Titre: Title:	Investigation of a Plasma Gurney Flap for Lift Enhancement
Auteur: Author:	Shinya Ueno
Date:	2010
Type:	Mémoire ou thèse / Dissertation or Thesis
Référence: Citation:	Ueno, S. (2010). Investigation of a Plasma Gurney Flap for Lift Enhancement [Mémoire de maîtrise, École Polytechnique de Montréal]. PolyPublie. https://publications.polymtl.ca/320/

URL de PolyPublie: PolyPublie URL:	https://publications.polymtl.ca/320/
Directeurs de recherche: Advisors:	Huu Duc Vo, & Njuki Mureithi
Programme: Program:	Génie mécanique

UNIVERSITÉ DE MONTRÉAL

INVESTIGATION OF A PLASMA GURNEY FLAP FOR LIFT ENHANCEMENT

SHINYA UENO

DÉPARTEMENT DE GÉNIE MÉCANIQUE

ÉCOLE POLYTECHNIQUE DE MONTRÉAL

MÉMOIRE PRÉSENTÉ EN VUE DE L'OBTENTION

DU DIPLÔME DE MAÎTRISE ÈS SCIENCES APPLIQUÉES

(GÉNIE MÉCANIQUE)

MAI 2010

UNIVERSITÉ DE MONTRÉAL

ÉCOLE POLYTECHNIQUE DE MONTRÉAL

Ce mémoire intitulé :

INVESTIGATION OF A PLASMA GURNEY FLAP FOR LIFT ENHANCEMENT

présenté par : UENO Shinya

en vue de l'obtention du diplôme de : Maîtrise ès sciences appliquées

et a été dûment accepté par le jury d'examen constitué de :

BALAZINSKI Marek, Ph.D., président

M. MUREITHI Njuki W., Ph.D., membre et directeur de recherche

M. VO Huu Duc, Ph.D., membre et codirecteur de recherche

M. REGGIO Marcelo, Ph.D., membre

ACKNOWLEDGEMENT

First of all, I would like to express the deepest appreciation to my advisor Professor Njuki W. Mureithi and my co-advisor Professor Huu Duc Vo for their guidance, encouragement, financial support and even their personally advice and assistance. This thesis presents my work, at the same time, this thesis presents their continuous guidance and encouragement for my work.

I would like to thank Mr. Bénedict Besner for his technical support for experimental approach. His personally advice made my laboratory life creative.

I am grateful to my three referees, Dr. Yuka Iga, Dr. Noriko Yui and Dr. Hiroshi Kanki. Their reference letters were essential to open the door to my master's degree.

I would like to acknowledge Dr. Kazuhiko Adachi. His guidance opened my eyes to study abroad. He was the key person to introduce me to Professor Njuki. W. Mureithi.

I would like to show my appreciation to Professor Toshiaki Ikohagi who was my former advisor and allowed me to leave Tohoku University Graduate School of Engineering for this study.

I would like to express my gratitude to my brilliant colleagues in our laboratory. I appreciate Kenny Huynh who allowed me to use his workstation when I had urgent simulations. His proof reading was very important assistance for me in the last minutes of this work. Philippe Versailles supported me for French translation of the RÉSUMÉ and CONDENSÉ EN FRANÇAIS. That was essential for this thesis. Xiaofei Xu was a good partner to discuss CFX simulations. His deep knowledge of the computational approach was very much helpful.

I am grateful to my parents, Kiyo Ueno and Kenji Ueno who have continuously encouraged my study and my life.

Last but not least, I am grateful to all people who contribute their life into technology progress. The life we have today is totally as a result of the endless effort of these people. It is an honor that I've been one of them.

RÉSUMÉ

Des essais en soufflerie à des nombres de Reynolds (Re) entre 1,0 x 10^5 et 1,8 x 10^5 ont été faits avec une pale NACA 4424 sur laquelle étaient installés des volets Gurney de 2 % et 4 %. Quatre positions (à 85 %, 90 %, 95 % et 100 % de la corde) étaient testées afin de déterminer l'effet de l'emplacement du volet sur l'augmentation de la portance; une position plus près du bord d'attaque permettant d'entreposer des volets qui seraient déployables. L'effet de leur hauteur a aussi été analysé et, conformément à la théorie, un plus grand volet induit une plus grande augmentation de portance. Cela a été observé pour toutes les positions étudiées, tout comme une extension de la plage d'opération en comparaison à l'aile sans volet. Aussi, pour un angle d'attaque constant et pour une hauteur de volet donnée, tous les emplacements en amont du bord de fuite ont présenté des accroissements de portance plus importants qu'à 100 % de la corde. Pour un volet de 2 % de hauteur, la localisation optimale pour obtenir la plus grande augmentation de portance (ΔC_L) est 85 % de la corde, alors que pour le contrôle du décrochage et la plage d'opération, il s'agit plutôt de 95 % de la corde. Un volet Gurney utilisant des actionneurs plasma a été conçu et testé à des *Re* variant de 1,2 x 10^5 à 1,8 x 10^5. Le « volet Gurney plasma » vise à éliminer la structure du volet Gurney conventionnel. Lors des essais, il était installé sur une pale NACA 4424 de 260 mm de corde et de 400 mm d'envergure. Les deux actionneurs plasma le composant étaient installés sur l'extrados et l'intrados du bord de fuite. Ils étaient activés de façon indépendante et les tests ont révélé que pris individuellement, ils contribuent de façon approximativement égale à l'augmentation de portance. Cette dernière est donc deux fois supérieure à celle qui serait obtenue avec une configuration à un seul actionneur. Alors que ΔC_L avec un volet Gurney standard est surtout causé par le retardement de l'écoulement sous l'intrados, celui-ci est plutôt dû à l'accélération de l'air au-dessus de l'extrados dans le cas du « volet Gurney plasma ». Cela contribue à étendre encore plus la plage d'opération pour de basses vitesses d'écoulement. Tandis qu'une pale sans volet ou avec un volet de 1 % de hauteur décrochait à une vitesse de 4,6 m/s, le volet Gurney de 2 % de haut et le « volet Gurney plasma » demeuraient dans les limites d'opération stable. Tout dépendant de la vitesse de l'air et de la puissance appliquée aux actionneurs, ΔC_L variait entre 0,02 et 0,18 pour le « volet Gurney plasma ». Puisque cette configuration présente deux actionneurs qui contribuent de façon égale à ΔC_L, elle est environ deux fois meilleure que tout autre système à un seul actionneur plasma.

Abstract

Wind tunnel tests for 2% and 4% Gurney flaps on a NACA 4424 wing were conducted at Reynolds numbers ranging from 1.0×10^5 to 1.8×10^5. Four different flap locations, 85%, 90%, 95% and 100%, were tested to investigate flap location effect for lift improvement since an upstream location is feasible to store deployable flaps. In the flap height study, as reported in the literature, higher flaps provided larger lift. This trend was observed for all flap locations in this study. In the location study, all Gurney flap configurations showed a wider wing operational range than the baseline wing. All upstream flaps showed higher lift than the 100% location flap for a given angle of attack and flap height. The optimal location of a 2% Gurney flap in the study was the 85% location in terms improvement, ΔC_L, and the 95% location in terms of stall control and wider operational range. A newly developed plasma "Gurney flap" was tested at Reynolds numbers ranging from 1.2×10^5 to 1.8×10^5. The plasma Gurney flap was intended to eliminate the physical structure of the Gurney flap and was installed on a 260 mm chord length and 400 mm wing span NACA 4424 airfoil. The Two SDBD plasma actuators comprising the plasma Gurney flap were installed individually on the suction side and the pressure side of the trailing edge. These two actuators were independently activated as well as the combined activation of the plasma Gurney flap. The tests revealed that each actuator individually contributes to the lift enhancement for nearly equal proportions, thus the combination of the two actuators performed twice as well as a single actuator. While the lift improvement by the physical Gurney flaps is mainly due to flow retardation on the pressures side, the lift enhancement of the plasma Gurney flap was mainly caused by the suction side flow acceleration. Because of these characteristics, the plasma Gurney flap is able to contribute wing operational range extension in the lower freestream velocity region. While the original and a 1% Gurney flap had stalled at 4.6 m/s freestream velocity, a 2% Gurney flap and the plasma Gurney flap wings remained within the wing operational ranges. The measured ΔC_L ranged from 0.02 to 0.18, depending on the freestream velocity and the power applied to the plasma actuators. Because the actuator configuration allows the installation of two plasma actuators nearly equal contribution to lift improvement, the setup can generate approximately twice the effect of any other single plasma actuator configuration.

CONDENSÉ EN FRANÇAIS

1. Introduction

La plupart des méthodes développées pour varier la force de portance le font en modifiant l'angle d'incidence de l'écoulement, ou en altérant l'écoulement autour de la pale à l'aide de surfaces mobiles de contrôle de portance telles que les becs de bord d'attaque, volets de bord de fuite et les ailerons.

Récemment, la technologie d'actionnement plasma a attiré l'attention en se montrant comme une approche alternative pour le contrôle des charges aérodynamiques. L'actionneur plasma est un dispositif simple constitué de deux électrodes décalées l'une par rapport à l'autre et séparées par un matériau diélectrique. Lorsqu'une différence de potentiel de plusieurs kilovolts et une fréquence de plusieurs kilohertz sont appliquées entre les électrodes, l'air dans le voisinage de l'électrode exposée est partiellement ionisé et accéléré par le champ électrique, ce qui induit un écoulement local qui prend généralement la forme d'un jet près de la paroi. En fait, cela équivaut à une force volumétrique qui accélère l'écoulement dans la couche limite. Ce dispositif peut donc être utilisé pour le contrôle de la portance et du décrochage des pales.

Des changements relativement petits dans la couche limite peuvent modifier l'écoulement global. Un exemple typique est le volet Gurney. Ce dispositif consiste en une structure rectangulaire installée perpendiculairement à la ligne de corde sur l'intrados, près du bord de fuite. La hauteur optimale du volet Gurney est en fait l'épaisseur locale de la couche limite. Bien qu'un volet plus épais induise tout de même une plus grande portance, cela se fait au détriment d'une traînée supérieure et d'un plus grand moment piqueur.

En plus du volet Gurney placé au bord de fuite, les volets placés en amont, connus sous le nom de « microtabs », sont particulièrement intéressants pour les applications dans le domaine éolien. Les « microtabs » fonctionnent exactement comme le volet Gurney. Ils sont installés en amont du bord de fuite, non seulement sur l'intrados, mais aussi sur l'extrados. Le fait qu'ils soient placés plus près du bord d'attaque constitue un avantage, puisque cela permet de les rétracter dans la structure de la pale et d'en faire des volets déployables. L'objectif de ces « microtabs » ne consiste pas uniquement à générer une portance supérieure, mais aussi à permettre un certain contrôle des charges aérodynamiques, ce qui ne peut pas être fait à l'aide des volets Gurney, qui sont fixes.

2. Objectifs

L'objectif ultime de la présente recherche est d'éliminer toutes les surfaces de contrôle qu'on peut observer sur une aile traditionnelle. La littérature concernant les volets Gurney et les « microtabs » montre que de minimes modifications à l'échelle de l'épaisseur de la couche limite entraînent un résultat significatif : l'augmentation de la portance. Cela implique que, bien que la vitesse maximale du jet induit par les actionneurs modernes est faible en comparaison avec la vitesse de l'écoulement dans les applications aéronautiques, ce dernier peut être affecté par l'actionneur plasma et, en conséquence, le contrôle de la portance de l'aile est potentiellement faisable.

Les ailes sans surfaces mobiles de contrôle de portance présentent plusieurs avantages. La première est la disparition des pénalités en termes de poids, de complexité mécanique, de coûts de production et d'entretien associés à ces surfaces et aux systèmes mécaniques et hydrauliques ou électriques qui les supportent. Le deuxième avantage est une portée accrue de l'aéronef découlant d'un volume de carburant plus élevé dû à la libération des espaces traditionnellement occupés par les surfaces mobiles et leur système de support. Finalement, on peut se libérer des compromis en performance aérodynamique imposés par l'implantation des surfaces mobiles et de leurs systèmes de support.

3. Méthodologie

L'effet du contrôle de l'écoulement par un volet Gurney peut être mesuré de deux façons : la mesure directe de la force de portance et la vélocimétrie par image de particules (VIP).

Les tests ont été faits dans une soufflerie en circuit fermé équipée d'une section d'essais de 0,61 m par 0,61 m par 2,4 m de longueur et équipée de parois transparentes. La température de l'air à l'intérieur de la soufflerie est contrôlée et l'incertitude sur la mesure de cette dernière est de ±1 °C. De plus, la série d'alvéoles et de maillages métalliques installée en amont de la section d'essais permet d'atteindre un bas niveau de turbulence (0,3 %). La vitesse de l'écoulement était obtenue à partir de la pression dynamique mesurée à l'aide d'une jauge de pression différentielle (DWYER INSTRUMENT, INC. Series 616 Differential Pressure Transmitter) ayant une résolution de 0,001 pouce d'eau (0,2499 Pa).

Le système de mesures de portance était situé sous la section de tests et avait été calibré en prévision des essais. Il est composé de deux balances ayant une résolution de 4.89×10^{-3}N

et 9.78 x 10^{-3} N, ce qui correspond respectivement à 0,02 % et 0,83 % de la force maximale mesurée lors des essais.

La VIP est une technique de visualisation d'écoulement utilisant dans ce cas-ci des particules d'huile d'olive pour suivre le déplacement des particules d'air. Deux photographies sont prises dans un court laps de temps, ce qui permet de déterminer le champ vectoriel de l'écoulement. Le système VIP calibré fournit différentes informations reliées à la vitesse de l'écoulement. En effet, les lignes de courant et les contours de vorticité sont calculés à partir du champ de vecteurs. Dans la présente étude, des champs vectoriels relatifs ont été utilisés pour analyser les changements dans la structure de l'écoulement en comparaison avec l'écoulement de base. Ces champs vectoriels relatifs étaient calculés en prenant le champ de vitesse moyenné pour une configuration donnée duquel on soustrayait le champ vectoriel de l'aile de base, pour la même vitesse globale d'écoulement. Cette approche a révélé comment les micro-modifications dans la couche limite induisent un effet significatif dans l'écoulement global.

4. Résultats

4.1 Étude de l'effet de la position et de la hauteur du volet Gurney

Des volets Gurney de différentes hauteurs, 2 % et 4 % de la corde, ont été installés à quatre positions différentes (à 85 %, 90 %, 95 % et 100 % de la corde) mesurées à partir du bord d'attaque d'une pale NACA 4424 de 6 pouces de corde. L'effet de la position et de la hauteur sur la portance était déterminé par des mesures de force. Comme énoncé dans la littérature, de plus grands volets Gurney induisent de plus importantes augmentations de portance.

Un résultat remarquable du présent travail est que lorsqu'installé à 100 % de la corde, le volet Gurney présente le plus petit accroissement de portance en comparaison à toutes les autres positions sur l'aile NACA 4424. Toutefois, la localisation optimale des volets dépend du profil de base. En effet, alors que 95 % de la corde a été identifiée comme la position optimale, d'autres chercheurs ont montré que les augmentations de portance avec un volet à 100 % de la corde dépassent celles observées pour les positions plus en amont.

L'effet de la hauteur des volets lors des mesures réalisées dans cette étude correspond à celui énoncé dans la littérature. De plus hauts volets fournissent de plus grandes augmentations de portance. Malheureusement, la traînée n'était pas mesurée lors des

essais. Or, il est rapporté dans la littérature que la pénalité en termes de traînée est non négligeable lorsque le volet excède l'épaisseur locale de la couche limite. Les calculs de l'augmentation absolue de portance par rapport à l'aile de base montrent qu'un volet Gurney d'une hauteur de 2 % positionné à 85 % de la corde induit le plus grand accroissement de cette force. L'augmentation de portance est moins sensible à la position du volet pour un volet de 4 % de haut que pour celui avec une hauteur de 2 %.

Le volet Gurney permet aussi d'obtenir une plus grande plage d'opération de l'aile, définie comme l'intervalle de vitesse de l'écoulement entrant pour laquelle il n'y a pas de séparation de la couche limite sur l'aile. Dans ce cas-ci, la configuration optimale est celle d'une aile avec un volet de 2 % de haut installé à 95 % de la corde. Tandis que toutes les pales, incluant celles équipées de volets Gurney moins optimaux, ont décroché lorsque la vitesse d'écoulement entrante a descendu à 10,3 m/s, l'aile optimisée (hauteur 2 %, position 95 %) n'entraîne pas le décrochage de ses couches limites et sa plage d'opération s'étend en deçà de cette vitesse. En somme, en ce qui concerne la plage d'opération, c'est le volet Gurney de 2 % de hauteur placé à 95 % qui fournit les meilleurs résultats.

4.2. Élaboration et étude du « volet Gurney plasma »

Le but de ce projet de recherche était d'évaluer la possibilité de remplacer le volet Gurney conventionnel par l'actionneur plasma. Le défi de cette recherche était d'étudier l'effet d'une configuration combinant deux actionneurs plasma pour accroître la génération de portance. Bien qu'une configuration à un actionneur ait déjà été étudiée, ce projet propose l'idée innovatrice d'installer un actionneur plasma sur chaque côté du bord de fuite d'une pale pour produire de meilleurs résultats en comparaison à l'effet d'un seul actionneur.

L'étude de l'effet de la position et de la hauteur du volet Gurney qui précède a montré les performances du volet lorsqu'il est placé en amont du bord de fuite. En se basant sur ces résultats, l'actionneur plasma sur l'intrados a été installé à 95 % de la corde de 26 cm d'une aile bâtie selon un profil NACA 4424 dans le but d'induire un tourbillon sur l'intrados ayant un axe parallèle au bord de fuite et se trouvant juste en amont de celui-ci, similairement à celui en présence d'un volet Gurney conventionnel. Un deuxième actionneur a été installé sur l'extrados à une position correspondant à 90 % de la corde. Cet emplacement a été choisi puisqu'il laissait un espace suffisant entre les deux actionneurs pour éviter une décharge électrique. L'actionneur sur l'extrados avait pour but d'empêcher la formation de

la bulle de séparation près du bord de fuite sur l'extrados. En présence d'un volet Gurney conventionnel, cette bulle est supprimée par la présence du tourbillon qui se forme juste en aval du volet de bord de fuite.

Les deux actionneurs étaient mis en marche de façon indépendante afin d'observer leur effet individuel avant d'analyser leur influence combinée. Les mesures de force ont montré que l'effet de chaque actionneur est du même ordre de grandeur. Quant à leur effet combiné, il correspond approximativement à la somme des contributions individuelles de chaque actionneur.

Les mesures VIP ont révélé la structure de l'écoulement lors de la mise en marche des actionneurs. Celui sur l'intrados a pour effet de retarder l'écoulement dans cette région. Simultanément, l'actionneur a pour effet d'accélérer l'écoulement sur l'extrados. Ces deux effets pris individuellement sont positifs en regard de l'augmentation de portance. Conséquemment, un accroissement de cette force a été observé lorsque l'actionneur sur l'intrados était en marche.

Les mesures de force faites dans la présente étude ont confirmé l'augmentation de portance induite par l'actionneur plasma situé sur l'extrados tel qu'on l'avait rapporté dans la littérature. Les mesures VIP ont non seulement permis de voir que cet actionneur plasma accélère l'écoulement au-dessus de l'extrados, mais il le ralentit aussi sous l'intrados. Ce phénomène s'explique par la plus grande circulation autour de l'aile induite par l'actionneur plasma placé sur l'extrados.

De plus, la structure de l'écoulement avec les deux actionneurs plasma en marche (volet Gurney plasma) a été comparée à celle obtenue avec un volet Gurney traditionnel. Les écoulements correspondants aux volets Gurney de 1 % et 2 % de hauteur, au volet Gurney plasma et à l'aile uniquement ont été mesurés. L'analyse des profils de vitesse a permis de constater un autre avantage à l'utilisation du volet Gurney plasma. Pour des écoulements de faible vitesse, alors que l'aile avec un volet Gurney de 1 % de hauteur a décroché, la couche limite sur l'extrados de l'aile avec le duo d'actionneurs plasma reste attachée. Cela s'explique par le fait que l'augmentation de la circulation autour de l'aile par le volet Gurney est principalement causée par le retardement de l'écoulement sur l'intrados, tandis que les actionneurs retardent l'écoulement sur l'intrados, mais accélèrent aussi l'écoulement sur l'extrados. Cette accélération de l'écoulement sur l'extrados a pour effet d'empêcher le décrochage de la couche limite et d'étendre par le fait même la plage d'opération.

5. Conclusion

Lors de l'étude de l'effet de la position et de la hauteur du volet Gurney, deux avantages de ce dernier ont été identifiés : l'augmentation de portance et la plus grande étendue de la plage d'opération. Le premier des deux a été mesuré pour plusieurs combinaisons de position et de hauteur de volet Gurney. Pour un profil NACA 4424, la plus petite augmentation de portance est observée lorsque le volet est positionné à 100 % de la corde. À l'opposé, le plus grand accroissement pour un volet d'une hauteur de 2 % se produit lorsqu'il est installé à 85 % de la corde. Pour les volets d'une hauteur de 4 %, l'augmentation de la portance est similaire pour toutes les positions en amont du bord de fuite et supérieure à celle observée avec un volet installé à 100 % de la corde. L'accroissement de portance est moins sensible à la position du volet pour un volet plus haut, tel qu'a démontré la comparaison des résultats entre les volets de 4 % et de 2 % de hauteur.

Le deuxième avantage, l'extension de la plage d'opération de l'aile, a été observé pour toutes les configurations de volet Gurney. Tandis que l'aile sans volet Gurney ni actionneur décrochait à une vitesse d'écoulement de 14,3 m/s, toutes les ailes avec un volet Gurney ne décrochaient pas, ce qui témoigne d'un agrandissement de la plage d'opération. De plus, les champs vectoriels relatifs mesurés à l'aide du système VIP ont révélé que le volet Gurney ne cause pas seulement un retard de l'écoulement sous l'intrados, mais aussi une accélération au-dessus de l'extrados. Cette augmentation de vitesse est liée à l'accroissement de la circulation autour de la pale induite par le retardement de l'écoulement entraîné par la structure du volet et le tourbillon en aval de ce dernier. Cette augmentation de la vitesse de l'écoulement sur l'extrados résulte en une extension de la plage d'opération en plus de l'augmentation de portance.

Le volet Gurney plasma présenté précédemment montre les deux mêmes avantages que le volet Gurney conventionnel, mais sans structure dépassant la surface de l'aile. Le principal accomplissement de cette recherche est l'élaboration de la configuration à deux actionneurs plasma qui combine l'effet de chaque actionneur. Les mesures de force ont permis de constater que chacun d'eux contribue de façon approximativement égale à l'augmentation de la portance. Cela est potentiellement supérieur à toutes les configurations à un seul actionneur, puisque celle élaborée dans cette recherche est équivalente à la somme de l'effet de deux actionneurs plasma.

Un autre avantage du duo d'actionneurs est une extension encore plus importante de la plage d'opération en comparaison au volet Gurney. Dans ce dernier cas, l'accélération de l'écoulement sur l'extrados est une conséquence de l'augmentation de la circulation autour de la pale. Toutefois, la configuration à deux actionneurs permet d'induire directement une force sur l'extrados pour accélérer l'écoulement près du bord de fuite, ce qui mène à un agrandissement de la plage d'opération.

Finalement, l'utilisation d'actionneurs plasma au lieu de volets Gurney permet de ne plus avoir recours à un système de déploiement et d'entreposage de la structure, ce qui permet du même coup leur utilisation dans plusieurs conditions de vol. Ces résultats présentent donc une approche alternative potentielle et réalisable pour le contrôle de la portance sans système mécanique.

TABLE OF CONTENTS

LIST OF TABLES

LIST OF FIGURES

LIST OF APPENDICES

CHAPTER 1

INTRODUCTION AND LITERATURE REVIEW

1.1 Review of Previous Studies

An aircraft requires variable lift during flight. To meet this requirement, all aircraft are equipped with flow control surfaces for low drag and high lift during takeoff, high drag and high lift during landing, and low drag and moderate lift when cruising. The high lift devices, known as slats and flaps were manually operated via cables in early airplanes and modern day smaller aircraft. Larger aircraft are equipped with hydraulic or electric actuators to drive these control surfaces. To improve flight efficiency, these devices must be retracted in cruising conditions in order not to induce additional drag. However, because of structural mechanism limitations, gaps between the movable surfaces cannot be eliminated or covered perfectly. A high tolerance design of these control surfaces increases manufacturing and maintenance costs therefore non-mechanical approaches have been considered.

Although ideas of surface flow control or active flow control were proposed in the early aviation history, many of these ideas were not realistic since the system requirements were mechanically complex or dependent on external pressure or suction sources. The main flow control ideas involved adding mass flow to the local boundary layer to induce a global flow effect.

One approach was a moving surface which replaced the wing leading edge curved surface by a rotating circular cylinder along the wing span. In this idea, by the cylinder rotation, a shear force is introduced in the boundary layer accelerating the flow at the leading edge. Another idea was surface suction. The surface suction system is equipped with several suction orifices to minimize the boundary layer thus controlling flow separation. However, this is not a practical approach since a lower pressure source is required. Another example is surface blowing which

adds high momentum flow to the boundary layer. Control of flow separation is achieved by a wall jet from a high pressure flow source. This system is not very practical since high pressure air for jet engines is at high temperature. High temperature resistant materials are not as light as aluminum alloy which is generally used for aircraft.

For practical applications, a principle similar to surface blowing is employed using leading edge and trailing edge flaps. The system works by bleeding flow from the airfoil pressure side to add momentum and delay flow separation, as shown in Figure 1.1.

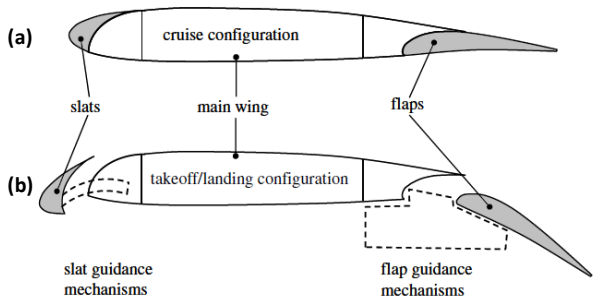

Figure 1.1 Slat and Flap: (a) Retracted (b) Deployed [1]

The Gurney flap is a rectangular plate located on the pressure side at the trailing edge of an airfoil. It is known as a simple and effective high lift device. The earliest concept of the Gurney flap was patented by Zaparka [2] in 1935 as a variation of split flaps. This flap was known in the 1960s as an application for racing car wings by Daniel Gurney. The goal was to obtain additional downward force to improve the traction. Lieback [3] introduced the idea in aeronautical applications in 1978.

Jeffrey [4] showed that the lift improvement of the Gurney flap is obtained by increasing circulation, a combination effect of vortex shedding behind the Gurney flap and flow retardation in front of the Gurney flap.

Bechert *et al*. [5] and Mayer *et al*. [6] tested the Gurney flap with several modifications to verify 3D effects. Slits, circular holes, rectangular holes and a unique 3D structure, similar to the detailed structure of dragonfly wings, were tested in a wind tunnel. These 3D modifications maintained similar lift and resulted in drag reduction.

Traub and Agarwal [7] combined the concept of the Gurney Flap and the jet flap. The Jet flap is a wing with orifices to bleed a jet and change flow around an airfoil as shown in Figure 1.2.

The authors intended to use the Gurney/jet flap for Unmanned Aerial Vehicle (UAV) lateral control. Variable lift and pitch moments were created by controlling the blowing jet supplied from an external high pressure source.

Figure 1.2 Wing with Jet Flap [8]

Shea and Smith [9] applied a synthetic jet at 92% and 95% chord locations. With a combination of synthetic jets, lift increase of up to 10% was achieved. Their experiments showed that a jet at the 95% chord location performed better than one at 92% chord.

Gurney flaps have also found their way into wind turbine applications where they are known as trailing edge microtabs. Following the demands of higher efficiency power production from reusable natural resources, the wind turbines required an increase in the size of the rotors. To do so, wind turbines are equipped with more robust hubs and rigid tower foundations since the top of the tower becomes heavier. Larger blades exposed heavier blade loads thus a mechanism to reduce the blade load is essential.

Stall control rotors are a simple approach to blade load control. The stall control rotor blades are fixed on the designed incident flow angle thus the systems are simple and relatively light weight. The blades are designed to stall at stronger wind to avoid blade overloading. The disadvantage of the stall control rotors is their relatively low efficiency since the natural wind speed varies but the blades are not able to follow the variable ambient flow conditions. This design requires statistical wind data at the installation site to optimize blade angle of attack and these studies increase cost.

Another major solution is pitch control rotors, which can vary the blade angle of attack adjusting it to the optimal value. Although this methodology is capable of following the oncoming natural wind, the design of the hubs is complex and the increase in weight of the system increases the construction costs.

A potential alternative approach is to embed micro devices, which control the surface flow and generate an equivalent effect to blade pitch control. One example of a small device which affects a macro phenomenon is the Gurney flap

Yen Nakafuji *et al* [10] embedded deployable microtabs on the pressure side and on the suction side at 95% chord location from the leading edge for dynamic lift control. Their computations on a GU25-5(11)-8 airfoil showed that the 95% chord had the best performance. The location is realistic for practical application since a forward location from the trailing edge makes it possible to store the mechanical systems of the deployable microtabs.

The microtabs at the trailing edge location performed better than at a 95% chord on a S809 airfoil in simulations made by Baker *et al*. [11]. The simulations showed that C_L with trailing edge tabs was higher than in the case of 95% and 90% chord tabs, however, the 95% case still exceeded the baseline. These studies implied that the optimal Gurney flap location depends on the airfoil profile.

The Plasma actuator was first reported in the mid-1990s. In the early days, the device was known for its boundary layer control capability. Later, the Plasma actuator was introduced into airfoil applications which had until then received little attention. Liu *et al*. [12] focused on the plasma actuator for aeronautical applications. Roth *et al*. [13] evaluated several dielectric materials, for aeronautical applications, which are able to induce higher jets while minimizing weight.

The plasma actuator airfoil application is feasible for Unmanned Aerial Vehicles (UAVs) applications because the device is simple, light weight and has wider flexibility in its installation. Santhanakrishnan *et al*. [14] considered the plasma actuators as an alternative flow control device for a lightweight UAV. Their tests showed approximately 60% positive and 30% negative shift on the lift curve by controlling the tip vortex created by the plasma actuator in lower freestream velocity conditions. Nelson *et al*. [15] installed the plasma actuator on the leading edge for UAV roll control in higher angle of attack. Their tests indicated an excellent roll control performance up to 35 degrees angle of attack.

Zhang *et al*. [16] simulated the plasma actuator installed at the trailing edge of a NACA 0012 airfoil. In their simulation, the plasma actuator was installed on the vertical surface of the

trailing edge to generate a downward wall jet. They assumed the height of the trailing edge vertical surface as the Gurney flap height. They obtained similar lift change as for a physical Gurney flap by Lee [17]. The simulations show lift to drag ratio improvement. The ΔC_L improved by approximately 0.2 in the linear section of the lift curve.

1.2 Objective

The ultimate objective of the present research is to eliminate all control surfaces from a wing. The literature on Gurney flaps and microtabs shows that micro scale changes up to the boundary layer thickness induce a macro scale outcome, the lift enhancement. This implies that even with the technology of the plasma actuator today, which is relatively weak relative to the freestream flow in aeronautical applications, the global flow can be affected by the plasma actuator thus wing lift control is potentially achievable.

The non-movable wings present several benefits. The conventional leading edge and trailing edge flaps are moving surfaces. These flaps therefore need to retract properly not to induce drag penalty and require to be deployed to the design locations when the control surface is operated. These design, including the mechanical components of the hydraulic or electric actuators, decrease wing aerodynamic efficiency, and increase manufacturing and operation cost. The flow control by the plasma actuators provides a simple wing structure and consequently the design and operation flexibility are extended. The proposed design of a new plasma "Gurney flap" uses two plasma actuators to improve airfoil circulation, as shown in Figure 1.3.

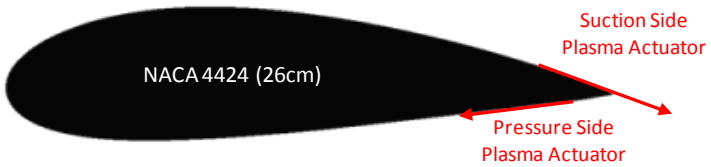

Figure 1.3 Proposed Design of Plasma "Gurney flap" for Non-Mechanical Approach

1.3 Thesis Outline

This thesis consists of five chapters. Introduction of this project is given in Chapter 1.

Chapter 2 and Chapter 3 are represented in journal paper form including their own abstract, introduction, experimental results and conclusions.

Chapter 2: The physical Gurney flap was tested to investigate flap location and height effect. An upstream flap has attracted the attention since the configuration provides sufficient structural volume and makes it possible to install a deployable flap.

Chapter 3: A newly developed plasma “Gurney flap” was tested. The physical structure of the Gurney flap was removed and replaced by the plasma actuator. This approach was intended to eliminate all mechanical surface control devices to achieve an alternative approach for non-movable wings.

Chapter 4: General discussion comparing the plasma Gurney flap to deployable Gurney flaps and morphing wings.

Chapter 5: Final conclusion and recommendations are presented here, followed by the references for Chapter 1, Chapter 4 and Chapter 5.

CHAPTER 2

A Location and Height Study of a Gurney Flap Installed on a NACA 4424 Airfoil

Shinya Ueno, Njuki W. Mureithi, and Huu Duc Vo,

École Polytechnique de Montréal,
Montréal, Québec H3T 1J4, Canada

2.1 Abstract

The performance of 2% and 4% Gurney flaps independently installed at four different locations, 85%, 90%, 95% and 100%, was investigated at Reynolds numbers ranging from 1.0×10^5 to 1.8×10^5. This study investigated the performance of a forward flap location since the forward section of the wing provides sufficient structural volume for the installation of a deployable flap. In the flap height study, as reported in the literature, higher flaps provided larger lift. This trend was observed for all flap locations. In the location study, all Gurney flap configurations showed wider wing operational range compared to the baseline wing. The best result was measured for the wing with a 2% Gurney flap at 95% chord. While the other wings stalled, the 2% Gurney flap at 95% chord remained within the operational range. The location study also revealed that a 2% Gurney flap at 85% chord had the highest performance in terms of lift change (ΔC_L) in the range of -4 to +6 degrees angle of attack. In all cases, for any given flap height, the 100% chord was found to always have the lowest lift change. The largest C_L improvements, approximately eight times and six times, were measured for the 4% flap at 95% chord and the 2% flap at 85% chord at -4 degrees angle of attack. PIV tests were also conducted to visualize the flow structure at -4 degrees angle of attack where the largest C_L improvement was measured. The velocity profile study at planes 10% and 20% chord downstream from the trailing edge revealed that the downstream flow of upstream flaps was deflected. The deflection was approximately 6 degrees for the 2% flap located at the 85% chord. This flow deflection was not measured in the downstream flow behind the 100% chord flap. This is one factor which caused upstream flaps performances to exceed that of the trailing edge flap. To recap, this study investigated the capability of forward location Gurney flaps. The optimal location of a 2% Gurney flap in the

study was the 85% chord in terms ΔC_L and the 95% chord in terms of stall control and increased operational range.

2.2 Introduction

Following the demands of higher efficiency power production from reusable natural resources, larger wind turbines are require leading to an increase in the size of the rotors. To support the rotors, wind turbines must be equipped with more robust hubs and rigid tower foundations. Larger blades result in higher blade loads thus a mechanism to reduce the blade load is essential.

Stall control rotors are a simple approach to blade load control. The stall control rotor blades are fixed at the design incident flow angles. The systems are simple and relatively light weight. The blades are designed to stall at high flow speeds to avoid blade overloading. The disadvantage of the stall control rotors is their relatively low efficiency since the natural wind speed varies but the blades are not able to follow the variable ambient flow conditions.

Another major solution is pitch control rotors, which can vary the blade angle of attack adjusting it to the optimal value. Although this method is capable of following the oncoming natural wind, the design of the hubs is complex and the increase in weight of the system increases the construction costs.

A potential alternative approach is to embed micro devices, which control the surface flow and generate an equivalent effect to blade pitch control. One example of a small device which leads to a macro phenomenon is the Gurney flap. The Gurney flap is a small rectangular plate located at the trailing edge. The concept of the trailing edge micro flap was patented by Zaparka [1] in 1935. Although the patented flap was a variation of the split flap, a fixed flap was used on racing cars in the 1960s by Daniel Gurney which attracted the attention of the aeronautics fields. The Gurney flap was examined by Lieback [2] for airfoil applications in 1978 and Jeffery [3] in 1996.

Although the typical flap height is 1% of chord [4], flap heights ranging from 0.21% to 5.0% were investigated by Cavanaugh *et al*. [4] in a wind tunnel. The tests showed that higher Gurney flaps generate larger lift, however, a large negative pitch moment was measured.

Three dimensional modifications to the Gurney flap were conducted by Meyer *et al*. [5]. The modifications were aimed to gain insight into the wake instability and drag reduction. The tests revealed that the drag reduction was achieved with relatively small lift reduction from the original Gurney flap configuration.

The trailing edge microtabs are also known as a type of Gurney flap. For lift and load control applications, active flaps are necessary, thus upstream located flaps have attracted more attention. Yen Nakafuji *et al*. [6] focused on microtabs for wind turbine blade load control. Their simulations and experiments showed that tab style flaps of up to the boundary layer height provide a macro scale effect. A deployable tab located at 95 % chord from the leading edge was the best compromise between optimal lift, drag and structural volume for storage of the deployable tabs. The lift benefit (ΔC_L) from the flap was 0.3, which was a 50% increase from the baseline. The result was the first report that demonstrated the global effect induced by the small device [6].

Chow and van Dam [7] simulated a deployable flap at 95% chord location on a S809 wind turbine airfoil. The location was optimized not only for aerodynamic performances but also for structural volume to store the flaps. The study includes a dynamic response of the flap deployment. The results show that the microtabs are clearly effective on cambered airfoils as a simple “on-off” type lift and load control device.

2.3 Experimental Methodologies

2.3.1 Wind Tunnel

Wind tunnel tests were conducted in a closed loop wind tunnel equipped with a test section of 0.61m by 0.61m, with a length of 2.4m and equipped with transparent optical windows. The wind tunnel temperature can be controlled by within 1 degree Celsius. Honeycomb screens installed upstream of the test section reduce the flow turbulence intensity to below 0.3%. Velocities were computed from the dynamic pressure measured by a DWYER INSTRUMENT, INC. Series 616 Differential Pressure Transmitter with a resolution of 0.001 in.W.C., equivalent to 0.2499 Pa.

2.3.2 Particle Image Velocimetry (PIV)

PIV is a flow visualization method that uses oil particles as tracers and measures the displacement of the particles thus displacement vector fields can be computed. The calibrated PIV system provides velocity information, from which streamlines and vorticity contours are computed.

Relative vector fields were used in this study to analyze detailed flow structure change from the baseline configuration. The relative vector fields were computed by subtracting the averaged velocity vector field of a given test configuration from the averaged velocity vector field of the baseline, at the same freestream velocity conditions. This approach revealed how a micro change in the boundary induces a macro effect in the ambient flow structure.

2.3.3 Force Measurement System

The force measurement system is located beneath the test section. The system is composed of two force balances to measure two components of the force generated by the airfoil. The resolutions of the two force balances are 4.89×10^{-03}[N], and 9.78×10^{-03}[N], which are 0.2% and 0.4% of the maximum force measured in the test. The system was validated before the tests.

2.3.4 Airfoil

A NACA 4424 airfoil was selected for the baseline because of its thicker profile. Although a deployable flap was not tested in this study, the upstream flap location provides better volume to store a deployable flap systems thus a wing with a capability of upstream flap installation is more attractive. A thicker profile is representative of the root of a large wind turbine blade.

The wing used in the wind tunnel tests was 0.15m (6 inch) in chord and had a 0.60m wing span. End plates were installed to minimize 3D effects. The force measurements were conducted on the original profile to acquire the baseline information, as shown in Figure 2.1.

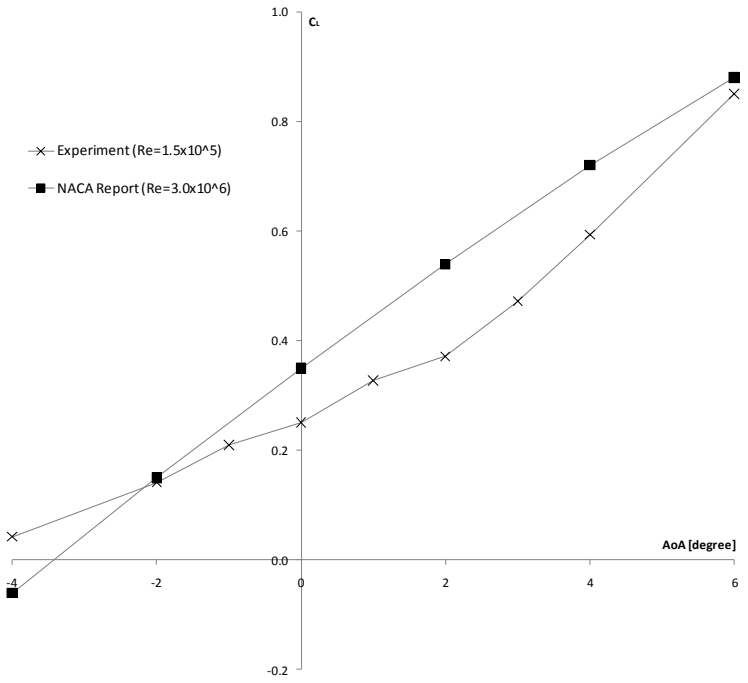

Figure 2.1 Test Wing Baseline Lift Curve

2.4 Wind Tunnel Force Measurements

2.4.1 Test Results

Lift force measurements for two different flap heights were conducted at four different flap locations. The absolute C_L values at Reynolds number 1.8 x 10^5 was plotted at a given flap location to validate the flap extension effect for a given location, as presented in Figure 2.2. The measured absolute C_L values at Reynolds numbers ranging from 1.0 x 10^5 to 1.8 x 10^5 are presented in Figure 2.3.

In Figure 2.2, solid symbols and open symbols represent 2% flap results and 4% flap results, respectively. As a general trend, 4% flaps are less sensitive to location change than 2% flaps.

At -4 degrees angle of attack, 2% flaps show a clear trend in the location effect on lift improvement, as shown in Figure 2.2(a). The 100% chord flaps provided the lowest lift improvement compared to other upstream flaps for a given flap height. The ΔC_L of the 4% flap at 100% chord was equivalent to the 2% flap effect at 85% chord. The 4% flap at 95% chord gives the highest lift among all configurations, as shown on Figure 2.2(a).

At -2 degrees angle of attack, the 85% chord flap provided the highest ΔC_L for 2% flaps as seen in Figure 2.2(b). For 4% flaps, the 90% and the 85% chord provided better ΔC_L although the 90% chord is slightly superior to the 85% chord flap, as seen in Figure 2.3(b). The 100% chord gives the lowest lift improvement for a given flap height.

At 0 degrees angle of attack, the 85% chord shows the largest and the 100% chord gives the lowest lift improvement for a given flap height.

At 2 degrees angle of attack, the trend of 2% flaps is the same as that of 0 degrees angle of attack; the 85% chord location has the largest effect and the 100% chord location has the lowest lift improvement. For 4% flaps, the 85% chord and the 95% chord location are equivalent and give the best lift improvement, while the 100% chord location shows the lowest performance.

At 4 degrees and 6 degrees angle of attack, the trend between the two cases is similar. While the 85% chord and the 95% chord location show the largest lift improvement for 2% flaps, the 90% chord and the 95% chord give the highest performance for 4% flaps.

The results for freestream velocity effects are presented in Figure 2.3. The general trend was that an increase in freestream velocity caused an increase in lift. As reported in the literature [4, 6-9], higher Gurney flaps provide higher lift performance in all configurations. The same result is reproduced in the present tests.

A unique trend was observed at 4 degrees angle of attack, and significant results for the wing operational range are observed at 6 degrees angle of attack.

At 4 degrees angle of attack, the four curves of a given flap height are separated into two groups, presented in Figure 2.3(e). In the 2% flap results, 85% and 95% chords belong to the higher ΔC_L group while 90% and 100% chords are in the lower ΔC_L group. In the 4% height results, 90% and 95% chords are in the higher ΔC_L group while 85% and 100% chords are in the lower group, as shown in Figure 2.3(e).

At 6 degrees angle of attack the wing operational range was extended for all Gurney flap wings, as shown in Figure 2.3(f). At 14.5 m/s freestream velocity, while the baseline airfoil stalled, all Gurney flap wings remained within the operational range. The best performance in terms of operational range extension was provided by the 2% Gurney flap at the 95% chord

location. At 10.3 m/s freestream velocity, all wings besides the wing fitted with the 2% flap at the 95% chord had stalled.

A similar trend to the 4 degrees angle of attack case was measured at 6 degrees angle of attack velocities higher than 16 m/s where all wings are within the operational conditions. The four curves for the 4% flap results fall into two groups which is exactly the same trend found for the 4 degrees angle of attack, as shown in Figure 2.3(e) and (f). In the 2% flap results, the higher ΔC_L group consists of the same locations with the same orders, however, the 90% chord location is now near the higher group while the 100% chord location has the lower performance in terms of ΔC_L.

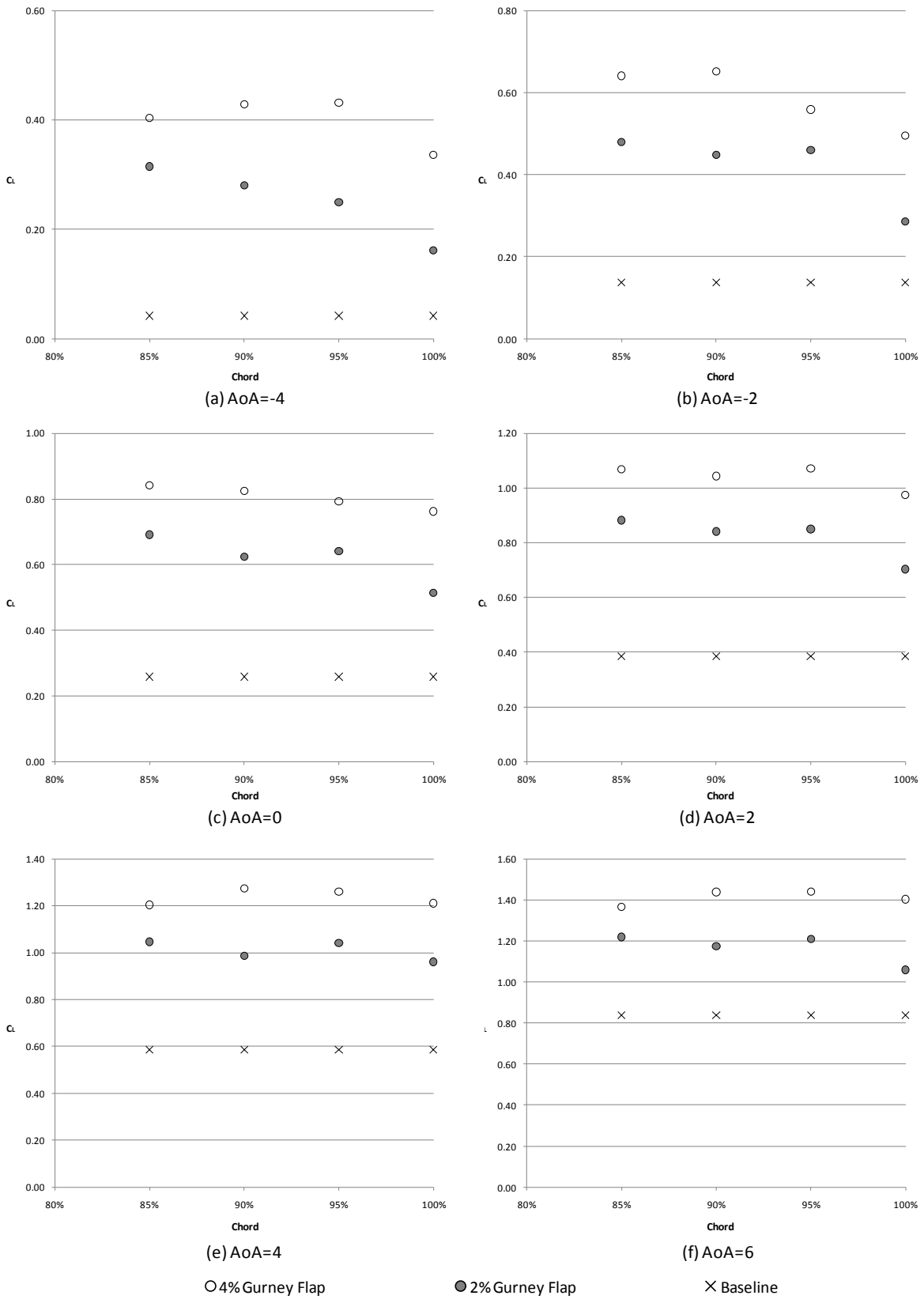

Figure 2.2 Variation of C_L with Four Different Locations at Reynolds Numbers of 1.8 x 10^5

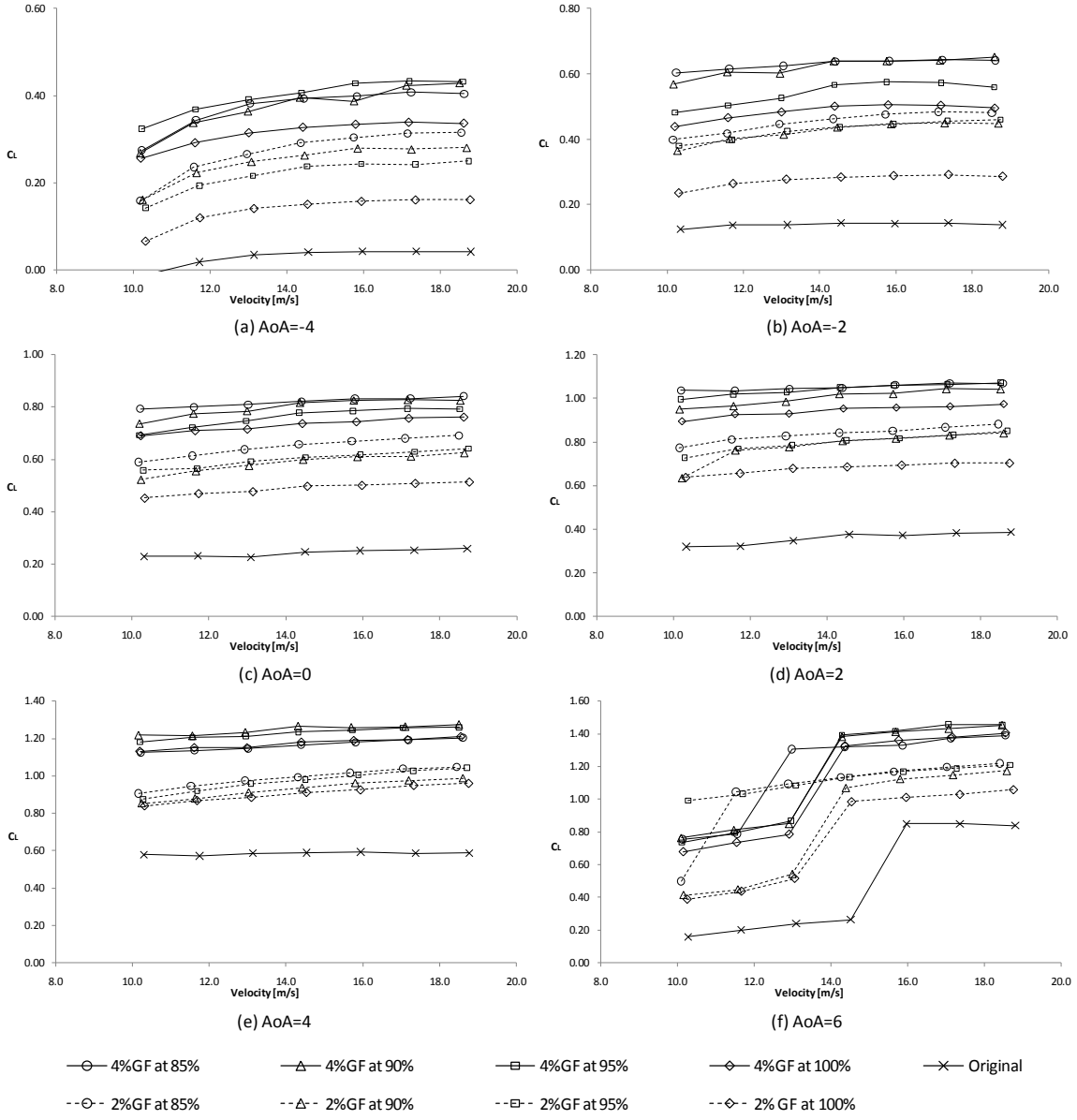

Figure 2.3 Variation of C_L with Four Velocities at Reynolds Numbers Ranged 1.0 x 10^5 ≤ Re ≤ 1.8 x 10^5

2.4.2 Gurney Flap Location and Height Study

The results of lift force measurements are organized by relative change of ΔC_L to highlight the ΔC_L improvement between the 4% and 2% height flaps at a given flap location, as presented in Figure 2.4. The results give lift sensitivity to flap extension at a given location.

At 85% chord, shown in Figure 2.4(a), apart from -4 degrees angle of attack, the relative ΔC_L deviations for different angles of attack fall within a narrow band. This result implies that for the 85% chord C_L is fairly insensitive to angle of attack.

At 90% chord, shown in Figure 2.4(b), the results fall into three groups. The lowest relative ΔC_L was recorded at -4 degrees. The middle group, with a relative ΔC_L of approximately 0.2, consisted of the angles -2, 0 and 2 degrees. The highest relative ΔC_L group consists of the two higher angles of attack, 4 and 6 degrees.

At 95% chord, shown in Figure 2.4(c), the results show a wider deviation, between 0.1 and 0.3, in terms of relative ΔC_L. The deviation does not show a clear trend with angles of attack.

At 100% chord, shown in Figure 2.4(d), the general trend was higher relative ΔC_L at higher angles of attack. The lift is sensitive to the flap extension for a given angle of attack with the exception of 4 degrees angle of attack.

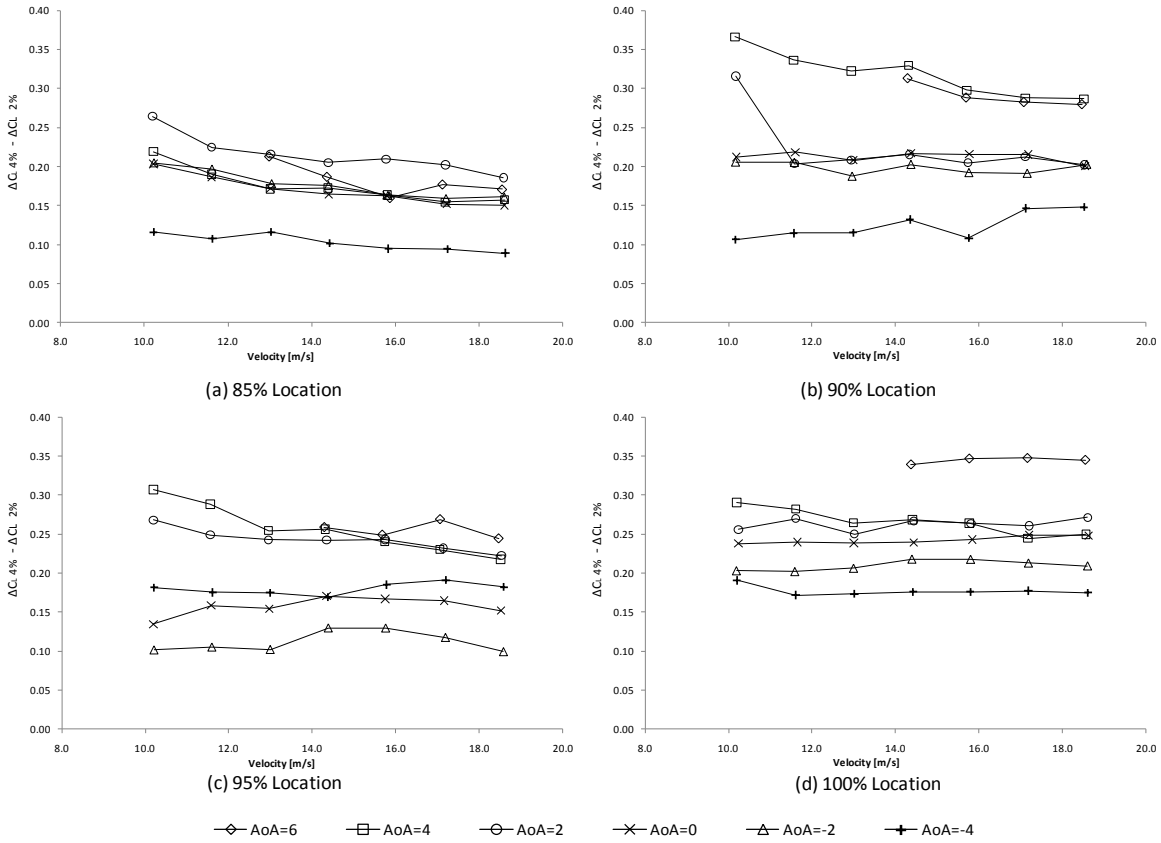

Figure 2.4 C_L Improvement from 2% Gurney Flap to 4% Gurney Flap at 85% Chord (a), 90% Chord (b), 95% Chord (c) and 100% Chord (d)

2.4.3 Discussion

Five papers are considered in this section. Three out of the five papers examined similar flap height to the current study, 2% and 4% flap, while others reported on 1% and 2% flap. Unfortunately, none of them selected the same airfoil profile.

Cavanaugh *et al*. [4] studied the Gurney flap height using an experimental approach. This study investigated 2% and 4% height flaps, as well as five other different flaps. A NACA 23012 wing was selected for the baseline profile in their study. The height study at a chord Reynolds number of 1.95 x 10^6 revealed that ΔC_L for the 2.08% flap was nearly 100% higher than ΔC_L for the 1.04% flap. The performance of the 4.00% flap was about 50% higher than that of the 2.08% flap in terms of ΔC_L. The results shows that between a 1% and a 2% Gurney flap, the ΔC_L

of a 2% flap was twice that of the 1% flap. In the case between a 2% and a 4% Gurney flap, the ΔC_L of the 4% flap was 50% larger than that of the 2%.

Baker *et al*. [8] conducted computational and experimental investigations of the effects of the Gurney flap location and height on a S809 wing. Wind tunnel tests were conducted at chord Reynolds number of 1.0×10^6. In the Gurney flap height study, three different heights, 1.1%, 1.6% and 2.2%, at 95% chord on the pressure side were tested. The test results showed that higher flaps caused larger lift improvement. The ΔC_L caused by the 2.2% height flap was approximately 100% larger than ΔC_L for the 1.1% height flap in the linear section of the C_L curve. The location study was conducted by comparing 90%, 95% and 100% chords on the pressure side. The ΔC_L for the 100% chord was approximately 100% higher than the ΔC_L of the 95% chord. There was no significant lift improvement between a 90% chord flap and the baseline in the linear section of the C_L curve.

Yen Nakafuji *et al*. [9] investigated location and height effect for three different height flaps at four different locations on a GU25-5(11)-8 wing by simulations and experiments. The height study was conducted with 0.5%, 1.1% and 1.7% flaps. The experiment showed that the 1.7% flap gave 9% higher C_L than the 1.1% flap, while the 0.5% flap gave 22% lower C_L than the 1% flap. The experimental results showed good agreement with simulations. From the simulation results, the 1.1% height flap was found to be optimal in terms of the lift to drag ratio. The location study was conducted at 90%, 95%, 97% and 100% chords. In their experiments, the three locations, 95%, 97% and 100% chord, were superior to the 90% chord which provides approximately 25% lower C_L than the other rear flaps. The study found to be the 1% flap at 95% chord was the optimal compromise between lift, drag and structure volume.

A Gurney flap height study on a NACA 0012 wing was reported by Liu *et al*. [10]. The symmetric airfoil was tested in a wind tunnel at $Re=4.74 \times 10^5$. Five different height flaps were tested including 2.0% and 4.12% flaps. The trend of the flap height was higher lift for higher height flaps. Between 2.0 % and 4.12% flaps, the ΔC_L improved approximately 70%.

In the current study, the ΔC_L from the baseline of a 100% chord flap on a NACA 4424 wing is presented on Figure 2.5(d). The ΔC_L of a 4% Gurney flap was nearly twice that of the ΔC_L of a 2%

Gurney flap in represented angle of attack. On a NACA 23012 wing [4], ΔC_L increased by approximately 50% between a 2% flap and a 4% flap. This result implies that the ΔC_L of the NACA 4424 wing is more sensitive to the flap extension. The 2% and 4.12% Gurney flaps on a NACA 0012 wing [9] provided closer values for the flap extension sensitivity to the NACA 23012 wing results. At 0 degrees angle of attack, a 2.0% flap and a 4.12% flap provided, respectively, 0.24 and 0.41 C_L improvement on a NACA 0012 wing. At the same angle of attack, a 2.0% flap and a 4.0% flap generate, respectively, 0.26 and 0.51 C_L improvement on a NACA 4424 wing in the current study. Thus ΔC_L improvement by the flap extension was 71% on the NACA 0012 and 95% on the NACA 4424.

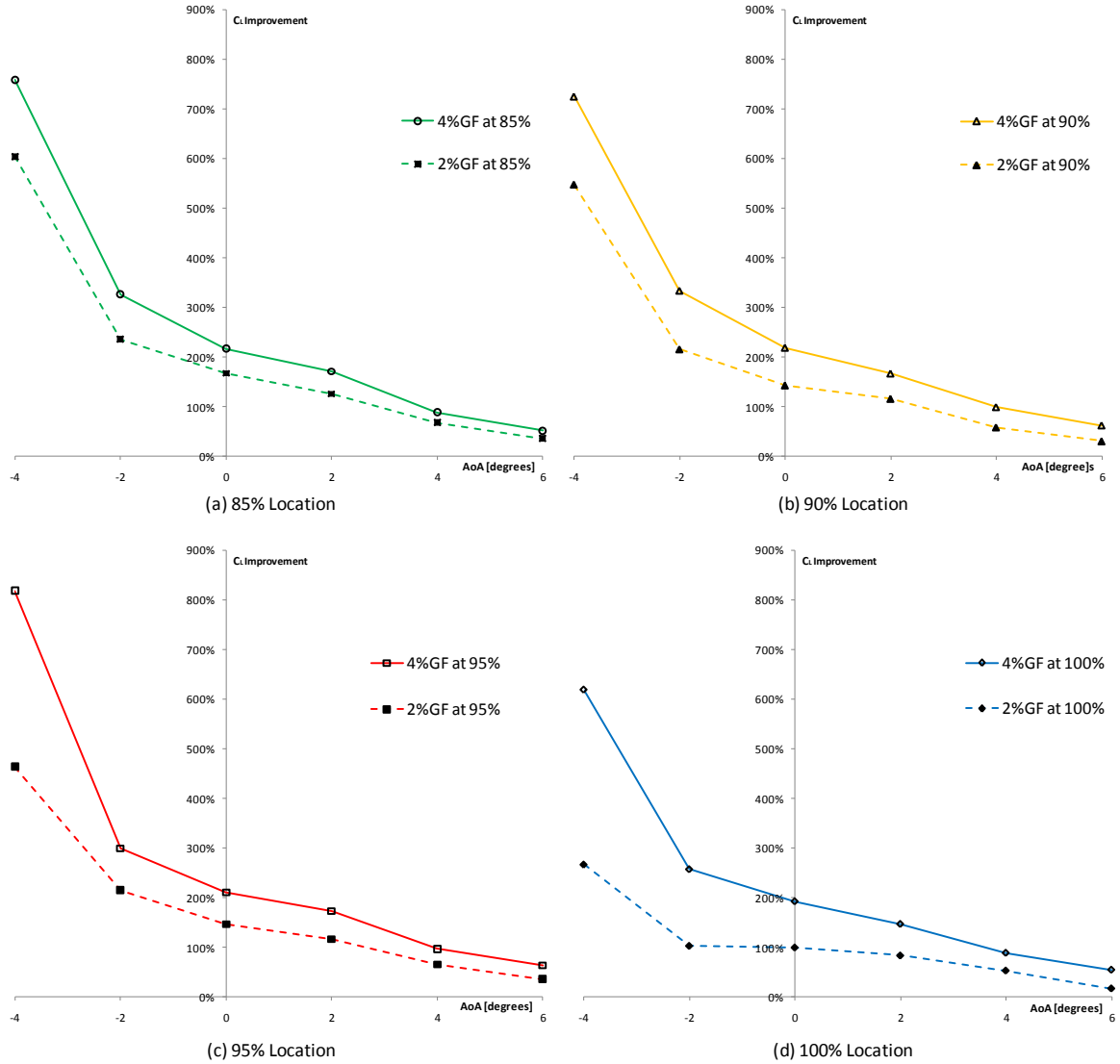

Figure 2.5 C_L Improvement Curve from Baseline Profile

The current results for 95% chord with 2% and 4% flaps do not correspond to the 1.1% and 2.2% flap results of Baker *et al*. [8] neither for the baseline profile nor for the flap height. However, both results show the same trend, higher flaps provide higher lift. In the current study, a 95% chord 4% flap provides approximately 25% to 50% lift improvement from the 2% flap performance, as shown in Figure 2.5(c).

Previous work and the current study have investigated the trend of the height effect on lift improvement. The flap extension effect for lift enhancement was measured for different baselines airfoils and different flap locations. This is because a relatively higher flap retards more flow, inducing higher stagnation pressure which raises the lift. Thus the flap extension causes lift enhancement for any given profile and flap location. Although the height effect is a general trend, the location effect is unique and depends on a baseline airfoil. The flap retards the pressure side flow, and at the same time offsets the flow stream away from the pressure side surface. This offset stream provides additional camber effect and lift is enhanced.

The location studies in the literature were conducted on a GU25-5(11)-8 wing [6] and a S809 wing [8]. The upstream flaps caused no change or had lower performance compared to the 100% chord flap on the two wings, however, the current study revealed that the location of 85%, 90% and 95% were superior to the 100% chord location. The different trend is explained by the profile difference of the pressure side trailing edge. For the GU25-5(11)-8 and S809 airfoils, the surface on the pressure side trailing edge is nearly flat. This means the height from the trailing edge to the tip of the flap is almost unchanged between the trailing edge flap and the upstream flaps. In the case of a NACA 4424 profile, the surface slope of the pressure side trailing edge provides additional thickness for the displacement from the trailing edge to the tip of an upstream flap. As Baker *et al*. [8] reported, higher flaps generate higher lift in forward locations. The additional thickness induces an additional camber effect, thus the upstream locations on a NACA 4424 wing provide positive results.

2.5 Velocity Profile Study of 2% Gurney Flap Airfoils

PIV tests were conducted to verify the flow structure change caused by the Gurney flaps. Relative velocity vector fields were computed at -4, 0 and 6 degrees angles of attack. In each configuration, 30 PIV images were recorded at 15Hz. A relative velocity vector field was computed by subtracting the averaged velocity vector field of the original profile from the averaged velocity vector field of the test wing with a flap, at a given freestream velocity. A schematic illustration of the camera view position is presented in Figure 2.6.

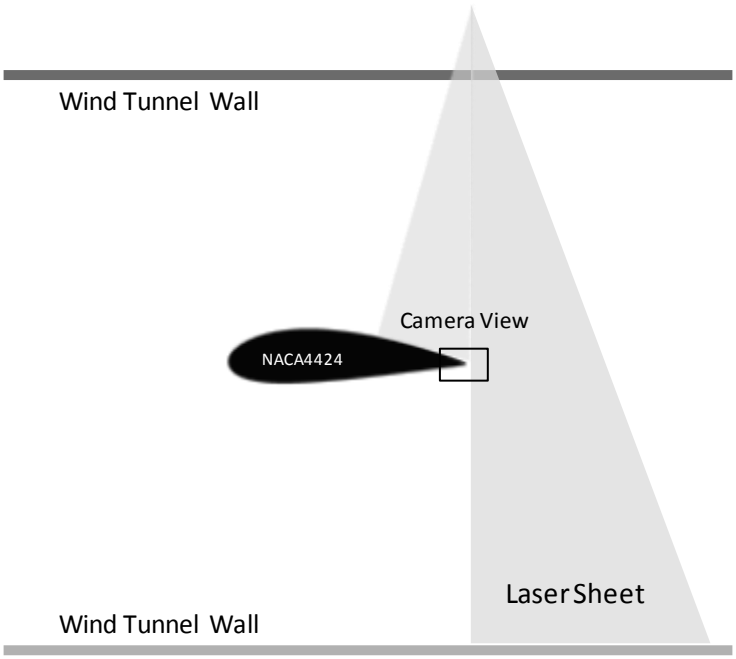

Figure 2.6 Camera View Position of 2% Gurney Flap Velocity Profile Study

The U velocity profile was extracted from the averaged relative velocity vector fields at 10% chord downstream from the trailing edge. Schematic sketches of the measurement planes are shown in Figure 2.7. The tests were conducted at 16.0 m/s freestream.

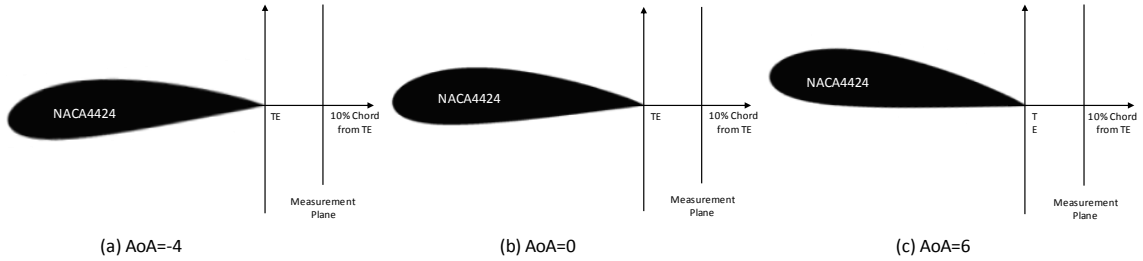

(a) AoA=-4 (b) AoA=0 (c) AoA=6

Figure 2.7 Measurement Plane of 20% Chord Downstream

At -4 degrees angle of attack, a 2% Gurney flap at the 85% chord was outstanding, as shown in Figure 2.8(a). On the suction side, the flow increase of the 90% chord flap and the 85% chord flap are nearly equivalent. The U velocity peak of these two flaps was nearly double that of the 100% chord location flap. On the pressure side, a negative U peak is measured, which shows that the flow on the pressure side is retarded by the Gurney flap. The negative U peak, the maximum velocity delay, for the 85% chord flap is approximately 3 times larger than for that of 100% chord flap. The result of the 90% chord flap is double of the 100% chord flap. The flow deceleration induced the largest lift improvement for the 85% chord flap. This was followed by the 95% chord flap and then the 90% chord flap. These performances are confirmed in the force measurements, shown in Figure 2.9. At -4 degrees angle of attack, ΔC_L for the 85% chord flap is the largest and the others follow in the same order of the velocity profile shown in Figure 2.8(a). The C_L improvement of the 85% chord was approximately six times larger relative to the baseline C_L.

In the case of 0 degrees angle of attack, the U peak values on the suction side upstream flaps are similar thus that of the effect flow retardation on the pressure side dominates the performance as shown in Figure 2.8(b). On the pressure side, a flap at 85% chord retarded the flow more than at 90% and 95% chords. Force measurement results in Figure 2.9 therefore show the highest performance at 85% and nearly equivalent performance for 90% and a 95% chords. The trailing edge, 100% chord, showed the lowest C_L improvement.

At 6 degrees angle of attack, the 100% chord caused the smallest flow change on the two surfaces, this resulted in the lowest lift improvement, as presented in Figure 2.8(c). The three upstream locations, 85%, 90% and 95% have comparable effects as confirmed in the force measurement results presented in Figure 2.9.

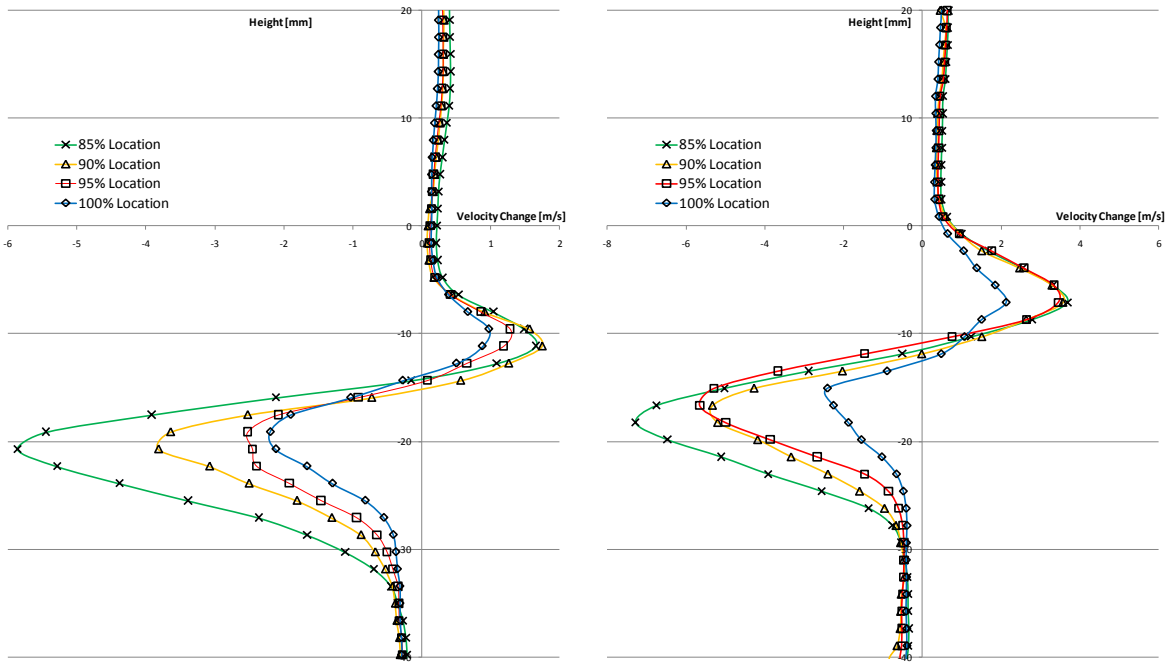

(a) AoA=-4

(b) AoA=0

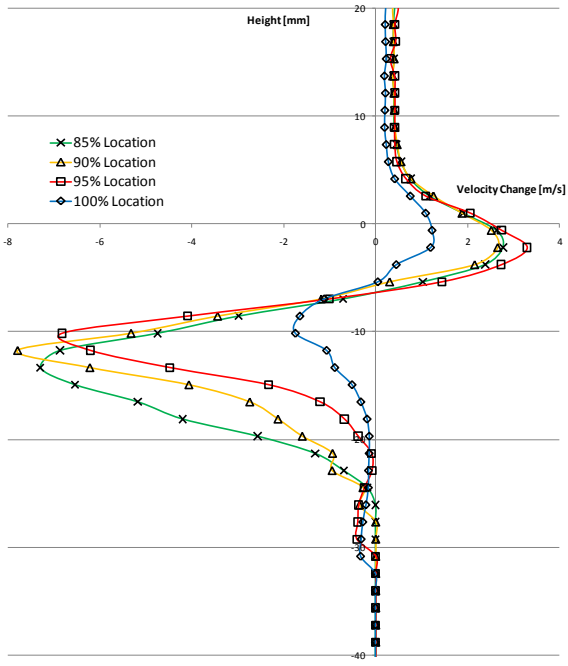

(c) AoA=6

Figure 2.8 Velocity Profiles of 10% Downstream Plane

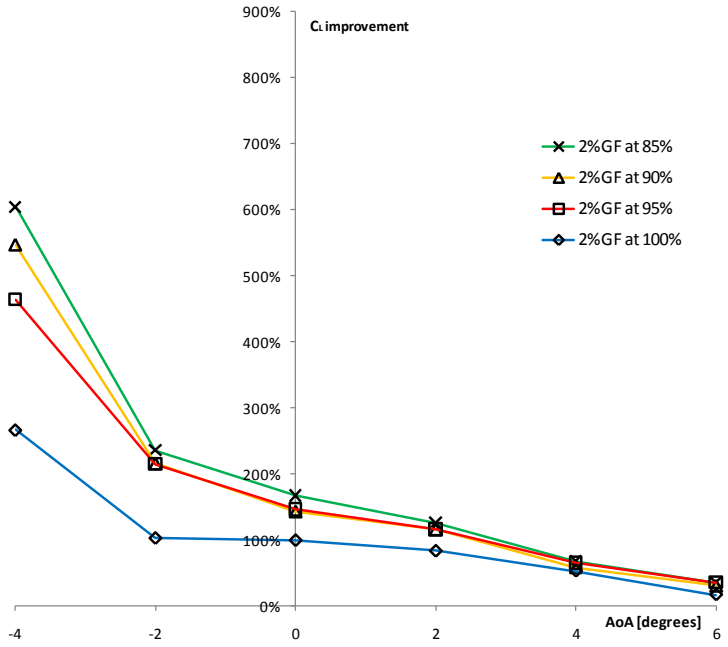

Figure 2.9 2% Gurney Flap C_L Improvement Curve

Relatively larger ΔC_L were measured for the negative angle of attack. The U velocity peak was extracted at the two planes 10% and 20% downstream from the trailing edge for -4 degrees angle of attack. The velocity profiles presented in Figure 2.10 show that the amount of the flow change is greatly dependent on the flap location, thus the C_L improvement ranged approximately 250% to 600%, as shown in Figure 2.9.

The results of the downstream flow study suggest another factor which induces relatively lower C_L improvement at 100% chord flap compared to other upstream flaps. In Figure 2.10, open symbols show data measured at the 20% downstream location thus the displacement of the U peak location between the two curves in Figure 2.10 represents the flow deflection between the two downstream planes. The three cases of upstream location flaps show flow deflections. However, no significant flow deflection was measured for the 100% chord case, in Figure 2.10(d). For the 85% chord flap, which gives the highest C_L improvement, the deflection angle between the two planes was 6.0 degrees. Schematic illustrations of the flow deflection are presented Figure 2.11.

Although the shift is small, the deflections were seen in the relative velocity vector field presented in Figure 2.12.

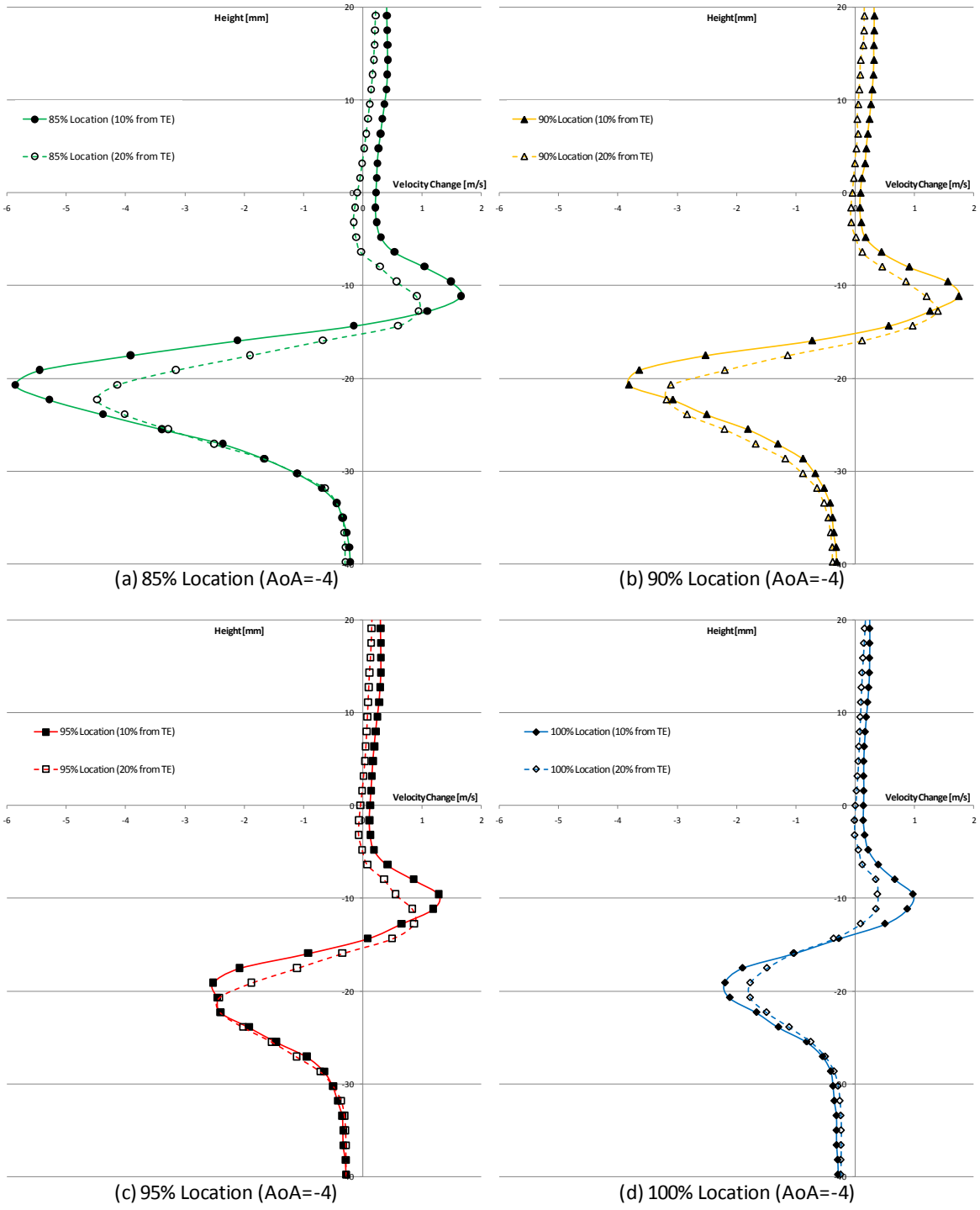

(a) 85% Location (AoA=-4)

(b) 90% Location (AoA=-4)

(c) 95% Location (AoA=-4)

(d) 100% Location (AoA=-4)

Figure 2.10 Velocity Profiles of 10% and 20% Downstream from TE in AoA=-4 deg.

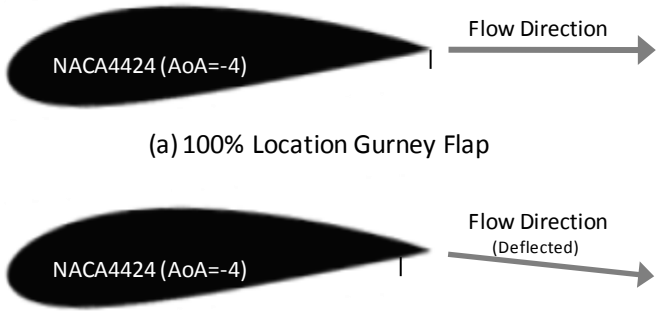

Figure 2.11 Schematic Illustration of Deflected Downstream Flow

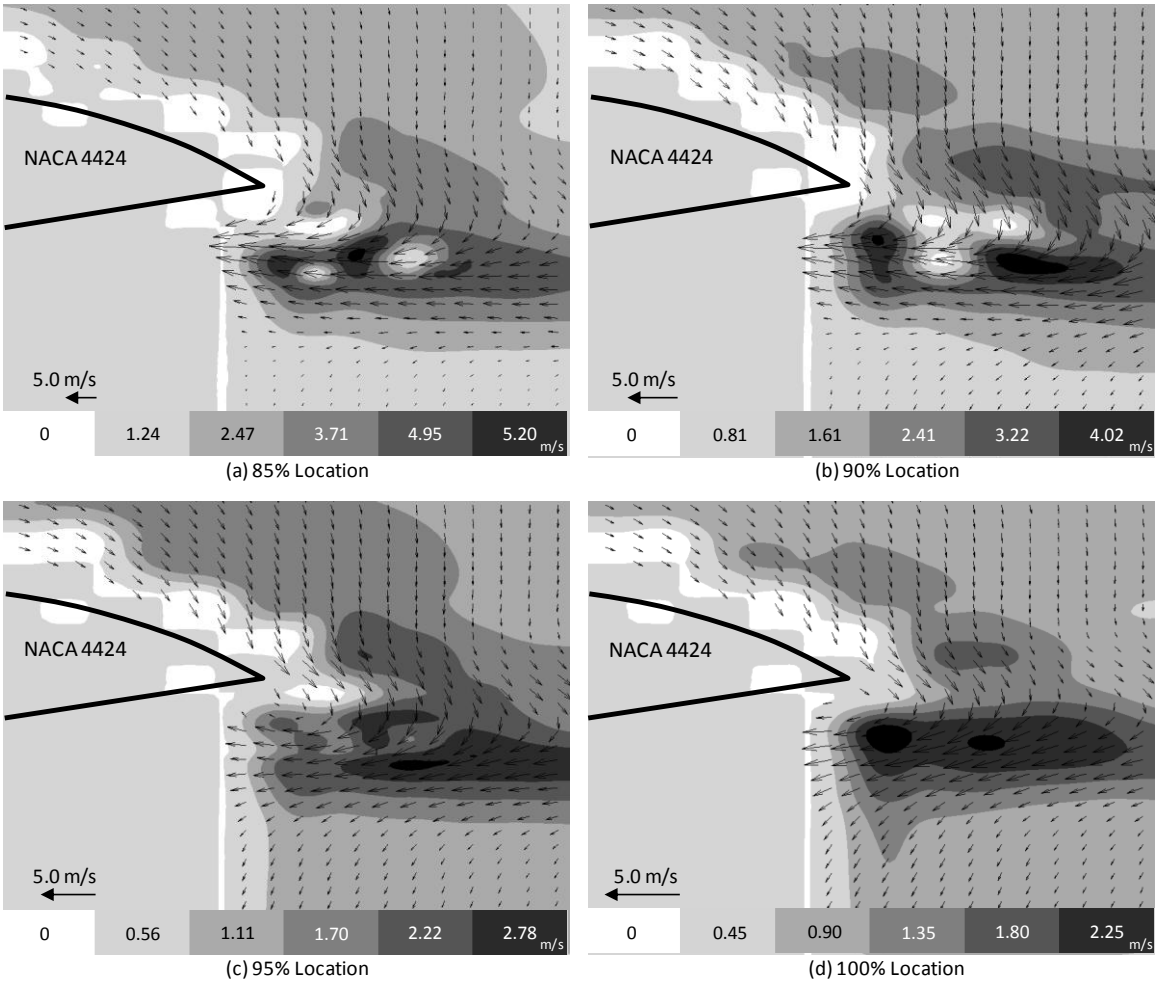

Figure 2.12 Averaged Relative PIV Vector Fields layered on Vector Contours at the Wing Trailing Edge

2.6 Conclusion

In most previous studies, the Gurney flap is located at the trailing edge because the trailing edge flap provided based on existing knowledge better C_L improvement than upstream flaps for some baseline profiles. However, the current study revealed that upstream location, exceed the performance of the trailing edge location on a NACA 4424 wing. A 2% height Gurney flap at 85% chord provided the highest performance in the range of -4 degrees to +4 degrees angle of attack. In terms of the wing operational range extension, a 2% Gurney flap at 95% was outstanding since the wing remained operational while all other wings including the baseline wing stalled at 10.5 m/s freestream velocity. The velocity profile study investigated the flow structure induced by the test flaps. The study revealed that variations in relative U velocity induced by the Gurney flap cause the deviation of the ΔC_L variations. This study also revealed that the downstream flow from the trailing edge is deflected by forward flap configurations but not deflected by the trailing edge flap thus these three wing performances exceeded that of the 100% chord flap.

All results point to the higher performance capability of upstream flaps. These results make these flap applications more realistic since the locations provide better structural volume to store of a deployable flap.

2.7 Reference

[1] Zaparka, E.F., "Aircraft and Control Thereof," U.S. Patent No. 19,412, January, 1935.

[2] Lieback, R.H., "Design of Subsonic Airfoils for high Lift," *Journal of Aircraft*, Vol. 15, No. 9, 1978, pp. 547-561

[3] Jeffrey, D.R.M., "Aerodynamics of the Gurney Flap," AIAA 96-2418, June, 1996.

[4] Cavanaugh, M.A, Robertson, P., and Mason, W.H., "Wind Tunnel Test of Gurney Flap and T-Strips on an NACA 23012 Wing," 25th AIAA Applied Aerodynamics Conference, 25-28 June 2007, Miami, FL, USA

[5] Meyaer, R., Hage, W., Bechert, D.W., Schatz, M., and Thiele, F., "Drag Reduction on Gurney Flaps by Three-Dimensional Modifications," *Journal of Aircraft*, Vol. 43, No. 1, Jan.-Feb., 2006, pp. 132-140

[6] Yen Nakafuji, D.T., van Dam, C.P., Smith, R.L and Collins, S.D., "Active Load Control for Airfoils using Microtabs," Journal of Solar Energy Engineering, Vol. 123, No. 4, Nov. 2001, pp. 282-289

[7] Chow, R., and van Dam, C.P., "Computational Investigation of Deploying Load Control Microtabs on a Wind Turbine Airfoil," AIAA-2007-1018, Jan. 2007

[8] Baker, J.P., Standish, K.J., and can Dam, C.P., "Two-Dimensional Wind Tunnel and Computational Investigation of a Microtab Modified airfoil," *Journal of Aircraft*, Vol. 44, No. 2, March-April, 1978, pp. 563-572

[9] Liu,T., Monefort, Liu, W.W., Pantula, S.R., and Shames, Q.A., "Static Extended Trailing Edge for Lift Enhancement: Experimental and Computational Studies," 3rd International Symposium on Integrating CFD and Experiments in Aerodynamics, 20-21 June 2007, Co, USA

CHAPTER 3

Development and Testing of a New Plasma "Gurney Flap" for Lift Enhancement

Shinya Ueno, Njuki W. Mureithi, and Huu Duc Vo,

École Polytechnique de Montréal,
Montréal, Québec H3T 1J4, Canada

3.1 Abstract

A plasma Gurney flap has been newly developed and tested in a low speed wind tunnel at up to 16 m/s freestream velocity. The plasma Gurney flap was installed on a NACA 4424 airfoil of 260mm chord length and 400mm wing span. The performance of the plasma Gurney flap at 0 degrees angle of attack was investigated and compared with the original profile as well as with a 1% and a 2% height physical Gurney flap. Force measurements and PIV flow visualization were conducted at Reynolds numbers ranging from 1.2×10^5 to 3.0×10^5. The two SDBD plasma actuators comprising the plasma Gurney flap were installed respectively, on the suction side and the on pressure side of the trailing edge. The two actuators were activated independently of simultaneously in the plasma Gurney flap configuration. The tests revealed that each actuator individually contributes to the lift enhancement by nearly equal proportions thus the combination of the two actuators performed twice as well as a single actuator. The PIV tests provided the downstream relative flow structure induced by the Gurney flap. Although the magnitude of the effect is smaller than the physical Gurney flaps, the plasma Gurney flap induces similar flow structure thus increasing lift. While the lift improvement by the physical Gurney flaps is mainly due to the flow retardation on the pressure side, the lift enhancement of the plasma Gurney flap is mainly caused by the suction side flow acceleration. Because of these characteristic, the plasma Gurney flap is also able to contribute to wing operational range extension in the lower freestream velocity regime. While the original and the 1% Gurney flap wing stalled at 4.6 m/s freestream velocity, the 2% Gurney flap and the plasma Gurney flap wings remained within the wing operational ranges. The ΔC_L measured in the tests ranges 0.02

to 0.18, depending on the freestream velocity and the power applied to the plasma actuators. The proposed plasma Gurney flap is configured to combine the effects of two actuators of comparable performance. The set up can therefore generate approximately double the lift improvement of any other single plasma actuator configuration.

3.2. Introduction

An aircraft requires variable lift during flight. To meet this requirement, all aircraft are equipped with flow control surfaces for low drag and high lift during takeoff, high drag and high lift during landing, and low drag and moderate lift when cruising. The high lift devices, known as slats and flaps were manually operated via cables in early airplanes and modern day smaller aircraft. Larger aircraft are equipped with hydraulic or electric actuators to drive these control surfaces. To improve flight efficiency, these devices must be stored in cruising conditions in order not to induce additional drag. However, because of structural mechanism limitations, gaps between the movable surfaces cannot be eliminated or covered perfectly. A high tolerance design of these control surfaces increases manufacturing and maintenance costs therefore non-mechanical approaches have been considered.

Although ideas of surface flow control or active flow control were proposed in the early aviation history, many of these ideas were not realistic since the system requirements were mechanically complex or dependent on external pressure or suction sources. The main flow control ideas involved adding mass flow to the local boundary layer to induce a global flow effect.

One approach was a moving surface which replaced the wing leading edge curved surface by a rotating circular cylinder along the wing span. In this idea, by the cylinder rotation, a shear force is introduced in the boundary layer accelerating the flow at the leading edge. Another idea was surface suction. The surface suction system is equipped with several suction orifices to minimize the boundary layer thus controlling flow separation. Another example is surface blowing which adds high momentum flow to the boundary layer. Control of flow separation is achieved by a wall jet from a high pressure flow source. This system is not realistic since an onboard high pressure flow source is necessary.

For realistic applications, a principle similar to surface blowing is employed using leading edge and trailing edge flaps. The system works by bleeding flow from the airfoil pressure side to add momentum and delay flow separation.

The Gurney flap is a rectangular plate located on the pressure side at the trailing edge of an airfoil. It is known as a simple and effective high lift device. The earliest concept of the Gurney flap was patented by Zaparka [1] in 1935 as a variation of split flaps. This flap was known in the 1960s as an application for racing car wings by Daniel Gurney. The goal was to obtain additional downward force to improve the traction. Lieback [2] introduced the idea in aeronautical applications in 1978.

Jeffrey [3] showed that the lift improvement of the Gurney flap is obtained by increasing circulation, a combination effect of vortex shedding behind the Gurney flap and flow retardation in front of the Gurney flap.

Bechert *et al*. [4] and Mayer *et al*. [5] tested the Gurney flap with several modifications to verify 3D effects. Slits, circular holes, rectangular holes and a unique 3D structure, similar to the detailed structure of dragonfly wings, were tested in a wind tunnel. These 3D modifications maintained similar lift and resulted in drag reduction.

Traub and Agarwal [6] combined the concept of the Gurney Flap and the jet flap. The authors intended to use the Gurney/jet flap for Unmanned Aerial Vehicle (UAV) lateral control. Variable lift and pitch moments were created by controlling the blowing jet supplied from an external high pressure source.

Shea and Smith [7] applied a synthetic jet at 92% and 95% chord locations. With a combination of synthetic jets, lift increase of up to 10% was achieved. Their experiments showed that a jet at the 95% chord location performed better than one at 92% chord.

Gurney flaps have also found their way into wind turbine applications where they are known as trailing edge microtabs.

The distribution of natural wind is unsteady thus controlling flaps or blade pitches are conventional methods for blade load control for wind turbines. These devices, however, result in heavy wind turbine designs. The required rigid foundation and support structure increase

construction costs therefore these requirements limit the location flexibility. A light weight, non-mechanical approach for wind turbine blade load control could be highly advantageous.

Yen Nakafuji *et al* [8] embedded deployable microtabs on the pressure side at 95% chord location from the leading edge for dynamic lift control. Their computations on a GU25-5(11)-8 airfoil showed that the 95% chord had the best performance. The location is realistic for practical application since a forward location from the trailing edge makes it possible to store the mechanical systems of the deployable microtabs.

The microtabs at the trailing edge location performed better than at a 95% chord on a S809 airfoil in simulations made by Baker *et al*. [9]. The simulations showed that C_L with trailing edge tabs was higher than in the case of 95% and 90% chord tabs, however, the 95% case still exceeded the baseline. These studies implied that the optimal Gurney flap location depends on the airfoil profile.

The plasma actuators are one potential method as a non-mechanical and light weight solution. The Plasma actuator was first reported in the mid 1990s. In the early days, the device was known for its boundary layer control capability. Later, the Plasma actuator was introduced into airfoil applications which had received little attention. Liu *et al*. [10] focused on the plasma actuator for aeronautical applications. Roth *et al*. [11] evaluated several dielectric materials, for aeronautical applications, which are able to induce higher jets while minimizing weight.

The plasma actuator airfoil application is feasible for Unmanned Aerial Vehicles (UAVs) applications because the device is simple, light weight and has wider flexibility in its installation. Santhanakrishnan *et al*. [12] considered the plasma actuators as an alternative flow control device for lightweight UAVs. Their tests showed approximately 60% positive and 30% negative shift on the lift curve by controlling the tip vortex created by the plasma actuator. Nelson *et al*. [13] installed the plasma actuator on the leading edge for UAV roll control. Their tests indicated an excellent roll control performance up to 35 degrees angle of attack.

Zhang *et al*. [14] simulated the plasma actuator installed at the trailing edge of a NACA 0012 airfoil. In their simulations, the plasma actuator was installed on the vertical surface of the trailing edge to generate a downward wall jet. They assumed the height of the trailing edge vertical surface as the Gurney flap height. They obtained similar lift change as for a physical

Gurney flap by Lee [15]. The simulations show lift to drag ratio improvement. The ΔC_L improved by approximately 0.2 in the linear section of the lift curve.

3.3. Experimental Facilities

3.3.1 SDBD Plasma Actuator

The single dielectric barrier discharge (SDBD) plasma actuator is composed of two electrodes separated by a dielectric material. By applying a high-frequency and high-voltage AC signal, a strong electric field is created. The field ionizes the surrounding air and forms a plasma. The ionized air accelerated by the electric field induces body force near the actuator. This approach is therefore physically different from conventional pneumatic devices which add mass flow.

There are three configurations for the location of the two electrodes, the upper overlapping design, the gapless design and the variable gap design [11]. Several materials were tested to find feasible choices for aeronautical applications [11]. The tests revealed that the Kapton stands out by having a better power to weight ratio [11].

The experiments in this paper were conducted with the gap less design using three layers of 0.2 mil (=0.2/1000 inch) Kapton tape as the dielectric material and one layer of 0.18mm aluminum-tined copper tape as the electrode material. The typical value of the excitation voltage was $25kV_{p-p}$. The actuation frequency was 6.0 kHz.

3.3.2 Wind Tunnel

Tests were conducted in a closed loop wind tunnel equipped with a test section of 0.61m by 0.61m, with a length of 2.4m and fitted with transparent optical windows. The wind tunnel temperature can be controlled to within 1 Celsius degree. Honeycomb screens installed upstream of the test section reduce the flow turbulence intensity to below 0.3%. Velocities were computed from the dynamic pressure measured by a DWYER INSTRUMENT, INC. Series 616 Differential Pressure Transmitter with a resolution of 0.001 in.W.C., equivalent to 0.2499 Pa.

3.3.3 Particle Image Velocimetry (PIV)

PIV is a flow visualization method that uses oil particles as tracers and measures the displacement of the particles thus displacement vector fields can be computed. The calibrated PIV system provides velocity information, from which streamlines and vorticity contours are computed.

Relative velocity vector fields were used in this study to analyze the detailed flow structure change from the baseline configuration. The relative velocity vector fields were computed by taking the averaged velocity vector field of given test configurations and subtracting from the averaged velocity vector fields of the baseline, obtained at the same freestream velocity conditions. This approach revealed how a micro change in the boundary induces a macro effect in the ambient flow structure.

3.3.4 Force Measurement System

The force measurement system is located beneath the test section. The system is composed of two force balances to measure two components of the force generated by the airfoil. The resolutions of the two force balances are 4.89×10^{-03}[N], and 9.78×10^{-03}[N], which are 0.3% and 0.9% of the maximum force measured in the test. The system was validated before the tests.

3.4 Plasma Gurney Flap PIV Flow Visualization Results

3.4.1 Plasma Gurney Flap Concept

One of the advantages of the Gurney flap is the relatively large effect obtained by a simple device. The lift enhancement generated by a Gurney Flap of adequate height is nearly equivalent to modern complex flaps. But at the same time, installing a Gurney flap at the trailing edge cannot be a way to replace the conventional flap system since an aircraft requires variable lift and drag during flight. Although adjusting the Gurney flap height provides variable lift, the mechanical system for the variable Gurney flap is still too complex.

The concept of the plasma “Gurney flap”, shown in Figure 3.1, involves replacing the physical structure of the Gurney flap by plasma actuators, which should keep the same flow structure and generate the same performance of the lift enhancement.

The suction side plasma actuator is expected to move or to eliminate the separation bubble, which forms near the trailing edge, and to increase flow curvature via the angled wall jet induced by the plasma actuator. These phenomena are intended to replace the circulation behind the physical Gurney flap.

The pressure side plasma actuator is intended to induce a spanwise vortex to decrease the pressure side flow thus raising the pressure.

The combined effect of these two actuators is increase effective camber and results in lift enhancement.

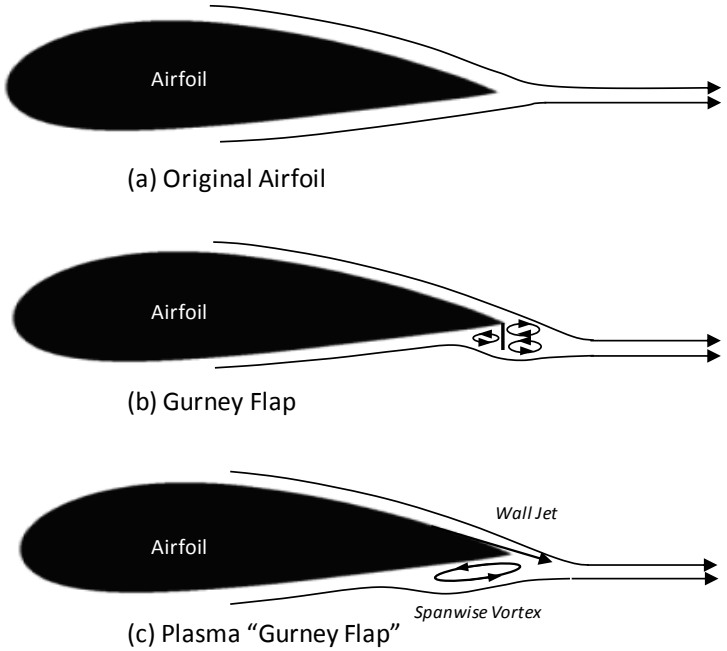

Figure 3.1 Plasma “Gurney Flap” Concept

3.4.2 Plasma Actuator Reverse Flow Test Results

The pressure side plasma actuator component of the plasma Gurney flap was tested to visualize the flow structure of the induced spanwise vortex. The plasma actuator was installed on a plate and the assembly was rigidly fixed on the wind tunnel floor. A schematic illustration of the setup geometry is shown in Figure 3.2.

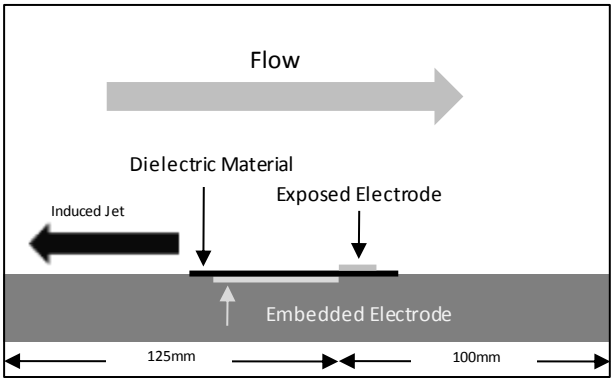

Figure 3.2 Plasma Actuator Reverse Flow Test Camera View

Two freestream velocities, 2.0 m/s and 13.3 m/s, were tested in addition to the zero flow condition. In each condition, an averaged velocity vector field was computed from 30 consecutive PIV images recorded at 15Hz with and without actuation. At 2.0m/s and 13.3m/s freestream conditions, to analyze the flow delay, the relative velocity vector fields were calculated by subtracting averaged velocity vector fields for the non-actuated cases from averaged vector fields obtained with actuation at the corresponding velocity. Vorticity and velocity contours were then generated from the relative velocity vector fields.

The relative velocity vector fields are shown in Figure 3.3(a), (c) and (e). The relative velocity contours are presented in Figure 3.3(b), (d) and (f). The left upper region in the figures is blank because of a shadow of a window frame which resulted the loss of flow information.

The results of the zero flow condition are shown in Figure 3.3(a) and (b). Unfortunately, the wall jet induced by the plasma actuator could not be recorded due to the strong laser reflection on the plate surface which masked particle image information. The existence of the wall jet is, however, implied by the ambient suction flow from the downstream region of the plasma actuator, presented in the Figure 3.3(a). Although this actuator geometry induces a “reverse” flow above the actuator, the spanwise vortex does not form since we have a zero upstream

flow condition. Another counter spanwise vortex was observed at the back end of the plasma actuator in Figure 3.3(a). A schematic illustration of the minor induced jet is presented in Figure 3.4. The vortex was induced by the two counter flows, the minor jet and the flow above the minor jet induced by the major wall jet suction effect. The induced minor jet was clearly observed in PIV tests. However, the plasma generating the minor jet was not visible, as shown in Figure 3.5. The photo in Figure 3.5 shows the activated plasma actuator used in this work. The minor jet is located at the edge of the exposed electrode away from the embedded electrode. On the velocity contours in Figure 3.3(b), the highest velocity recorded in this measurement was up to 0.18 m/s in the plasma region. The second fastest flow is near the wall at the downstream side of the plasma actuator and is a part of the minor induced jet.

There are few publications discussing backward flow induced by the plasma actuator. Santhanakrishman and Jacob [15] recorded the vortex behind the major wall jet in their PIV measurements. Jayarawan *et al*. [16] developed a mathematical model of the plasma actuator. In their simulations, a minor wall jet was induced on the side of the embedded electrode because of the existence of an electric field near the electrode's side away from the embedded electrode.

The flow field shown in Figure 3.3(c) is obtained at 2.0 m/s freestream velocity. The flow structure in this configuration is not similar to the zero flow conditions. Because of the existence of the freestream flow, the suction flow caused by the wall jet can only occur in the downstream region of relatively slow flow in the near wall region. The effect appears as a flow velocity decrease of up to 1.13 m/s, shown in Figure 3.3(d). The spanwise vortex exists as a circulation above the plasma actuator.

The result for the fastest ambient flow condition, 13.3 m/s freestream velocity, are shown in Figure 3.3(e) and (f). The phenomenon is not a simple spanwise vortex generation but multiple vortexes were induced. A part of the induced wall jet is recorded on the relative velocity vector field, in Figure 3.3(e). At the tip of the wall jet, the flow separated from the wall thus forming a spanwise vortex. The fastest relative flow velocity recorded in the measurements was 0.45 m/s, shown on the relative velocity contours in the Figure 3.3(f). This speed occurs within the core flow of a vortex, separated from the spanwise vortex generated by the induced wall jet.

These tests imply that in the spanwise vortex generation, the maximum velocity induced by the plasma actuator in the zero flow conditions is not the maximum velocity. Faster flows were measured at freestream conditions.

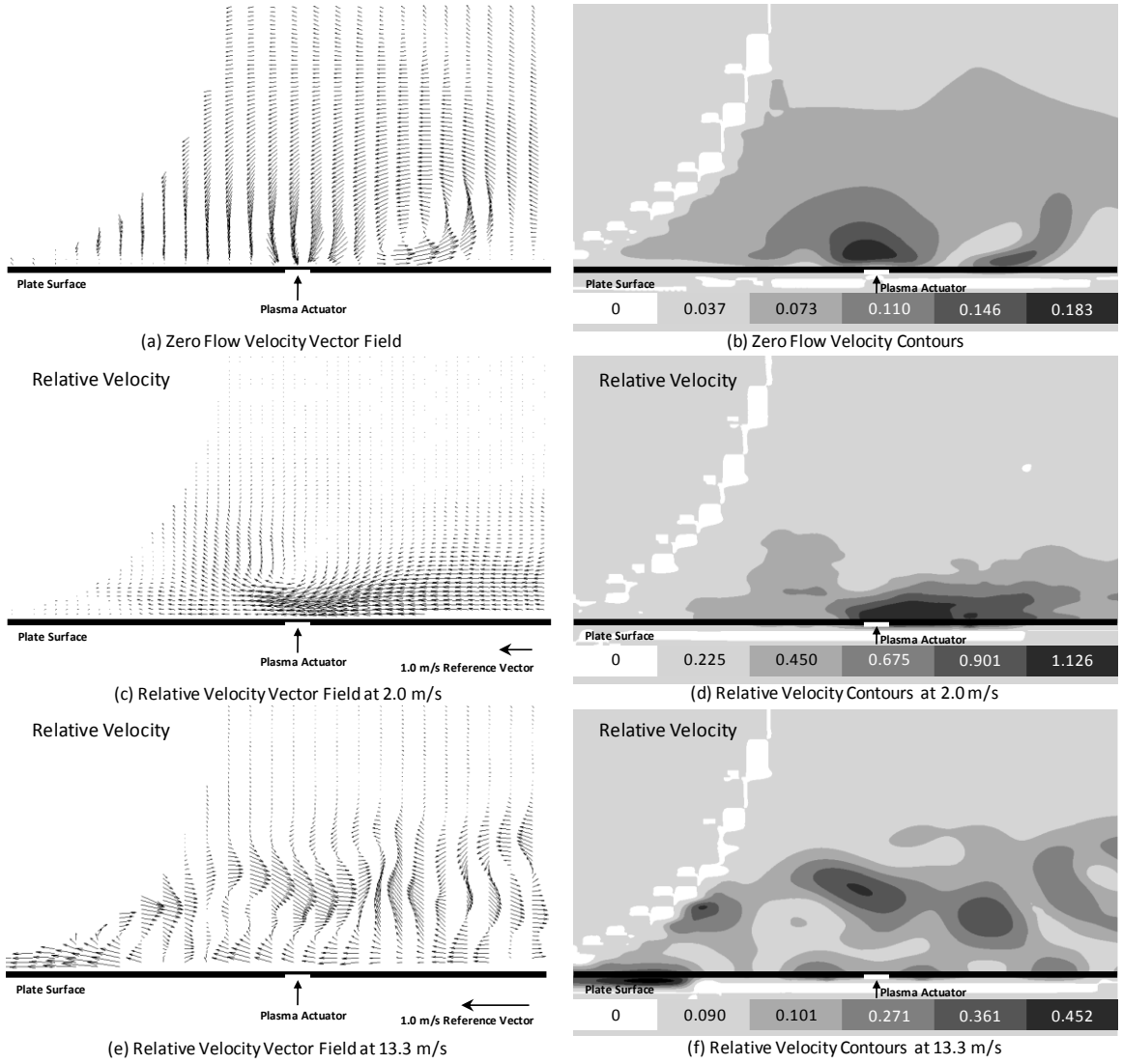

Figure 3.3 Relative Velocity Vector Fields superimposed on Vorticity Contours (a), (c), (e) and Relative Velocity Contours (b), (d), (f)

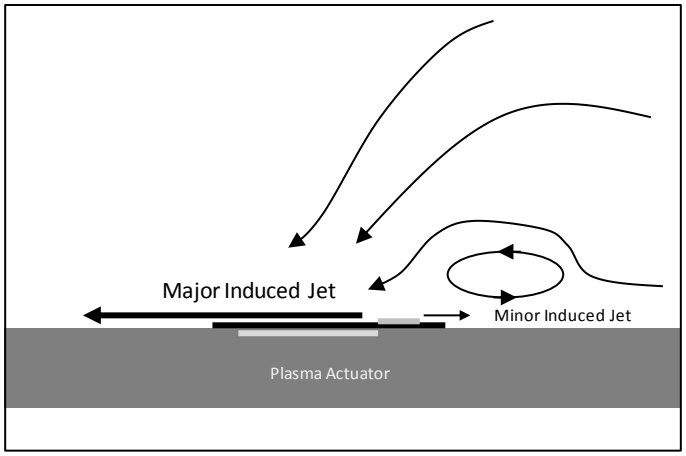

Figure 3.4 Minor Induced Jet and Vortex

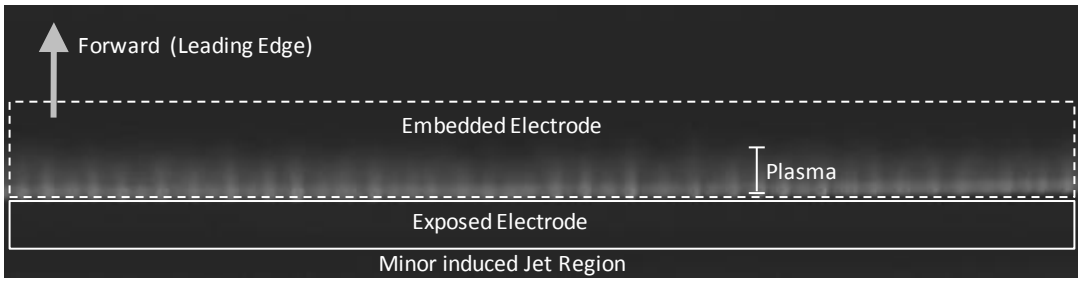

Figure 3.5 Activating Plasma Actuator Photo with Electrode Arrangement Illustration

3.4.3 Plasma Gurney Flap Component Tests

The flow structure induced by the components of the plasma Gurney flap was also visualized using PIV. A NACA 4424 wing profile was selected because of its thickness. The thicker profile provides adequate structural volume for the actuator cable arrangement and proper distance between the two actuators to avoid electrical discharge. The wing used for the PIV tests had a 26cm chord and a 60cm span which fit the 61cm width of the wind tunnel test section. The wing was installed the pressure side up to allow PIV flow visualization on the pressure side. A schematic illustration of the wing setup and of the camera view field is shown in Figure 3.6(a). During the tests at zero freestream flow, the actuators were initially activated individually before the double activation of the plasma Gurney flap configuration. The same process was repeated at freestream velocity of 8.0 m/s. Velocity vector fields were analyzed with the same

post processes to compute a relative velocity vector fields from a pair of averaged vector fields with and without actuation by subtracting the latter from the former.

The actuator configuration is shown in Figure 3.6(b). The suction side plasma actuator was installed at approximately 90% chord from the leading edge. The pressure side actuator was located at 95% chord from the leading edge.

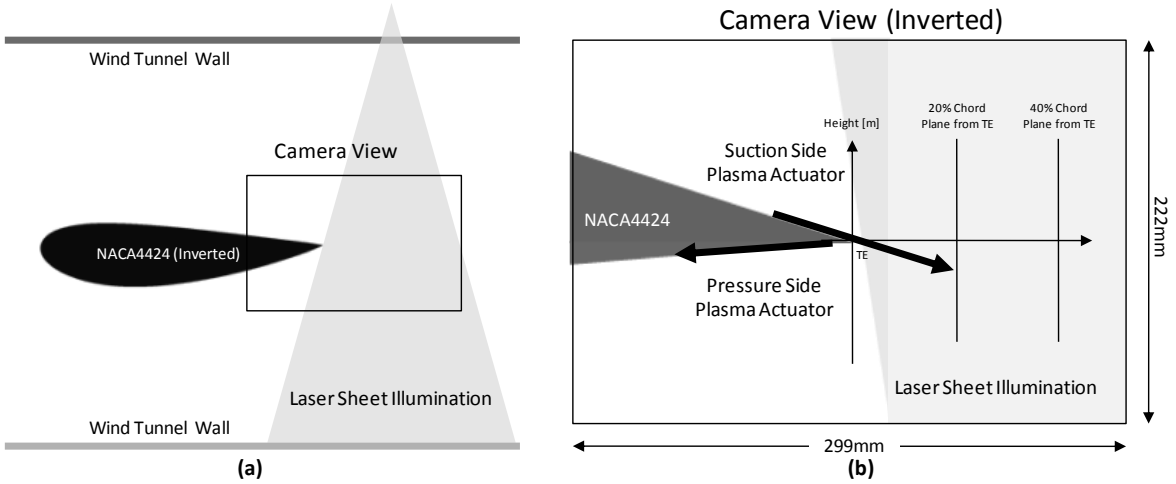

Figure 3.6 Test Setup Geometry (a) and Camera View Field Showing Two Planes for Velocity Profile Study (b)

Since the wall jet induced by the pressure side plasma actuator was outside of the range of the laser illumination, the wall jet could not be visualized. However, the ambient suction flow could be clearly observed as shown in the Figure 3.7(a).

The wall jet was observed on the suction side plasma actuator activation at zero flow conditions, as shown in Figure 3.7(b). A straight core stream was generated which had a velocty of up to 0.75m/s.

The resulting flow with combined actuatation of the plasma Gurney flap is shown in Figure 3.7(c). Although the observed phenomenon is a wall jet induced by the suction side plasma actuator, the effect of the pressure side plasama actuator is observed as an increase the twist of the wall jet of the suction side plasama actuator. Thus the effective camber is increased, as presented in Figure 3.7(c).

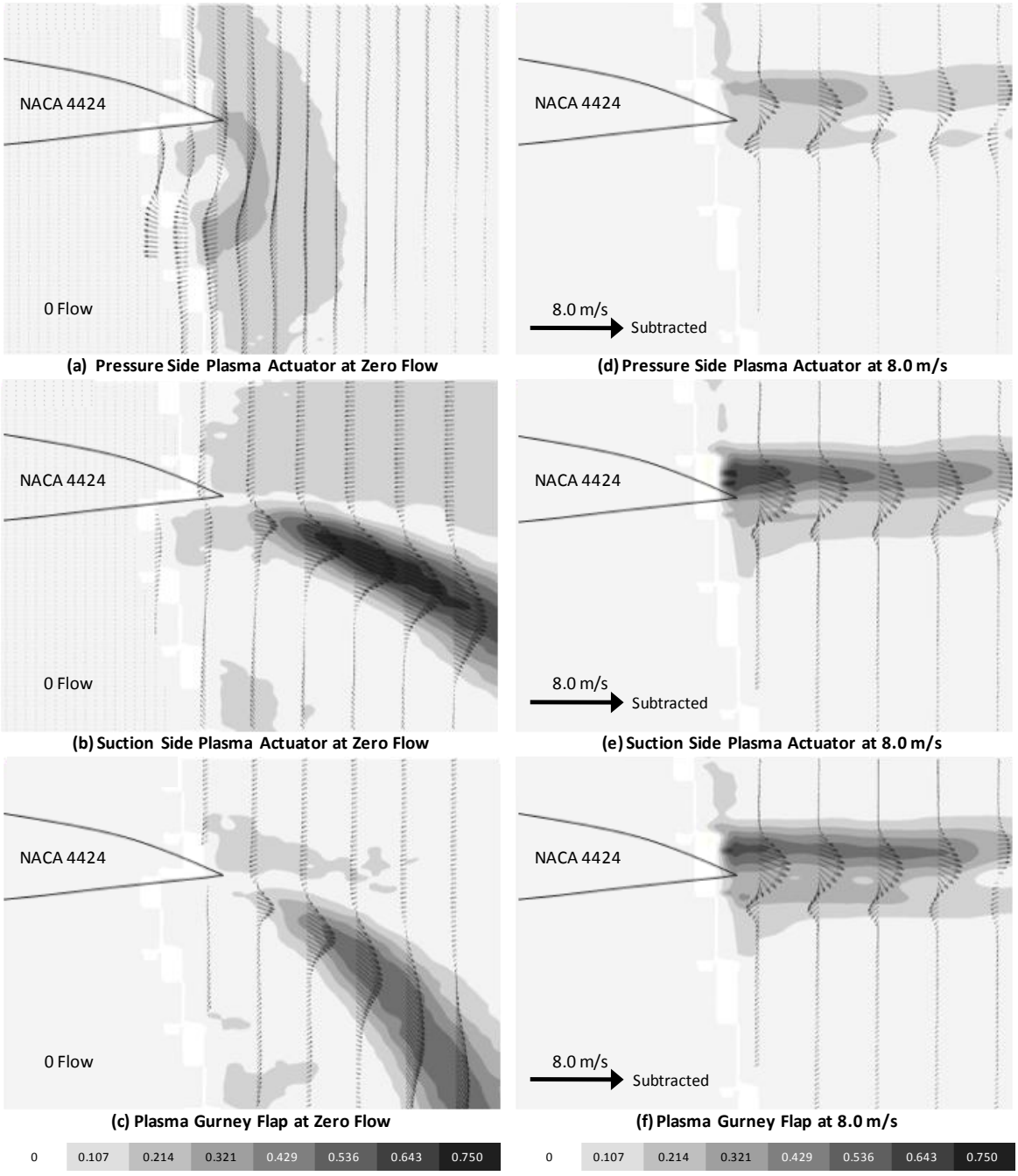

Figure 3.7 Velocity Vector Field for Zero flow conditions (a)-(c) and Relative Velocity Vector Field at 8.0 m/s (e)-(f)

A velocity profile study was conducted at two planes located at 20% and at 40% chord downstream from the trailing edge, as shown schematiclly in Figure 3.6(b). The velocity profiles provided in Figure 3.8 and Figure 3.9 are U velocity components for each measurement plane shown in Figure 3.6(b) at zero flow conditions and at a freestream velocity of 8.0 m/s. The data

was exported from the averaged velocity vector fields for zero flow conditions and the relative velocity vector fields for a freestream velocity of 8.0 m/s are shown in Figure 3.8 and Figure 3.9, respectively.

At zero flow conditions, the suction effect of the pressure side actuator is wide and weak, hence the U velocity profile of at the 20% and 40% chord downstream location shows nearly no flow, as presented in Figure 3.8(a).

A shift in the U velocity peak height at the 20% and the 40% chord downstream planes was observed for the suction side actuator activation, as shown in Figure 3.8(b). The U velocity peak heights of the two planes were shifted from -0.017m to -0.039m. From this result the angle of the wall jet was calculated to be 23 degrees deflected from the freestream direction.

For the plasma Gurney flap configuration, a combined effect of the two actuators was observed. The peak U velocities are nearly equal in the two planes, however, deflection is increased. A deflection angle of 35 degrees was computed from the peak shift of the U velocity. This result implies that because of the suction flow on the pressure side, the flow deflection is increased and thus the effective camber of the wing is enhanced.

At the freestream velocity of 8.0m/s, Figure 3.9, the shift of the U velocity peak was not as significant as at the zero flow conditions.

The flow deflection was not observed for the pressure side actuator activation, as seen in Figure 3.9(a). The actuator retarded the pressure side flow by up to 0.2m/s.

The flow is slightly shifted for the suction side actuator activation, as shown in Figure 3.9(b). The flow increase on the suction side is more significant than that of the pressure side.

The combined actuation of the plasma Gurney flap showed similar flow structure to that of the suction side actuation, as shown in Figure 3.9(c). The U velocity peak on the pressure side is nearly equivalent to that of the suction side actuation. While the suction side actuator induced velocity reduction was 0.18m/s, the reduction maximum U velocity on the plasma Gurney flap was 0.20m/s. The actuator improves the airfoil circulation and enhanced lift.

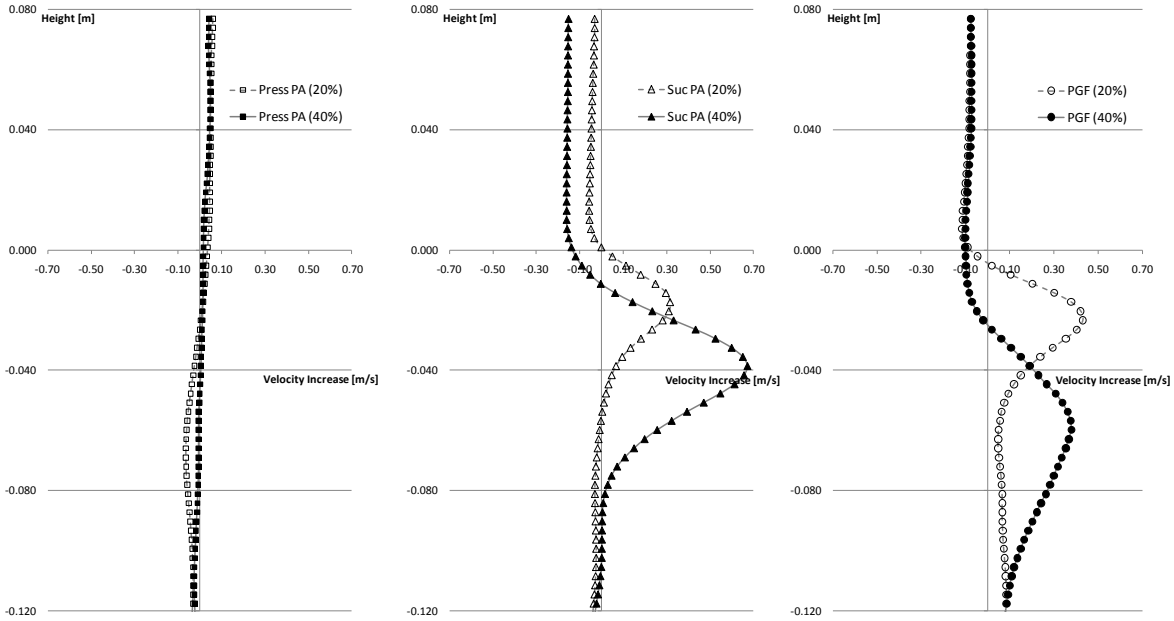

(a) Pressure Side Plasma Actuator **(b)** Suction Side Plasma Actuator **(c)** Plasma Gurney Flap

Figure 3.8 Velocity Profiles of 20% & 40% Locations in Zero flow conditions

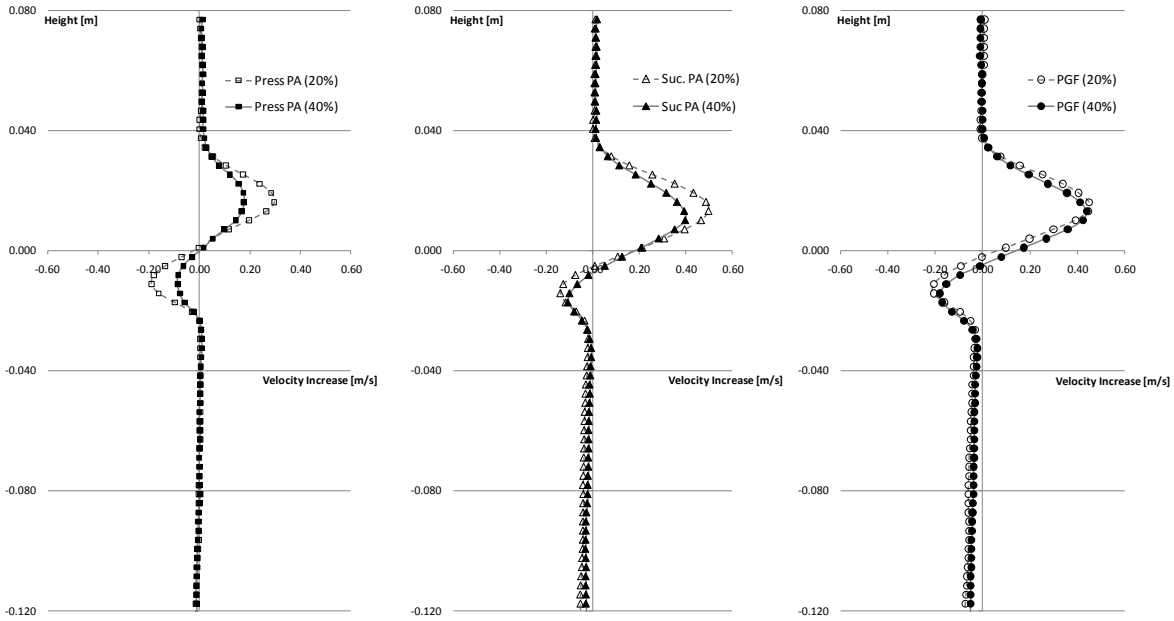

(a) Pressure Side Plasma Actuator **(b)** Suction Side PA Plasma Actuator **(c)** Plasma Gurney Flap

Figure 3.9 Relative Velocity Profiles of 20% and 40% locations at 8.0 m/s

3.5 Force Measurements

3.5.1 Plasma Gurney Flap Component Study

Force measurements were conducted to verify the lift improvement of a single plasma actuator as well as double actuation of the plasma Gurney flap. The tests were conducted in the wind tunnel at Reynolds numbers ranging from $1.0X10^5$ to $2.6X10^5$ corresponding to freestream velocities ranging from 6.0 m/s to 16.0 m/s.

The tests revealed that activation of each single plasma actuator contributes nearly equal proportions to ΔC_L. The ΔC_L obtained by the double actuation of the plasma Gurney flap shows good agreement with the sum of the ΔC_L by the two single actuations except for freestream velocities between 8.0 m/s and 12.0 m/s, corresponding to the Reynolds numbers $1.2X10^5 <Re<1.9X10^5$ in Figure 3.10. This result implies that the activation effect is linear and the two actuators contribute equally in terms of ΔC_L.

The plasma actuator installed on the suction side trailing edge is reported as the plasma flap by He and Corke [18]. They tested a 90% chord plasma actuator on the suction side trailing edge. The actuator was installed on a NACA 0015 airfoil and tested at a 21 m/s freestream velocity in a wind tunnel. The plasma actuator was comprised of two layers of 4mil Kapton tape and operated at a voltage of $7kVP_{-P}$ in steady actuation. The measured ΔC_L was 0.051 at $Re=1.8X10^5$. This result, plotted in Figure 3.10, was 46% greater than the linear interpolated value of the same configuration, the suction side plasma actuator in this work. The ΔC_L of the plasma Gurney flap is approximately 50% greater than the result of He and Corke [18], as seen in Figure 3.10.

Because the two studies did not provide information in the force generated by the plasma actuator, the two results are not easily comparable. However, the advantage of the new plasma Gurney flap is to combine the two single plasma actuator characteristics for lift enhancement thus the plasma Gurney flap is potentially superior to any single actuator configuration in airfoil applications.

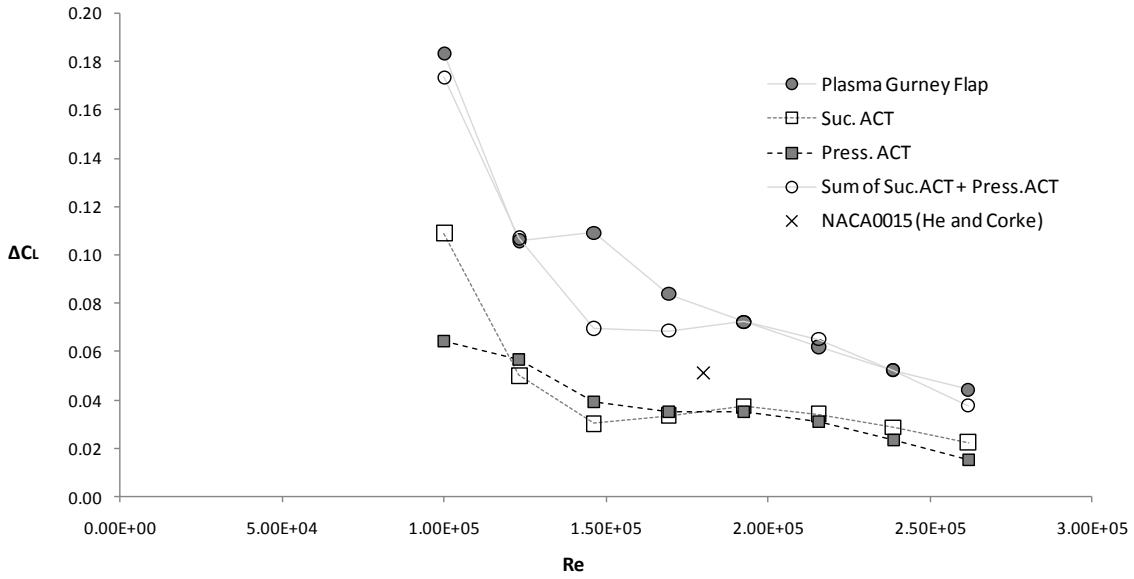

Figure 3.10 Experimental Results of Plasma Actuator Trailing Edge Applications

3.5.2 Plasma Actuator Power Study

The generation of force is governed by ion density, plasma volume and the applied electric field [19] thus the output power of the plasma actuator is dependent on the power input. The two configurations in Table 3.1 were tested in this section to verify the effect of the input power change.

In the dual power supply setup, in Table 3.1, a power supply was connected to each plasma actuator independently. In this case, because the power was supplied to the two plasma actuators individually, the total power supplied was twice of each element. The typical values of the voltage and current were 35.6V and 2.3A and that was the output of the power supply.

In the single power supply setup, in Table 3.1, a single power supply was connected to the two plasma actuators. The typical value of the voltage and current was 35.7V and 3.9A and that was the output of the power supply.

Table 3.1 Input Power Configurations

Case	Configuration	Unit Power [W]	Total Power [W]	ΔPower [%]
Dual Power Supply	Power Supply x2	81.9	163.8	18
Single Power Supply	Power Supply x1	139.2	139.2	-

The results of the two cases in Table 3.1 are shown in Figure 3.11. The mathematically doubled values of the single power supply result are plotted as empty squares. The results show good agreement between the dual power supply setups; thus doubling the supplied power leads to a doubling of the lift increase ΔC_L.

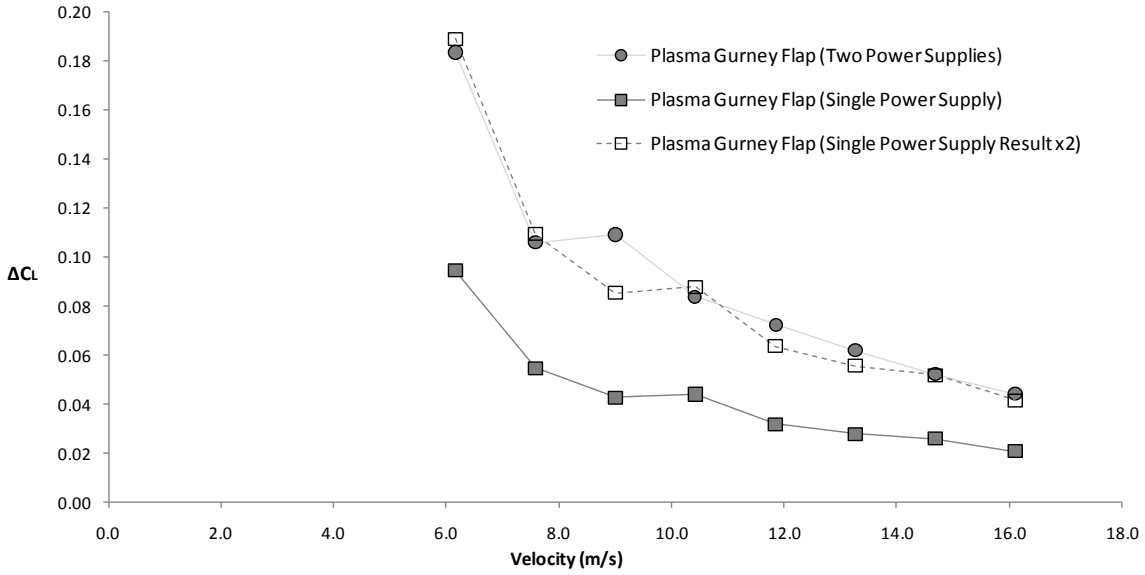

Figure 3.11 Plasma Gurney Flap Power Study Results

3.6 Plasma Gurney Flap Flow Structure Study

3.6.1 Plasma Gurney Flap Global Effect Study

PIV tests were conducted to visualize the plasma Gurney flap global effect for three different freestream velocities. A laser sheet introduced downstream illuminated the two surfaces of the wing. The top and the bottom regions of the camera view field were not covered by the laser illumination, as shown in Figure 3.12. In thes tests, the power applied to the two actuators was generated by single power supply. The typical output value of the power supply was 35.5V and 3.8A.

An expected phenomenon was two streets of velocity change which is comprised of relatively faster flow on the suction side and relatively slower flow on the pressure side. From the

previous relative velocity profile study in Figure 3.9(c), the peak of the velocity change is estimated the be nearly parallel to the freestream flow direction.

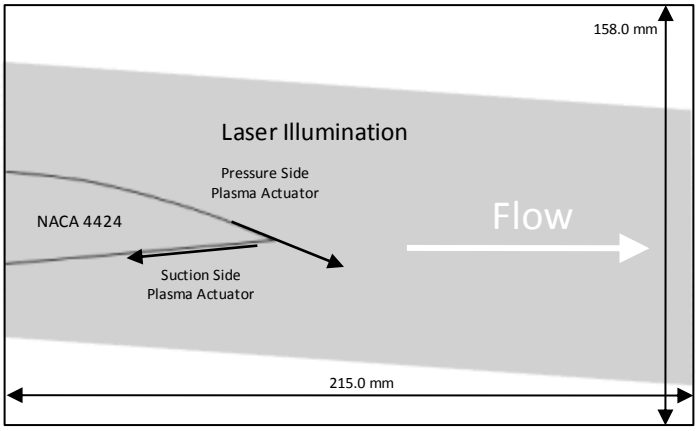

Figure 3.12 Camera View Field for Global Effect Study

Relative velocity vector fields were computed from this PIV test. The relative velocity vector fields are shown in Figure 3.13(a), (b) and (c). The relative velocity contours are presented in Figure 3.13(d), (e) and (f).

The two streets of varying velocity regions are observed in the results shown in Figure 3.13. The phenomenon is clearly visible for 6.0 m/s and 7.4 m/s freestream velocities, Figure 3.13(d) and (e). The streets of velocity change are less clearly defined at 8.7 m/s, as presented in Figure 3.13(f).

In the relative velocity vector fields in Figure 3.13(a)-(c), velocity decreases on the pressure side while it increases on the suction side. These effects are induced by the retardation effect by the spanwise vortex on the pressure side and the acceleration by the wall jet on the suction side. As a result, the circulation on the wing is increased and the lift enhanced.

On the pressure side, flow retardation is widely distributed in the pressure side cascade while flow retardation in the downstream region has a relatively narrower distribution.

On the suction side, the distribution of the accelerated flow is narrower thus most of the relative flow velocity change occurs near the surface of the suction side. These results can be explained as follows, the suction side plasma actuator accelerates the flow near the wall which has a relatively low velocity thus significant acceleration is seen on the relative velocity vector fields.

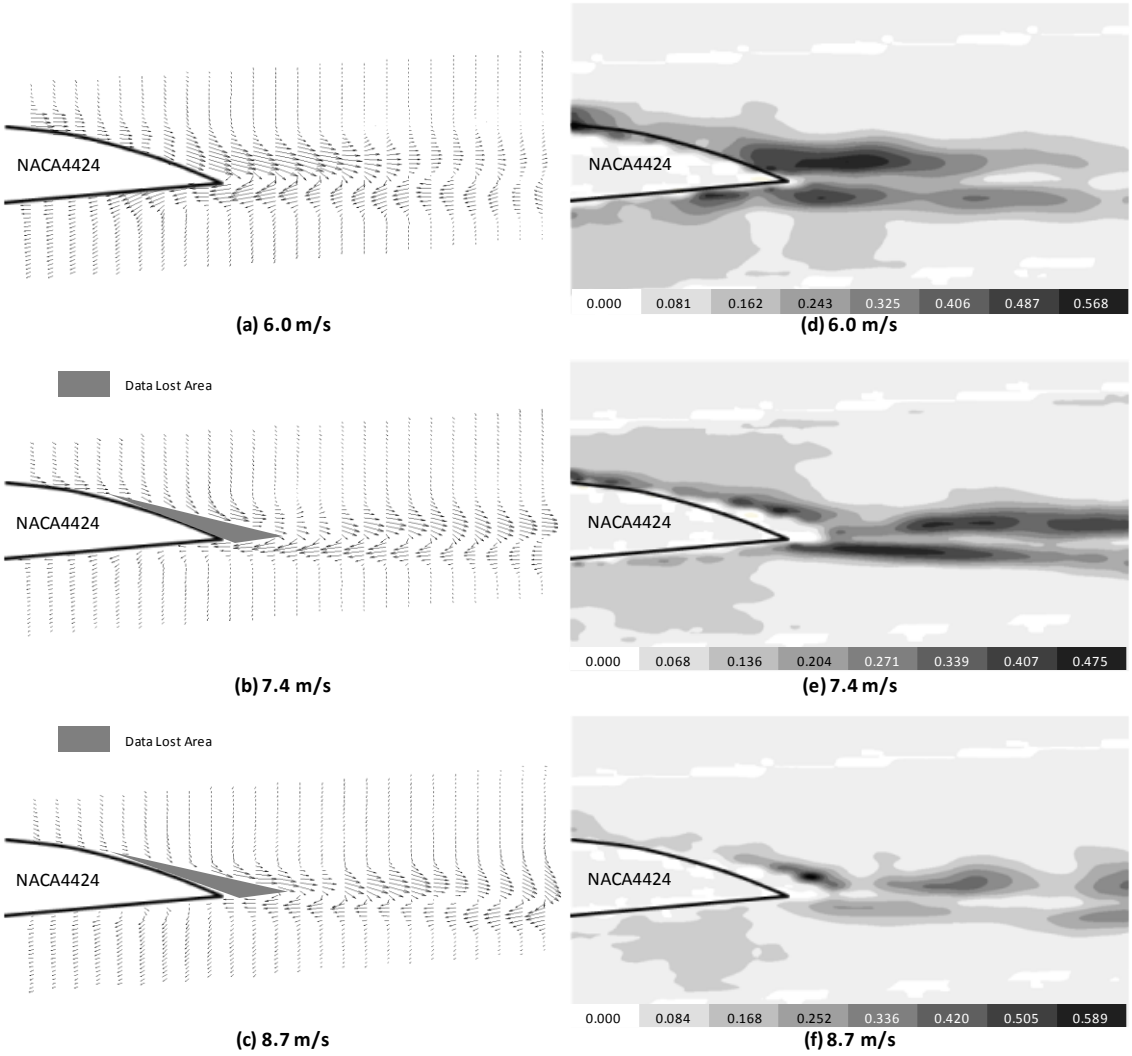

Figure 3.13 Relative Velocity Vector Fields (a)-(c) and Relative Velocity Contours (d)-(f)

3.6.2 Detailed Flow Structure Study

The PIV tests showed a local flow decrease in the downstream region and a global flow decrease on the airfoil pressure side cascade. Although the spanwise vortex is not visualized in the previous tests, the flow structure implies the existence of the spanwise vortex. A illustration of the spanwise vortex which is expected from the downstream and upstream flow structure is schematically shown in Figure 3.14. A detailed flow study was conducted next to observe the spanwise vortex in detail.

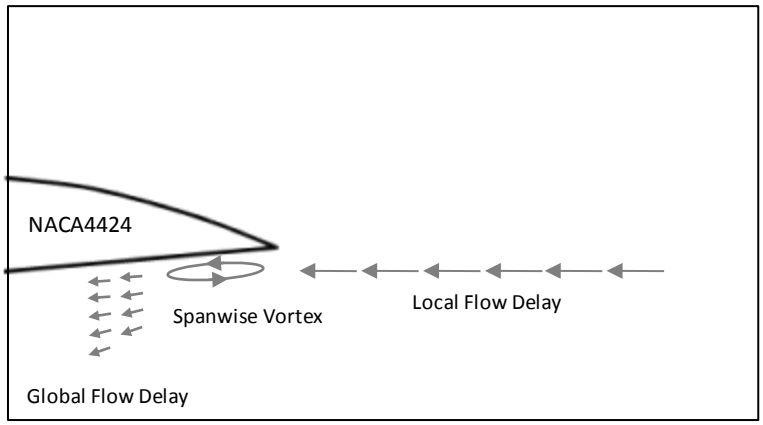

Figure 3.14 Spanwise Vortex

The PIV camera was focused on the pressure side trailing edge where the spanwise vortex is expected to be located. A schematic illustration of the camera view field is presented in Figure 3.15. The tests were conducted at the same velocities used in the global flow study. Relative velocities were computed by the same process as in the former tests.

The relative velocity vector fields are presented in Figure 3.16(a)-(c). In Figure 3.16(d)-(f), the relative velocity streamlines are superimposed on the corresponding contours.

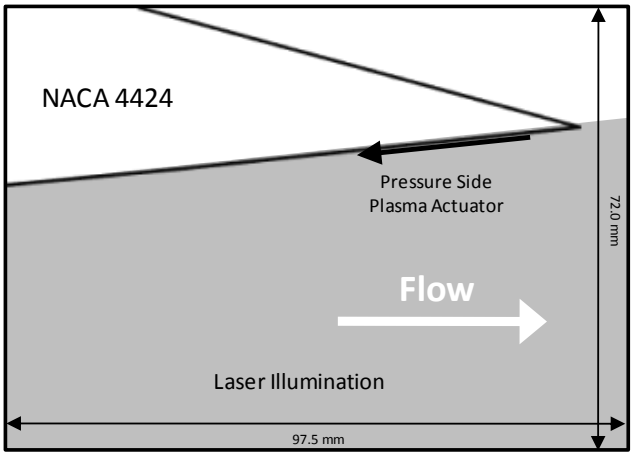

Figure 3.15 Camera View Field for Detailed Flow Study

In the results, a spanwise vortex is observed near the trailing edge. A part of the local flow delay is seen as narrower distributed relatively larger vectors at the trailing edge tip in Figure 3.16(a)-(c).

The local flow delay is shifted to the global flow delay in the pressure side cascade as depicted in Figure 3.14. A part of the local flow delay is observed in the relative velocity contours as a darker color region, which represents faster flow, near the tip of the wing.

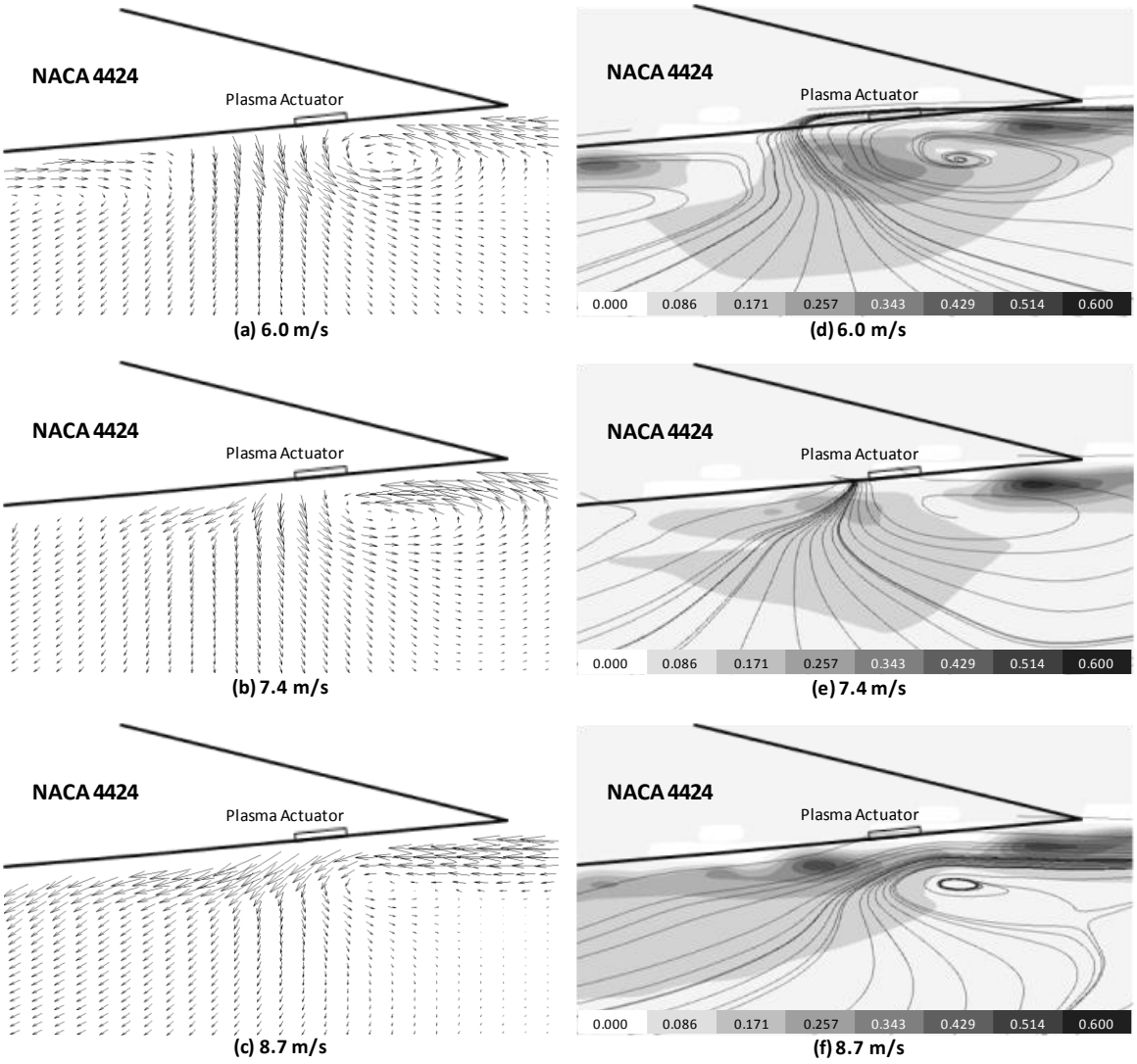

Figure 3.16 Relative Velocity Vector Fields (a)-(c) and Relative Velocity Contours (d)-(f)

3.6.3 Physical Gurney Flap versus Plasma Gurney Flap PIV Comparison

A comparison of the downstream flow structure of the physical Gurney flap and the plasma Gurney flap was conducted using the PIV results. Two Gurney flaps, 1% and 2%, were selected for this comparison. A schematic illustration of the camera view is presented in Figure 3.17.

The flaps were made of 1mm thick wood strips attached by thin aluminum tape. The aluminum tape, typically 0.18mm thick, was formed to fix the flap at right angles to the surface.

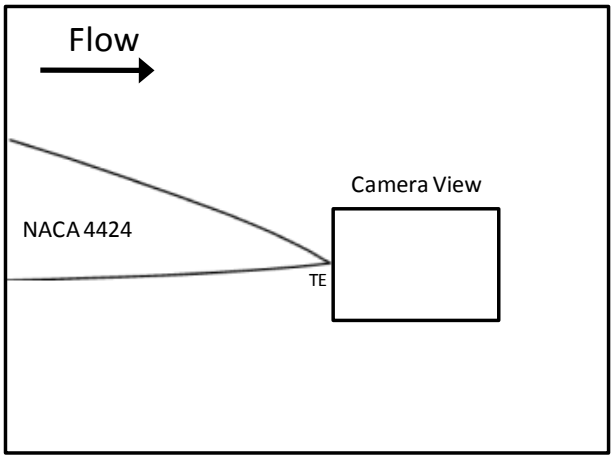

Figure 3.17 Camera View Field for Physical versus Plasma Gurney Flap Comparison

On the relative velocity contours in Figure 3.18(d)-(f), two streets of the high speed flow are observed as two regions of darker contour colors. The two streets are the suction side flow increase and the pressure side flow retardation, both relative to the baseline flow.

Most of the flow structure is similar in all three cases. However, some differences are observed in the detailed flow structure. Although the downstream flow is deflected by the physical Gurney flap configurations in Figure 3.18(a) and (b), less deflection is observed for the plasma Gurney flap, as seen in Figure 3.18(c). Another trend was that while larger relative flow retardation is observed on the pressure side for the physical Gurney flaps, faster relative flow was observed on the suction side when using the plasma Gurney flap. Either flow changes induce circulation increase and increasing lift in both cases.

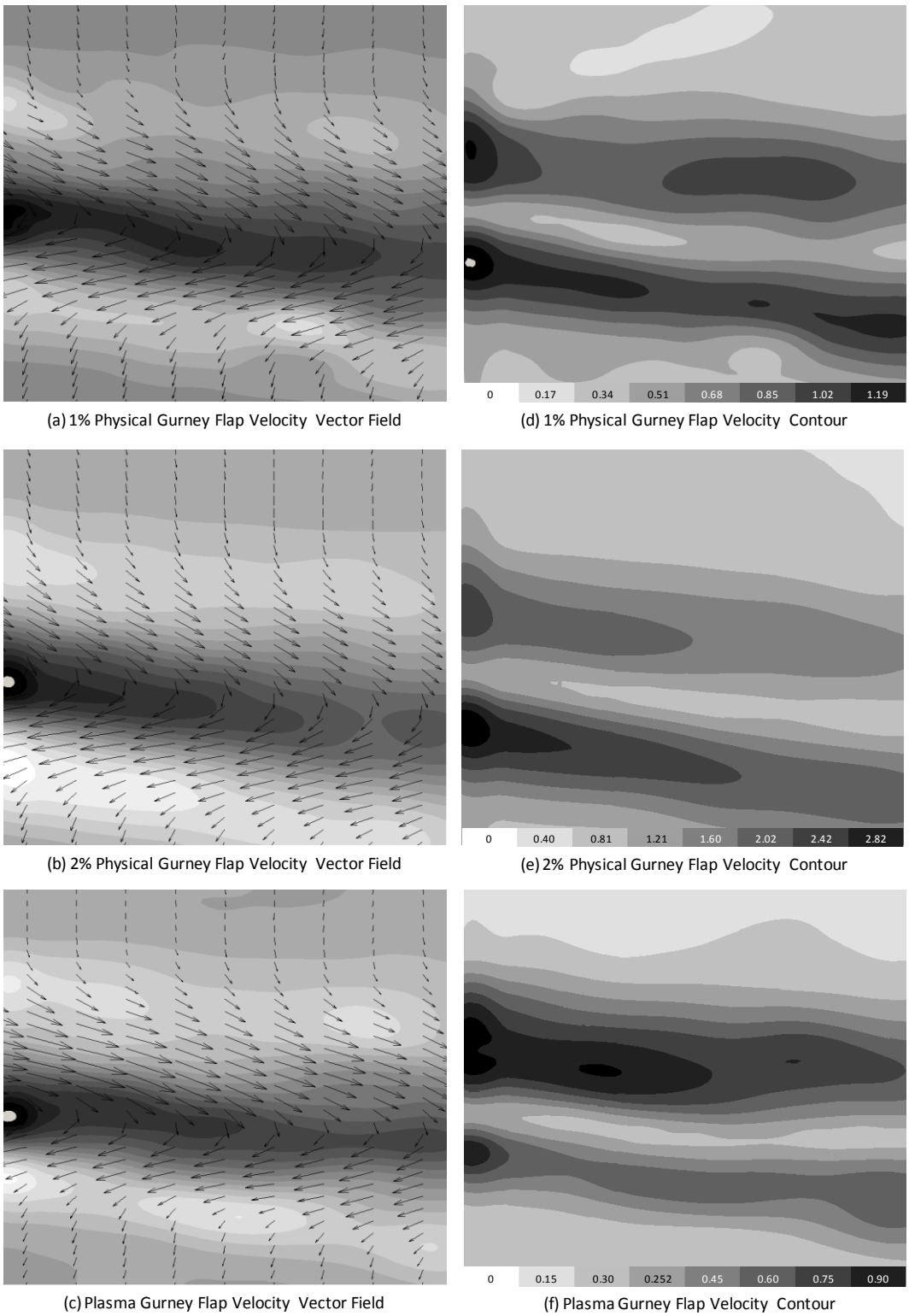

(a) 1% Physical Gurney Flap Velocity Vector Field

(d) 1% Physical Gurney Flap Velocity Contour

(b) 2% Physical Gurney Flap Velocity Vector Field

(e) 2% Physical Gurney Flap Velocity Contour

(c) Plasma Gurney Flap Velocity Vector Field

(f) Plasma Gurney Flap Velocity Contour

Figure 3.18 Relative Velocity Vector Fields Superimposed on Vorticity Contours (a)-(c) and Relative Velocity Contours (d)-(f) at a Freestream Velocity of 6.0 m/s

To provide insight into the detail flow structure change in the downstream region, a flow profile study was conducted at the two planes, 10% and 20% downstream from the trailing edge. The relative U velocity profiles were extracted from the PIV results at two different freestream velocities, 5.9 m/s and 14.1 m/s to validate the ambient velocity effects. The geometry of the two measurement planes is presented in Figure 3.19.

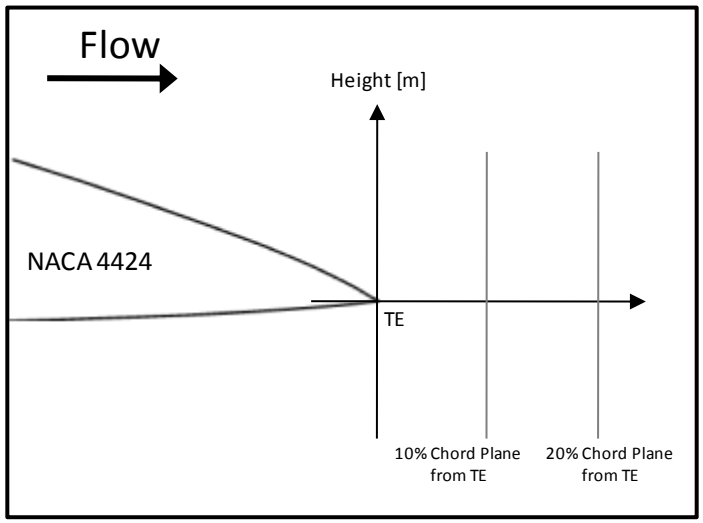

Figure 3.4 Camera View Geometry Physical and Plasma Gurney Flap Comparison

The major trends of the relative flow structure in all cases are the same, flow velocity increase on the suction side and flow velocity decrease on the pressure side, as shown in Figure 3.20. The major difference is the response to the freestream flow. The flow structure change is greater for the physical Gurney flaps as the freestream velocity increases, compared to the flow structure change for the plasma Gurney flap.

For the physical Gurney flap cases, flow change on the pressure side is more significant than on the suction side. This is because the main benefit of the physical Gurney flap is induced by the flap on the pressure side. The flap decelerates flow causing pressure rises on the pressure side. Another effect induced by the flap is flow offset. The pressure side flow stream is offset by the flap. Flow on the suction side obtains more flow curvature since the pressure side flow is offset by the flap therefore the camber effect is improved. This effect is magnified in a higher flap since the flap induces more pressure rise on the pressure side and hence more offset flow.

In Figure 3.20(b) and (c), the flow retardation is always larger than flow increase on the suction side. This is observed at all freestream velocity.

At the 10% chord location at 14.1 m/s, the maximum flow retardation by the 1% flap is approximately 2.4 m/s as shown in Figure 3.20(b) while the 2% flap retards flow by up to 5.5 m/s as shown in Figure 3.20(c). As discussed before, higher flaps generate larger effects.

The flap height camber effect is also measured for the two flaps in Figure 3.20(b) and (c). Between the two measurement planes, 10% and 20% downstream, flow deflection is observed as peak U velocity displacements. The peak shift between the dotted line and the solid line at a given freestream velocity represents the flow deflection between the 10% and the 20% chord locations. A larger deflection is observed for the 2% flap in Figure 20(c).

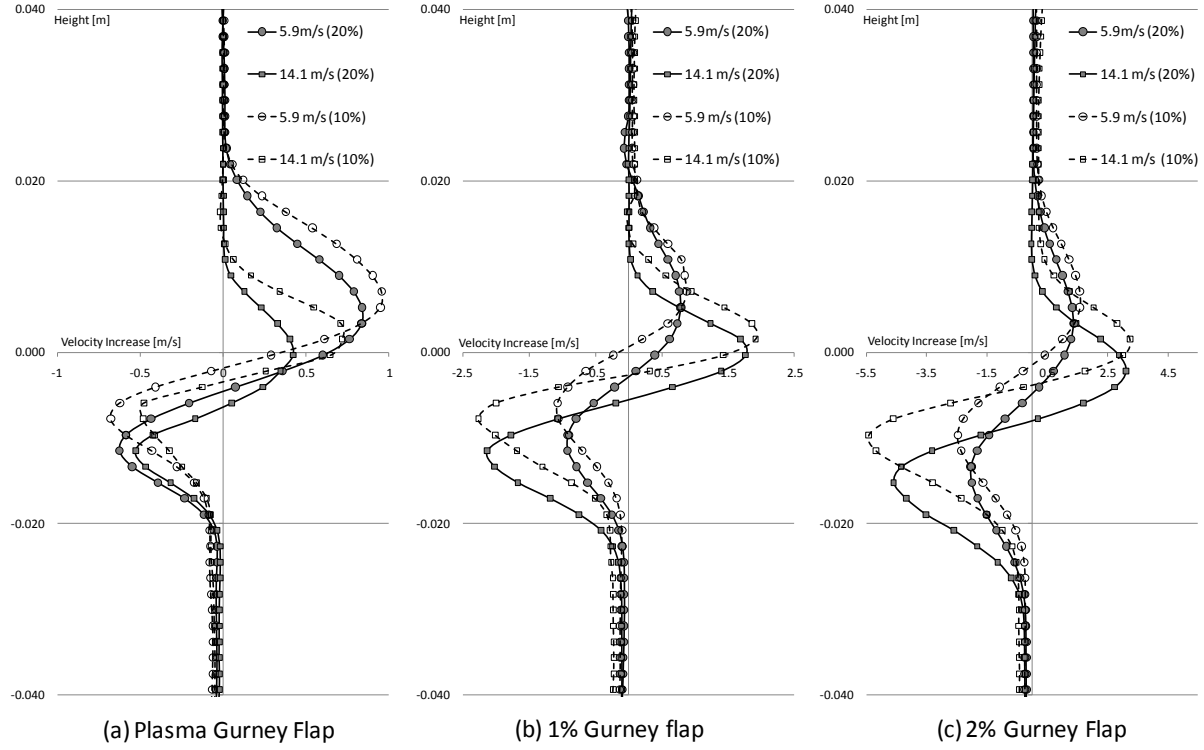

(a) Plasma Gurney Flap (b) 1% Gurney flap (c) 2% Gurney Flap

Figure 3.20 Flow Profiles at 10% and 20% Downstream Planes for Physical and Plasma Gurney Flap Comparison

The detailed flow structures and differences between physical Gurney flaps and the plasma Gurney flap effects were were studied. The flow profiles at 10% location are plotted at each freestream velocity, as shown in Figure 3.21(a) and (b).

While the flow structure change for a physical Gurney flap is dominated by pressure side flow retardation with minimal suction side acceleration, the plasma Gurney flap directly accelerates the suction side flow while at the time flow is decelerated by the spanwise vortex on the pressure side trailing edge.

At 5.9 m/s, the Physical Gurney flap flow retardation is superior to that of the plasma Gurney flap as shown in Figure 3.21(a). Note, however, that flow acceleration of the plasma Gurney flap exceeds that of the 1% Gurney flap.

At 14.1 m/s, the flow change by the plasma Gurney flap is, however, lower than that of the physical Gurney flap as presented in Figure 3.21(a).

These results imply that because the flow on the suction side is directly accelerated by the plasma actuator, the flow change on the suction side potentially exceeds the performance of the physical Gurney flap depending on the force generated by the actuator.

The direct flow acceleration makes it possible to extend the wing operational range to the lower velocity regime. The physical Gurney flap itself also improves the wing operational range. The present results, however, reveal that the plasma Gurney flap is able to exceed the physical Gurney flap performance in terms of the wing operational range extension.

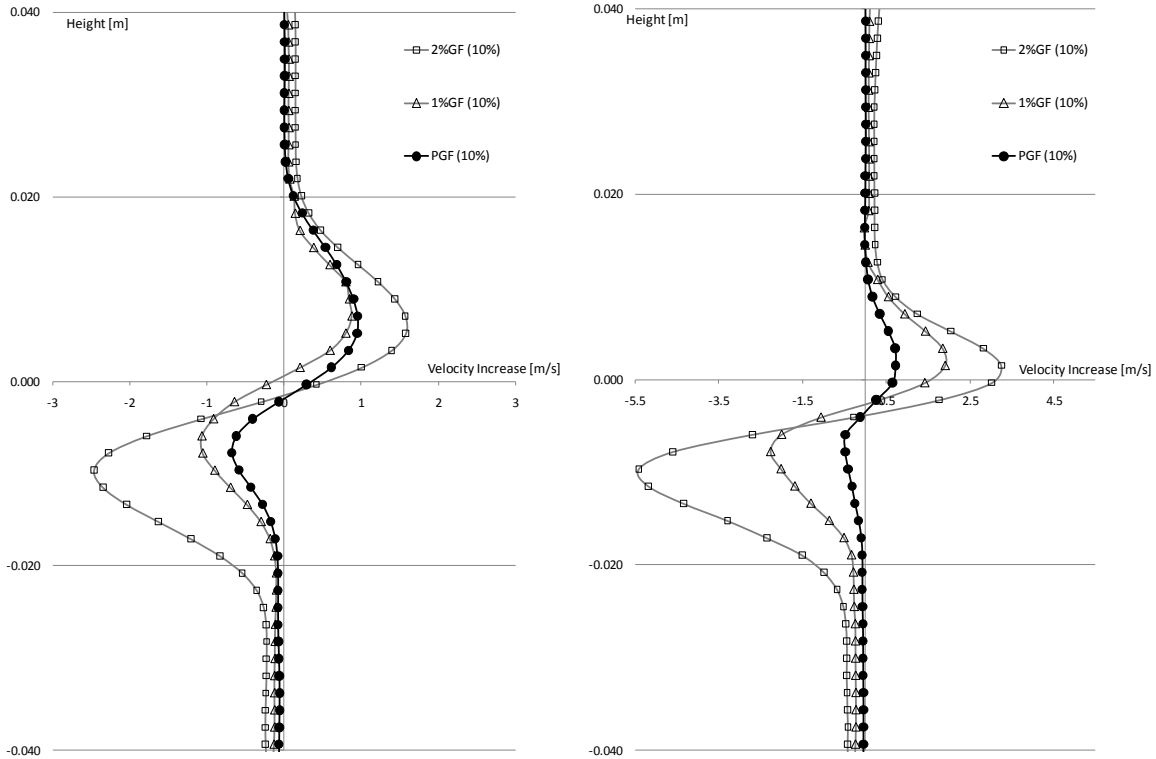

(a) 5.9 m/s (b) 14.1 m/s

Figure 3.21 Velocity Profiles of 2%GF, 1%GF and PGF in 5.9m/s (a) and 14.1m/s (b)

At 5.9 m/s, the flow increase on the suction side flow of the plasma Gurney flap was superior to that of the 1% Gurney flap. Another PIV test was conducted at a freestream velocity of 4.7 m/s. This test was intended to observe the wing operational range extension by the plasma Gurney flap.

As the results presented in Figure 3.22 show, the plasma Gurney flap remained within the operational range while the baseline and the 1% Gurney flap wing stalled. Although the 2% Gurney flap wing also remained within the operational range at the same time, as the force generation capability of the plasma actuator continues to increase, the plasma Gurney flap is potentially superior to the physical Gurney flap.

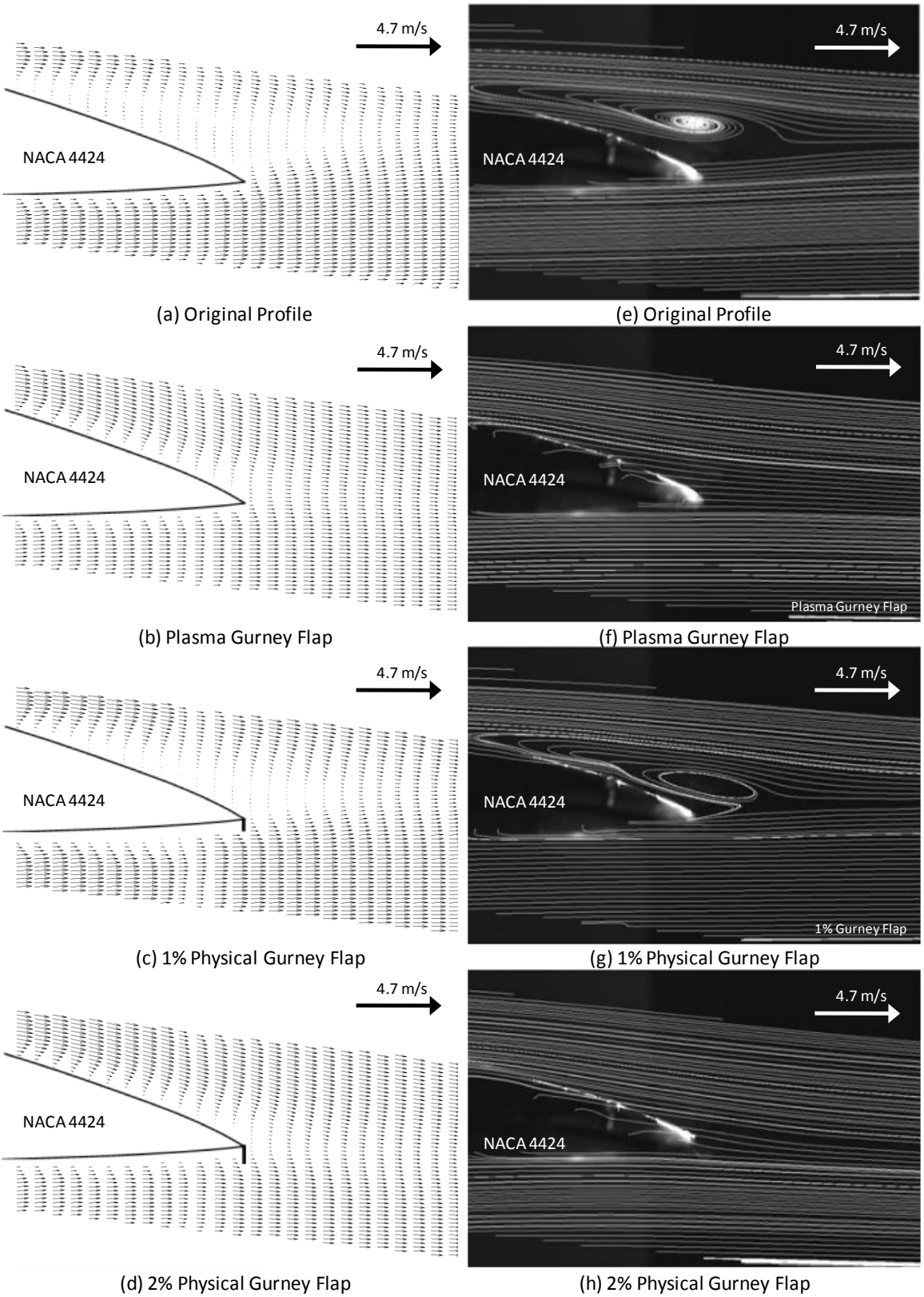

Figure 3.22 Velocity Vector Fields (a)-(d) and Streamlines (e)-(h) for Physical and Plasma Gurney Flap Comparison

3.7 Conclusion

The Plasma “Gurney flap” achieved the two advantages of the physical Gurney flap without any protruding structure outside of the airfoil profile. The achievement in this study on the plasma Gurney flap was the introduction of the double plasma actuator configuration, which was capable of combining the effects individual components. The force measurements showed that the individual actuators contribute nearly equally to the combined activation of the plasma Gurney flap. This potentially exceeds any single plasma actuator configuration, since the effect of the plasma Gurney flap is equivalent to the sum of two single actuator results.

One more advantage of the plasma Gurney flap over the physical Gurney flap was the extension of the wing operational range. The geometry of the plasma Gurney flap makes it possible to directly induce a force on the suction side flow at the trailing edge. This leads to a greater extension of the wing operational range.

Finally, the plasma Gurney flap completely eliminates the need to a deploy and store mechanical systems, making it feasible for variable flight conditions. These results present a potential and feasible alternative approach to lift control by a non-mechanical methodology.

3.8 Reference

[1] Zaparka, E.F., "Aircraft and Control Thereof," U.S. Patent No. 19,412, January, 1935.

[2] Lieback, R.H., "Design of Subsonic Airfoils for high Lift," *Journal of Aircraft*, Vol. 15, No. 9, 1978, pp. 547-561

[3] Jeffrey, D.R.M., "Aerodynamics of the Gurney Flap," AIAA 96-2418, June, 1996.

[4] Bechert, D.W., Meyer, R. and Hage, W., "Drag Reduction of Airfoils with Miniflaps," AIAA paper, 2000-2315 (2000)

[5] Meyaer, R., Hage, W., Bechert, D.W., Schatz, M., and Thiele, F., "Drag Reduction on Gurney Flaps by Three-Dimensional Modifications," *Journal of Aircraft*, Vol. 43, No. 1, Jan.-Feb., 2006, pp. 132-140

[6] Traub, L.W. and Agarwal, G., "Aerodynamic Characteristics of a Gurney/Jet Flap at Low Reynolds Numbers," *Journal of Aircraft*, Vol. 45, No. 2, Mar.-Apr. 2008, pp. 424-429

[7] Shea, P. R. and Smith, D.R., "Aerodynamic Control of a Rectangular Wing Using Gurney Flaps and Synthetic Jets," AIAA 2009-886 (2009)

[8] Yen Nakafuji, D.T., van Dam, C.P., Smith, R.L and Collins, S.D., "Active Load Control for Airfoils using Microtabs," Journal of Solar Energy Engineering, Vol. 123, No. 4, Nov. 2001, pp. 282-289

[9] Baker, J.P., Standish, K.J., and can Dam, C.P., "Two-Dimensional Wind Tunnel and Computational Investigation of a Microtab Modified airfoil," *Journal of Aircraft*, Vol. 44, No. 2, March-April, 1978, pp. 563-572

[10] Liu, C. and Roth, J.R., "Atmospheric Glow Discharge Plasma for Aerodynamic Boundary layer Control," Proceeding of 21st IEEE International Conference on Plasma Science, Sante Fe, NM, June 6-8, 1994, ISBN 7803-2006-9, pp.97-98

[11] Roth, J.R. and Dai, X., "Optimization of the Aerodynamic Plasma Actuator as an Electrohydrodynamic (EHD) Electrical Device," 44th AIAA Aerospace Science Meeting and Exhibit, 9-12 January, 2006, Reno Nevada

[12] Santhanakrishnan, A., Pern, N. J., Ramakumar, K., Simpson, A., and Jacob, J.D., "Enabling Flow Control Technology for Low Speed UAVs,"AIAA Infortech Aerospace, September 26-29, 2005, Washington, DC

[13] Nelson, R. C., Corke, T. C., Hesham Othman, C. H., and Matsuno. T., “Modification of the flow Structure over a UAV Wing for Roll Control,” 45th Aerospace Science Meeting, January 8-11, 2007, Reno, Nevada

[14] Zhang, P.F., Liu, A.B. and Wang, J.J., ”Aerodynamic Modification of a NACA 0012 Airfoil by Trailing-Edge Plasma Gurney Flap,” AIAA Journal, Vol. 47, No. 10, October 2009

[15] Lee, T., ”Aerodynamic Characteristic of Airfoil with Perforated Gurney-Type Flaps,” *Journal of Aircraft*, Vol. 46, No. 2, 2009, pp. 542-448

[16] Jayaraman,B., Cho,Y.C., and Shyy,W. “modeling of Dielectric Barrier Discharge Plasma Actuator,” 38th AIAA Plasmadynamics and Lasers Conference, 25-28 June 2007, Miami, FL

[17] Santhanakrishman, A., and Jacob, J.D., “On Plasma Synthetic Jet Actuators,” 44th AIAA Aerospace Science Meeting and Exhibit, 9-12 January 2006, Reno, Nevada

[18] He, C., and Corke, T.,C., “Plasma Flaps and Slats: An Application of Weakley Ionized Plasma Actuators,” *Journal of Aircraft*, Vol. 46, No. 3, May-June, 2009, pp. 864-873

[19] Gregory, J.W., Enloe, C.L., Font, G.I. and McLaughlin, T. E., “Force Production Mechanisms of a Dielectric-Barrier Discharge Plasma Actuator,” 45th AIAA Aerospace Science Meeting and Exhibit, 8-11 January 2007, Reno, Nevada

3.9 Appendices

3.9.1 Wind Tunnel Velocity Validation

The wind tunnel velocity validation was conducted to validate the velocity measured by a pitot-dynamic tube and built in static ports on the wind tunnel. A pitot-static probe was used to measure the reference velocities. Because of the installation flexibility, the pitot-dynamic tube was feasible for the measurement setup thus the velocity corrections were necessary from this validation results.

The wind tunnel was operated with empty test section to validate the velocity information comparing with the data from two different instruments, the pitot-static probe and the combination of the pitot-dynamic tube and the built in static ports.

In the results with empty test section, the error for the measurement set up was negligible, 0.42% lower from the velocities from the pitot-static probe. Aster the tests with empty test section, an airfoil was installed and the same process was repeated. The results for the measurement setup showed two different trends, the group of the baseline wing and the plasma Gurney flap, and the group of the Gurney flap configurations, as shown in Figure 3.23. The former is without physical structure and the lalter is similar configuration equipped with a Gurney flap, thus two different velocity calibration equations were derived.

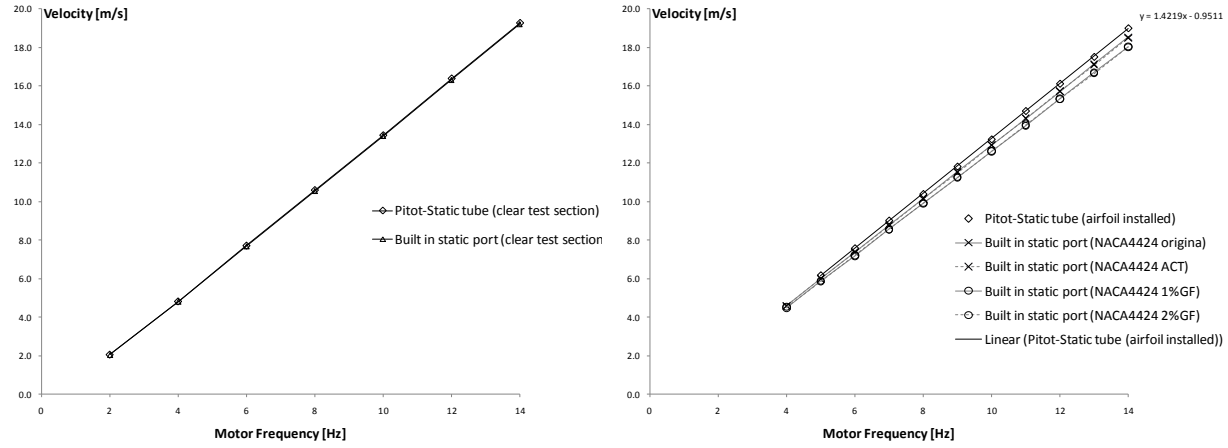

Figure 3.23 Wind Tunnel Velocity Validation with Empty Test Section (left) and Airfoil Installed Test Section (right)

For the original profiles and the actuator activations:

$$V_{actual} = 1.02V_{measured} + 0.058$$

For the 1% Gurney Flap configurations and the 2% Gurney flap configurations:

$$V_{actual} = 1.053V_{measured} - 0.011$$

3.9.2 Force Balance

The force measurement system is organized with two force balances placed beneath an L shape structure. Figure 3.24 shows the principle of the system. An airfoil was installed at location A in Figure 3.24. The two vertical force components, $\boldsymbol{F_1}$ and $\boldsymbol{F_2}$ were measured by balance 1 and balance 2 located under the location B and location C. The lift $\boldsymbol{L}$ was calculated $\boldsymbol{L = F_1 + F_2}$ as shown in Figure 3.24.

The resolution of $\boldsymbol{F_1}$ and $\boldsymbol{F_2}$ was 4.89 x 10^{-03}[N], and 9.78 x 10^{-03}[N], which was 0.28% and 0.9% of the maximum force, measured in the tests.

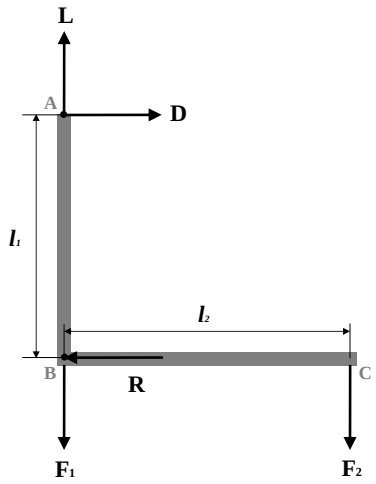

Figure 3.24 Force Components and Structure Geometry

The force measurement system was validated to compare with the applied force and the measured force. Figure 3.25 shows the validation result. The error in the outlet value was -0.21% from an input value.

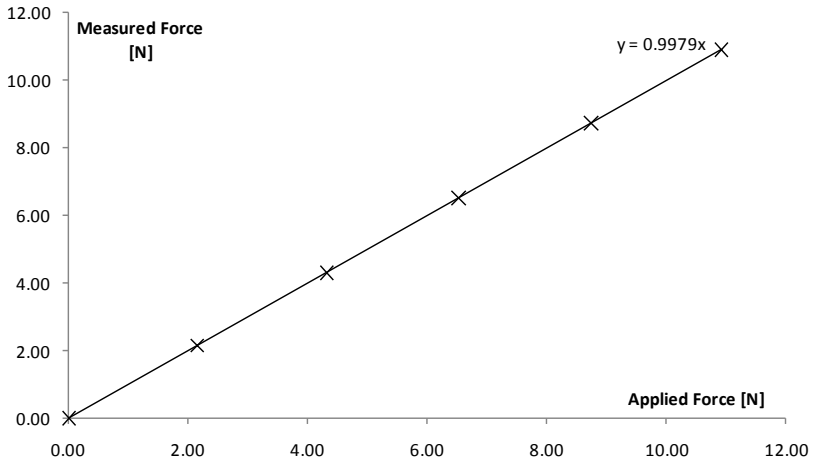

Figure 3.25 Force Validation Result

3.9.3 AIAA Journal Submission

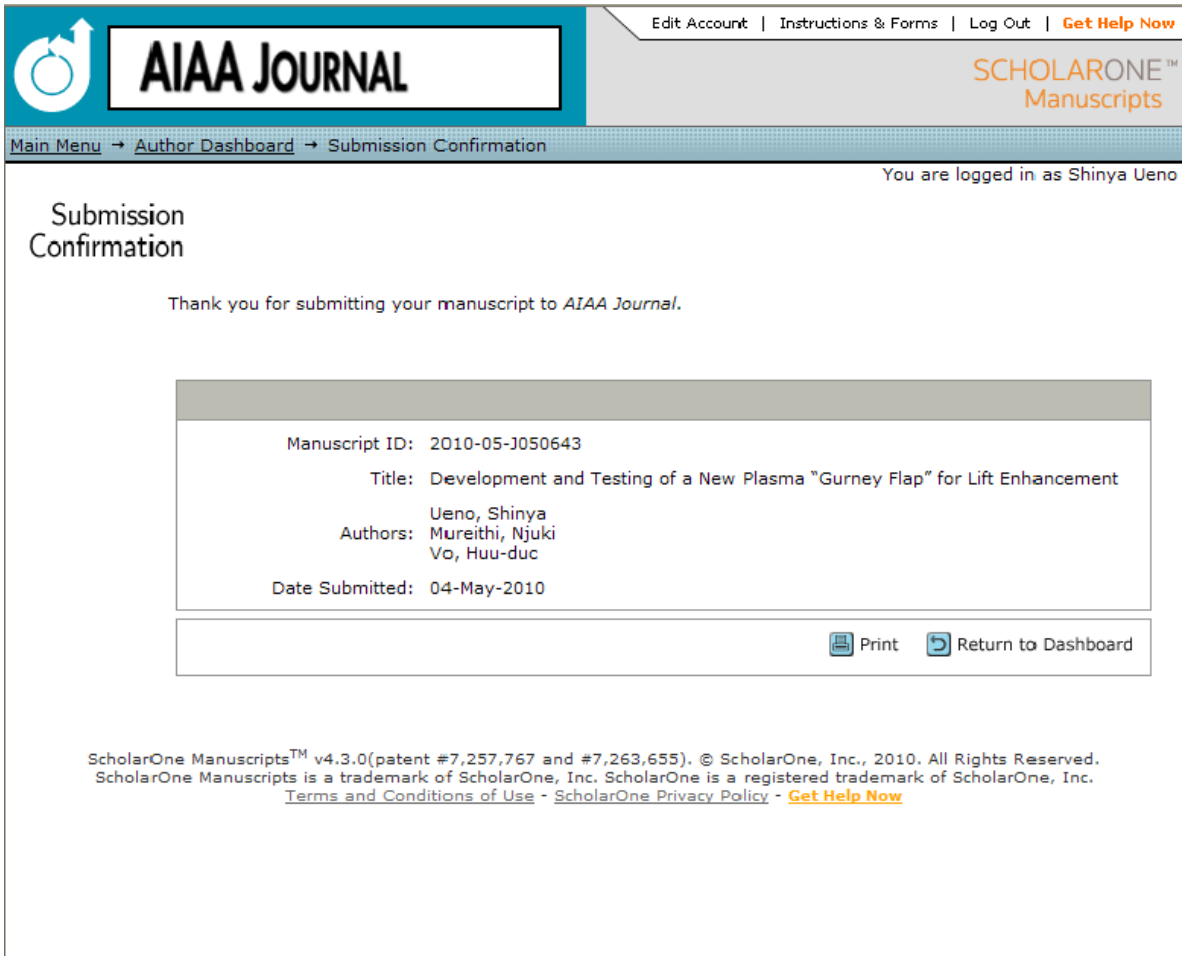

Figure 3.26 Screenshot of AIAA Journal Submission

CHAPTER 4

GENERAL DISCUSSION

Two advantages, lift enhancement and wing operational range extension were measured in the physical Gurney flap study. The study revealed the superior performance of the upstream flap configuration which also provides for a structural volume to store the deployable flap.

The lift enhancement and the wing operational range extension were observed in the development and testing of an innovative new plasma "Gurney flap". The additional benefit of the plasma Gurney flap was further extension of the operational range in addition to the original target of lift enhancement without the physical structure of the Gurney flap.

In this Chapter, the plasma Gurney flap is compared with the variable Gurney flap, and then discussed relative to the morphing wing, which is another potential alternative approach to replace conventional control surfaces.

4.1 Variable Gurney Flaps versus Plasma Gurney Flaps

Besides fixed Gurney flaps and microtabs, variable Gurney flaps and microtabs are discussed here for comparison with the plasma Gurney flaps.

The aim of the current Gurney flap location study was to investigate the potential of the upstream flap since the location makes it possible to provide a structural volume which the deployable flap can be stored. Movable components require adequate clearances. These mechanical clearances on airfoils are generally seen as grooves on the wing surfaces. Although variable Gurney flaps are relatively simple compared to conventional flaps, they are still mechanical components thus adequate clearance is essential.

Yen Nakafuji *et al*. [10] investigated a remotely activated flap in addition to their fixed flap studies. The investigation was focused on the aerodynamic effect of the gaps caused by the deployable flap. A 1% deployable flap was embedded at 95% chord on a GU25-5(11)-8 wing having 0.305m chord and 0.838 wing span. The flap was remotely driven by an electro-

mechanical linkage and servo-motor actuation system. Wind tunnel tests at Re=1.0x10^6 showed lower C_L improvement dependent on the gap width compared with an equal height fixed flap at the same location, as shown in Figure 4.1.

Figure 4.1 (a) Fixed Flap (b) Deployable Flap with Gaps

The result is presented in Figure 4.2. The study examined three different non-dimensional gaps, defined as the ratio of the gap to the flap height. At 0 degrees angle of attack, while a 1% solid flap provides 50% C_L improvement, 0.5:1, 1:1 and 2:1 gap width to flap height configurations provide 42%, 33% and 20% C_L improvement, respectively. This result implies that the advantage of the Gurney flap, which is a relatively simple configuration, is reduced since the deployable Gurney flap requires high tolerance design to achieve the equivalent aerodynamic benefit of the fixed Gurney flap.

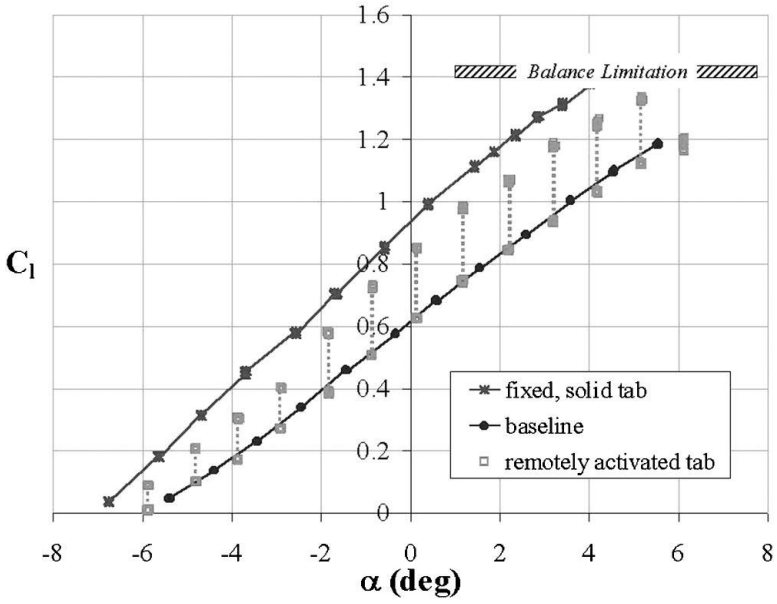

Figure 4.2 Lift Curve of Fixed and Deployable Flap of a 1% and 95% location on a GU25-5(11)-8 wing [10]

The advantage of the plasma Gurney flap is that no gap exists on the surface because the plasma actuator can be installed completely flush to the surface, as presented in the schematic illustration of Figure 4.3. The major advantage of the plasma Gurney flap is that it is a completely non-movable approach for lift and load control. A hingeless wing provides several benefits compared to the conventional flap and the deployable Gurney flap. The gap of the deployable Gurney flap causes the performance decrease [10]. At the same time, the gap on a wing is known to be a source of viscous drag, acoustic noise and radar reflection. The structure of a non-movable wing decreases manufacturing and operational costs because the arrangement of the flaps as well as the mechanical systems composed of the hydraulic and electric actuators require complex wing structure designs.

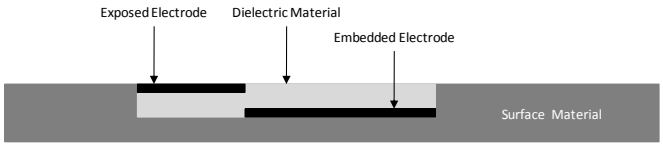

Figure 4.3 Schematic Illustration of Flush Surface Plasma Actuator

Another advantage of the plasma Gurney flap is extension of the wing operational range. This effect was measured in the physical Gurney flap as well. However, the effect of the plasma Gurney flap potentially exceeds that of the physical flap. Most of the flow structure for the physical and plasma Gurney flap is similar; increased flow on the suction side and retarded flow on the pressure side. Although the flow increase on the suction side is caused by the flow retardation by the flap in the physical Gurney flap configuration, the flow is directly accelerated on the suction side by the plasma actuator in the plasma Gurney flap. The difference in the flow structure appears in the lower limit of the wing operational range because in that situation the flow increase on the suction side of the physical Gurney flap is relatively weaker than that of the plasma Gurney flap. The phenomenon was observed in the PIV and the lift force measurements in this study. While wing with a 1% physical Gurney flap stalled, the plasma Gurney flap remained within the operational range at 4.7 m/s freestream velocity. The effect is governed by the force generated by the plasma actuator thus the application range will continue to expand as plasma actuator technology improves.

4.2 Morphing Wings versus Plasma Gurney Flaps

Morphing wings have attracted attention due to their lower drag compared to conventional flap wings because no hinge gaps exist on the wing surface thus the drag is reduced. The concept involves modifying the airfoil profile to change the surface flow without using conventional flaps. An example is presented in Figure 4.4. Full scale flight tests were conducted in the mid-1980s with the wing called the Mission Adaptive Wing.

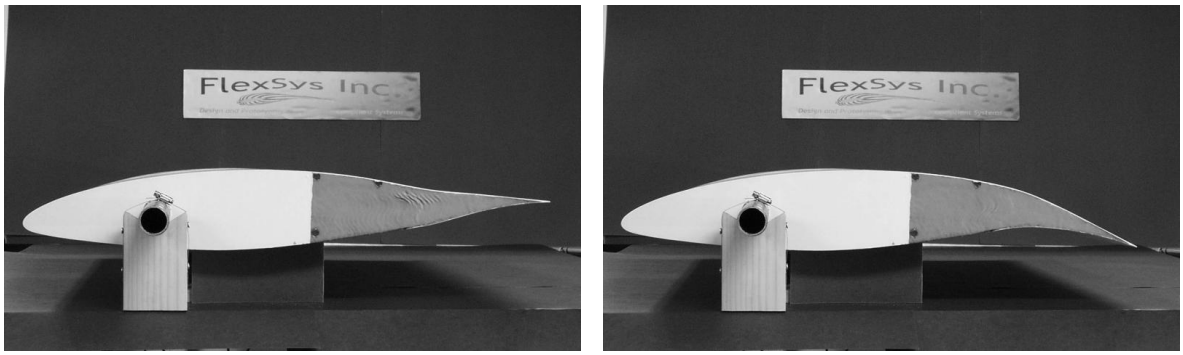

(a) (b)

Figure 4.4Variable Geometry TE Wind Tunnel Model shown in -10 degrees (a) and +10degrees (b) [23]

Mission Adaptive Wing is a concept of an aircraft wing which is capable of changing the profile by modifying the wing shape to reduce drag and enhance lift. The concept was tested by modifying F-111 aircraft wings in the mid-1980s. The shape of the leading and trailing edges of the test wings were mechanically varied by conventional rigid-link mechanisms. The flight tests proved the concept was superior to the conventional leading edge and trailing edge flaps in terms of aerodynamic performance [22].

The benefit of the morphing wing is reduced drag and higher lift. The wing is able to adjust to the optimal wing profile during flight. The major technologies of the morphing wings are the leading and trailing edge profile change and the camber control by a mechanical approach. The replacement of these mechanical approaches by smart materials and smart structures are the subject of ongoing research.

The common advantage between the morphing wing and the plasma Gurney flap is the absence of hinge gaps. The morphing wings are potentially superior to the plasma Gurney flap in terms of energy consumption. While the plasma Gurney flap requires the plasma actuator

activation when flow control is needed, the morphing wing does not require steady activation once the actuators are deployed and locked. The disadvantage of the plasma Gurney flap can be removed or minimized by unsteady activation of the plasma actuator. A disadvantage of the morphing wing is complex wing structure composed of many hinge and link systems. The plasma Gurney flap is superior to the morphing wings in terms of wing structure simplicity and storage space for other electric systems and fuel or butteries.

The plasma Gurney flap is superior to the morphing wing at the lower end of the wing operational range. Although flow separation is not avoidable for the morphing wings, the plasma Gurney flap is able to extend the operational range by directly accelerating the suction side flow which would otherwise separate and stall the wing at the lower end of the operational range. The capability of current plasma actuators is in the range of the Unmanned Aerial Vehicles. However, the technology evolution can potentially extend the application range to full size aircraft. Even in the UAV range, the operational range extension provides lower cruising and landings speed which has attracted attention because of the advantage of steady observation for a static or low-speed target and safe landing over a short range in urban environments.

CHAPTER 5

CONCLUSION AND RECOMMENDATIONS

5.1 Conclusion

The Gurney flap location and Height study revealed the upstream flap capability and height effect for a given flap location. All wings equipped with a Gurney flap had higher lift compared to the baseline wing. All upstream flaps provided higher lift than the 100% location flap for a given flap height. For 2% height flaps, a clear trend of the location effect was measured. The highest lift improvement was achieved by a 2% flap at 85% location for any given angle of attack. The height study shows that higher flaps provide higher lift in any given flap location.

The wing operational range was extended to the lower freestream velocity region by the physical Gurney flap. This trend was measured for all Gurney flap configurations. The most outstanding result was measured with a 2% flap at 95% location. While all the other wings stalled, the wing with the 2% flap at 95% location remained within the operational at 10.5 m/s freestream velocity.

An innovative new concept of the plasma “Gurney flap” was developed and tested in the wind tunnel. The force measurements revealed that the two plasma actuators comprising the plasma Gurney flap contribute approximately the same magnitude lift change individually thus the combined effect of the plasma actuators is nearly the sum of the two actuators. The flow structure study revealed that there is a similarity of the relative flow between the plasma Gurney flap from the baseline and the physical Gurney flap but the plasma Gurney flap potentially exceed the physical Gurney flap in terms of the suction side flow increase because the plasma actuator is able to accelerate the flow directly. The force measurements show that an equivalent effect is provided by the plasma Gurney flap. At the highest freestream velocity, although the performance of the plasma Gurney flap is lower than that of the physical Gurney flap, technology improvement of the plasma actuator is expected to rapidly extend the

performance of the plasma Gurney flap. The highest C_L improvement from the baseline in the force measurements was ΔC_L=0.18 at 6.0 m/s freestream velocity.

From these results, the lift control capability by the plasma Gurney flap was investigated and confirmed. A non-movable approach for lift and load control has been developed in this study and been shown to have very promising potential.

5.2 RECOMMENDATIONS

The force measurements in this Thesis covered only the lift component but not the drag component. For further study, drag comparison between the physical Gurney flap and the plasma Gurney flap is important. Although test results for the current study imply drag for the plasma Gurney flap wing is slightly higher than for the baseline wings, the system needs to be improved for drag study.

There are two major factors which prevented drag measurement in the current setup. One is drag from the airfoil support and the other is cable stiffness.

Usually, the support is covered by a sheath to prevent drag from acting on the airfoil support. A sheath can be a solution but a better idea is to install the airfoil vertically to minimize the exposed are of the airfoil support. In this setup, strain gages are installed on the wind tunnel test section and cables are connected from the bottom of the test section. This setup can minimize the effect of cable stiffness.

A mechanical system to adjust the airfoil angle of attack will be essential to improve data quality. This will improve both data quality of lift and drag component measurements.

Although the power of the plasma actuators is lower than full scale aeronautical applications, simulations will help to estimate the necessary power in faster freestream conditions. From these studies, requirements for associated technology, power supply and amplifiers, can be determined. This will give detailed information on which components need technological improvement to make plasma actuator aeronautical application practically feasible.

REFERENCE

[1] Zierath, A., Woernle, C., and Heyden, T., "Elastic Multibody Models of Transport Aircraft High-Lift Mechanisms," *Journal of Aircraft*, Vol. 46, No. 5, 1978, pp. 1513-1524

[2] Green, L.L., Cruz, J., "Uncertainty Analysis for a Jet Flap Airfoil," 2006 Fall Simulation Interoperability workshop, 10-15 Sep. 2005, Orland, FO, USA

[3] Zaparka, E.F., "Aircraft and Control Thereof," U.S. Patent No. 19,412, January, 1935.

[4] Lieback, R.H., "Design of Subsonic Airfoils for high Lift," *Journal of Aircraft*, Vol. 15, No. 9, 1978, pp. 547-561

[5] Jeffrey, D.R.M., "Aerodynamics of the Gurney Flap," AIAA 96-2418, June, 1996.

[6] Bechert, D.W., Meyer, R. and Hage, W., "Drag Reduction of Airfoils with Miniflaps," AIAA paper, 2000-2315 (2000)

[7] Meyaer, R., Hage, W., Bechert, D.W., Schatz, M., and Thiele, F., "Drag Reduction on Gurney Flaps by Three-Dimensional Modifications," *Journal of Aircraft*, Vol. 43, No. 1, Jan.-Feb., 2006, pp. 132-140

[8] Traub, L.W. and Agarwal, G., "Aerodynamic Characteristics of a Gurney/Jet Flap at Low Reynolds Numbers," *Journal of Aircraft*, Vol. 45, No. 2, Mar.-Apr. 2008, pp. 424-429

[9] Shea, P. R. and Smith, D.R., "Aerodynamic Control of a Rectangular Wing Using Gurney Flaps and Synthetic Jets," AIAA 2009-886 (2009)

[10] Yen Nakafuji, D.T., van Dam, C.P., Smith, R.L and Collins, S.D., "Active Load Control for Airfoils using Microtabs," Journal of Solar Energy Engineering, Vol. 123, No. 4, Nov. 2001, pp. 282-289

[11] Baker, J.P., Standish, K.J., and can Dam, C.P., "Two-Dimensional Wind Tunnel and Computational Investigation of a Microtab Modified airfoil," *Journal of Aircraft*, Vol. 44, No. 2, March-April, 1978, pp. 563-572

[12] Liu, C. and Roth, J.R., "Atmospheric Glow Discharge Plasma for Aerodynamic Boundary layer Control," Proceeding of 21st IEEE International Conference on Plasma Science, Sante Fe, NM, June 6-8, 1994, ISBN 7803-2006-9, pp.97-98

[13] Roth, J.R. and Dai, X., "Optimization of the Aerodynamic Plasma Actuator as an Electrohydrodynamic (EHD) Electrical Device," 44th AIAA Aerospace Science Meeting and Exhibit, 9-12 January, 2006, Reno Nevada

[14] Santhanakrishnan, A., Pern, N. J., Ramakumar, K., Simpson, A., and Jacob, J.D., "Enabling Flow Control Technology for Low Speed UAVs,"AIAA Infortech Aerospace, September 26-29, 2005, Washington, DC

[15] Nelson, R. C., Corke, T. C., Hesham Othman, C. H., and Matsuno. T., "Modification of the low Structure over a UAV Wing for Roll Control," 45th Aerospace Science Meeting, January 8-11, 2007, Reno, Nevada

[16] Zhang, P.F., Liu, A.B. and Wang, J.J., "Aerodynamic Modification of a NACA 0012 Airfoil by Trailing-Edge Plasma Gurney Flap," AIAA Journal, Vol. 47, No. 10, October 2009

[17] Lee, T., "Aerodynamic Characteristic of Airfoil with Perforated Gurney-Type Flaps," *Journal of Aircraft*, Vol. 46, No. 2, 2009, pp. 542-448

[18] Jayaraman,B., Cho,Y.C., and Shyy,W. "modeling of Dielectric Barrier Discharge Plasma Actuator," 38th AIAA Plasmadynamics and Lasers Conference, 25-28 June 2007, Miami, FL

[19] Santhanakrishman, A., and Jacob, J.D., "On Plasma Synthetic Jet Actuators," 44th AIAA Aerospace Science Meeting and Exhibit, 9-12 January 2006, Reno, Nevada

[20] He, C., and Corke, T.,C., "Plasma Flaps and Slats: An Application of Weakley Ionized Plasma Actuators," *Journal of Aircraft*, Vol. 46, No. 3, May-June, 2009, pp. 864-873

[21] Gregory, J.W., Enloe, C.L., Font, G.I. and McLaughlin, T. E., "Force Production Mechanisms of a Dielectric-Barrier Discharge Plasma Actuator," 45th AIAA Aerospace Science Meeting and Exhibit, 8-11 January 2007, Reno, Nevada

[22] "Advanced Fighter Technology Integration F-111 Mission Adaptive Wings", *proceeding of symposium held at NASA Ames Research Center*, NASA Conference Publication 3055, April 1989

[23] Kota, S., Hetrick, J. Osborn, R., Paul, D., Pendleton, E. Flick, Peter, and Tilmann, C., "Design and application of compliant mechanisms for morphing aircraft structures," *proceedings of SPIE*, Vol. 5054, 2003, pp. 24-33.

APPENDICES

APPENDIX I

DETAILED FLOW STUDY (AoA=-4)

Figure I.1 Camera View Field of Detailed Flow Study at AoA=-4

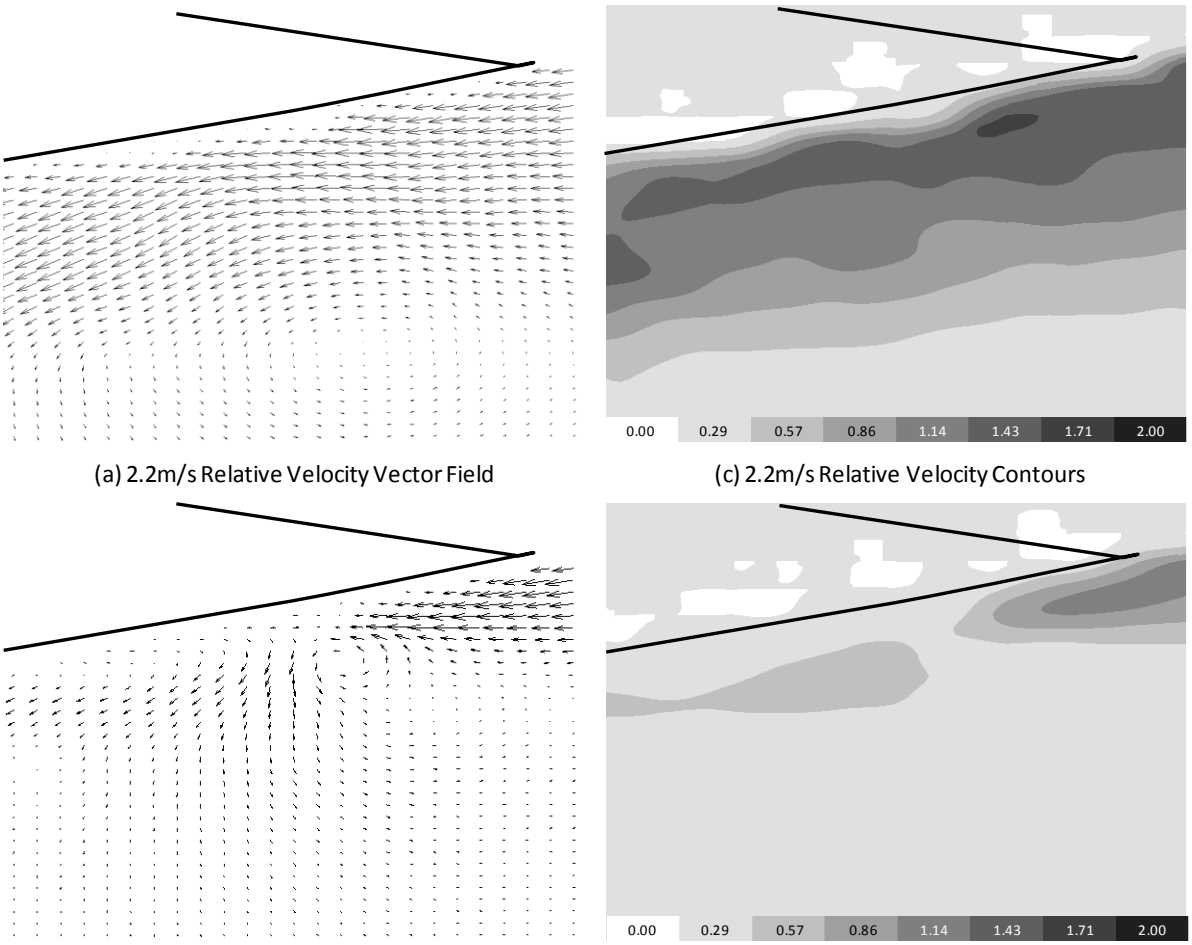

(a) 2.2m/s Relative Velocity Vector Field

(c) 2.2m/s Relative Velocity Contours

(b) 3.6m/s Relative Velocity Vector Field

(d) 3.6m/s Relative Velocity Contours

Figure I.2 Detailed Flow Study at AoA=-4: Relative Velocity Vector Fields (a) and (b) and Relative Velocity Contours (c) and (d)

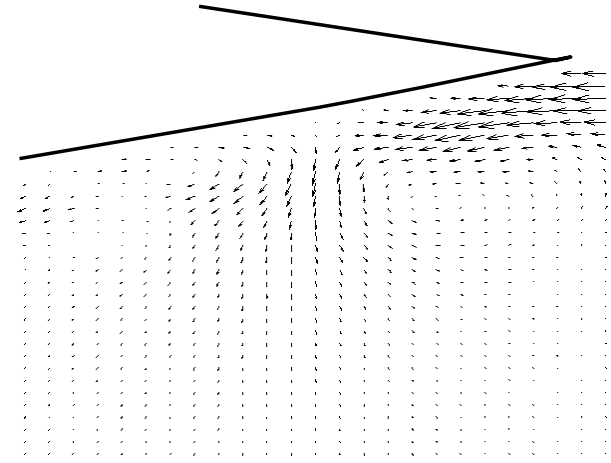

(c) 5.2m/s Relative Velocity Vector Field

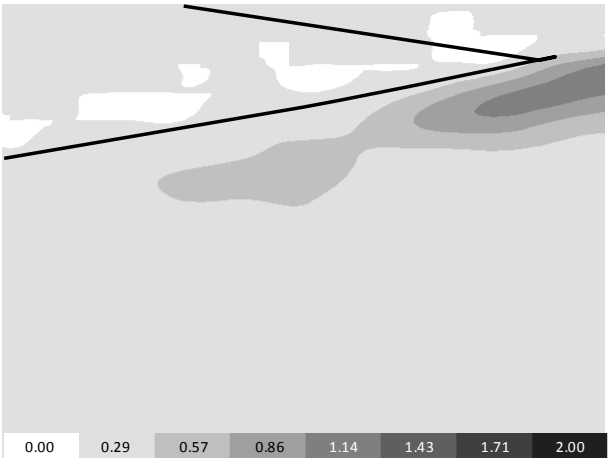

(d) 5.2m/s Relative Velocity Contours

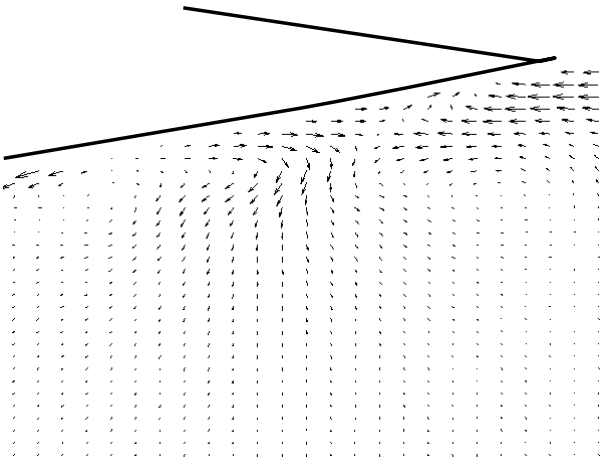

(b) 6.6m/s Relative Velocity Vector Field

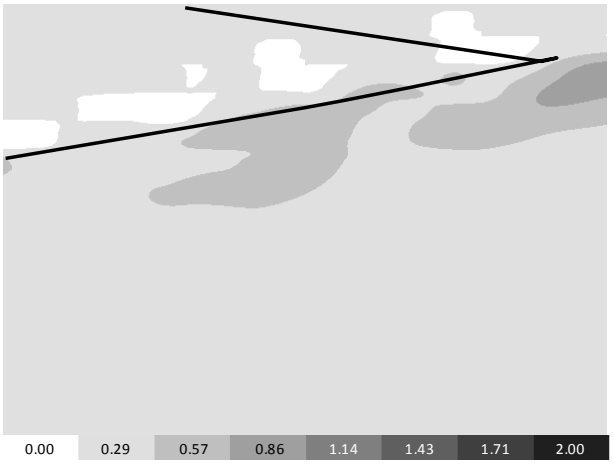

(e) 6.6m/s Relative Velocity Contours

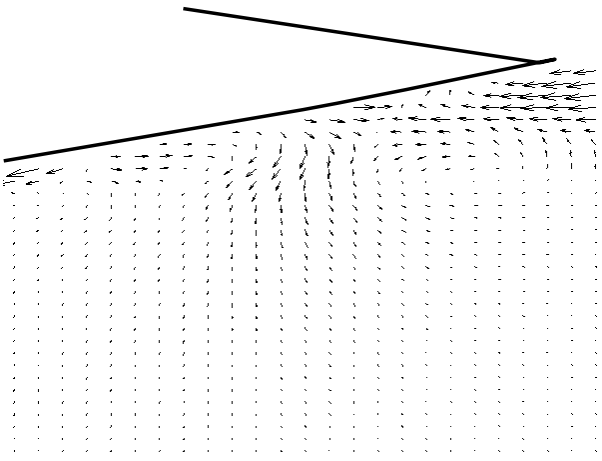

(c) 8.2m/s Relative Velocity Vector Field

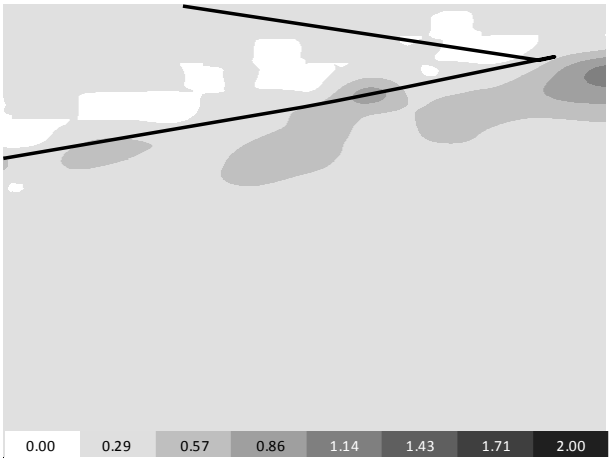

(f) 8.2m/s Relative Velocity Contours

Figure I.3 Detailed Flow Study at AoA=-4: Relative Velocity Vector Fields (a)-(c) and Relative Velocity Contours (d)-(f)

APPENDIX II

DETAILED FLOW STUDY (AoA=+2)

Camera View Field

Figure II.1 Camera View Field of Detailed Flow Study at AoA=+2

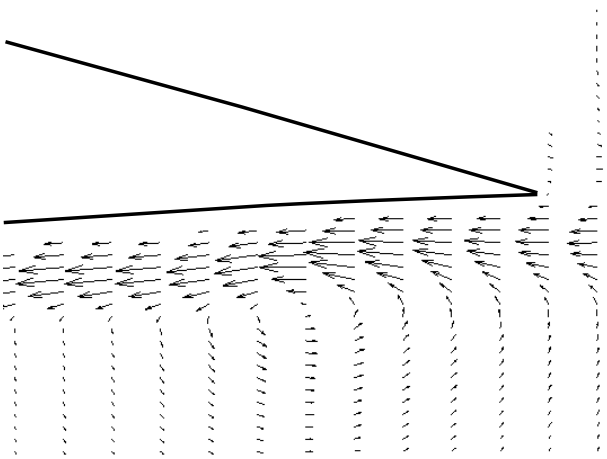

(a) 2.2m/s Relative Velocity Vector Field

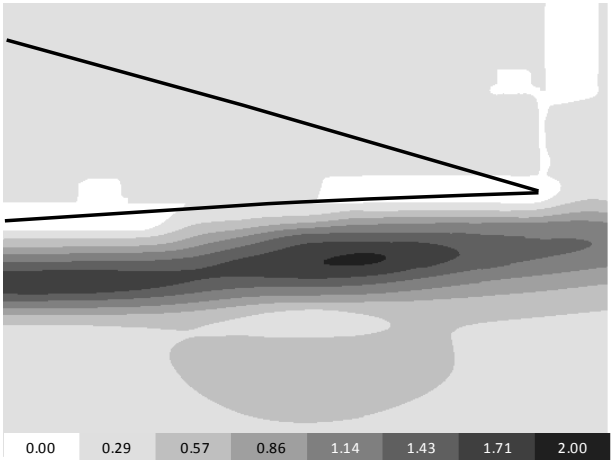

(e) 2.2m/s Relative Velocity Contours

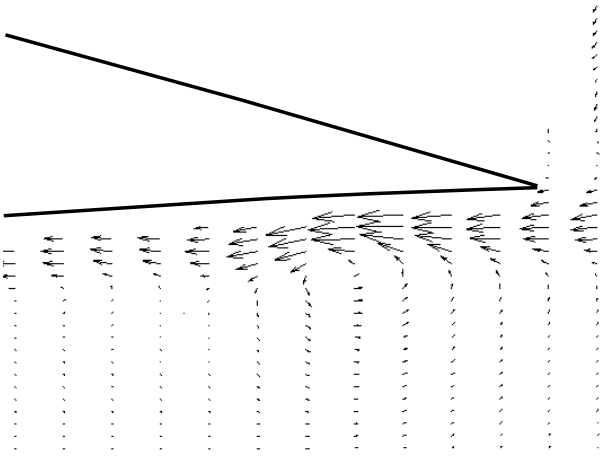

(b) 3.6m/s Relative Velocity Vector Field

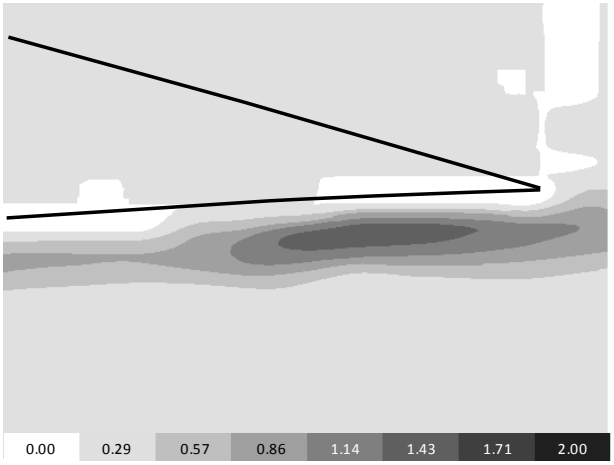

(f) 3.6m/s Relative Velocity Contours

Figure II.2 Detailed Flow Study at AoA=+2: Relative Velocity Vector Fields (a) and (b) and Relative Velocity Contours (c) and (d)

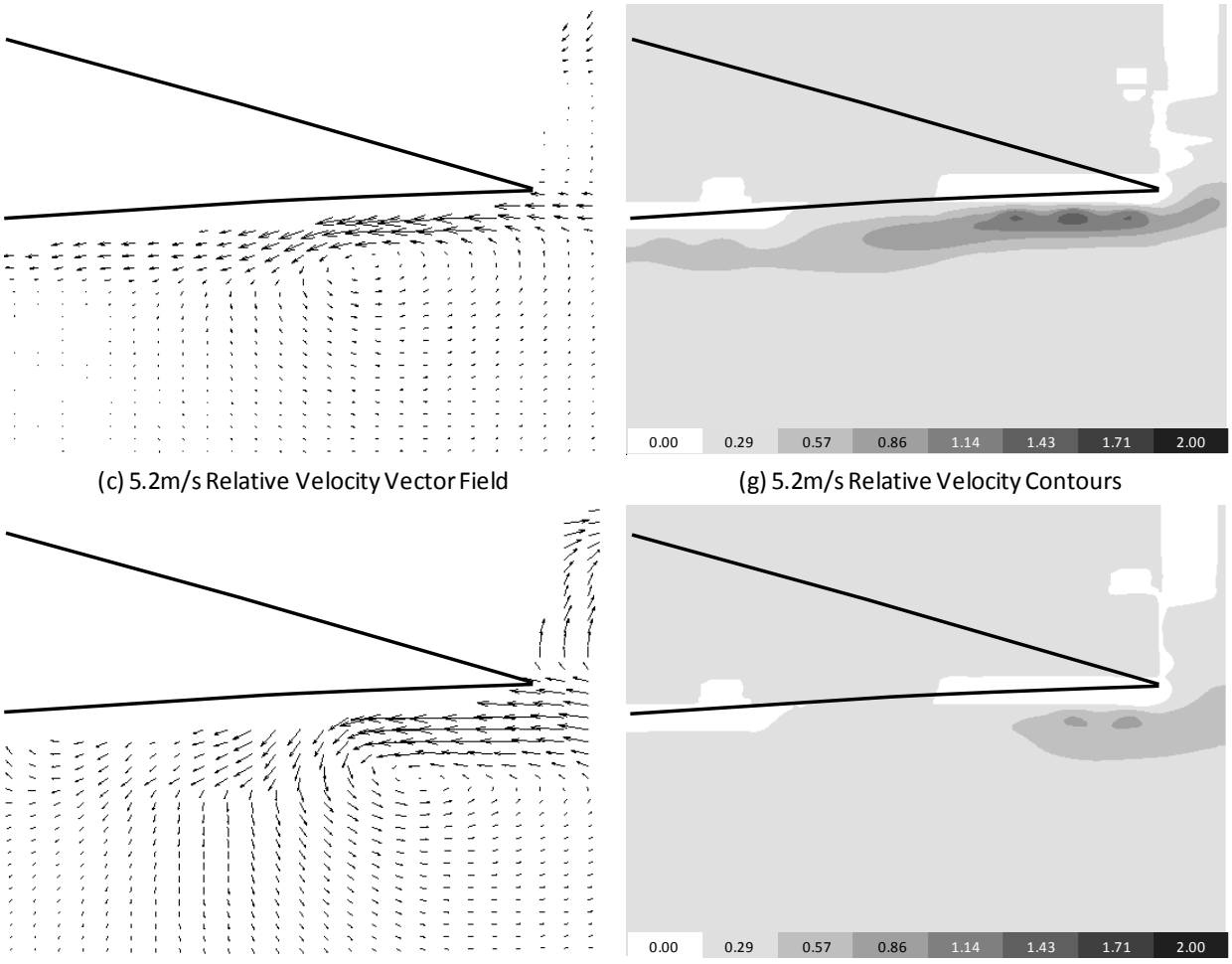

(c) 5.2m/s Relative Velocity Vector Field

(g) 5.2m/s Relative Velocity Contours

(d) 6.6m/s Relative Velocity Vector Field

(h) 6.6m/s Relative Velocity Contours

Figure II.3 Detailed Flow Study at AoA=+2: Relative Velocity Vector Fields (a) and (b) and Relative Velocity Contours (c) and (d)

APPENDIX III

DETAILED FLOW STUDY (AoA=+4)

Figure III.1 Camera View Field of Detailed Flow Study at AoA=+4

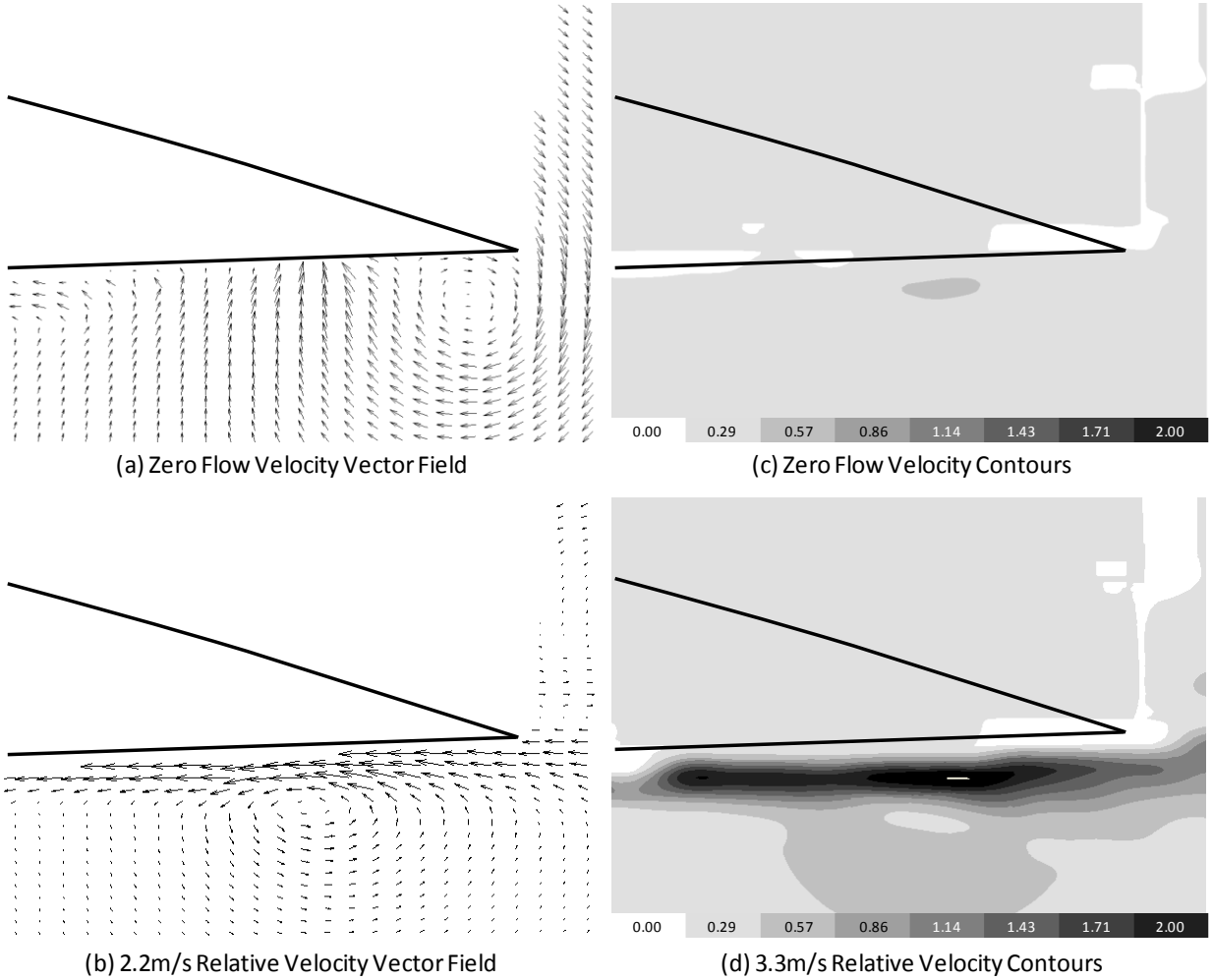

Figure III.2 Detailed Flow Study at AoA=+4: Velocity Vector Field (a), Relative Velocity Vector Field (b), Velocity Contours (c) and Relative Velocity Contours (d)

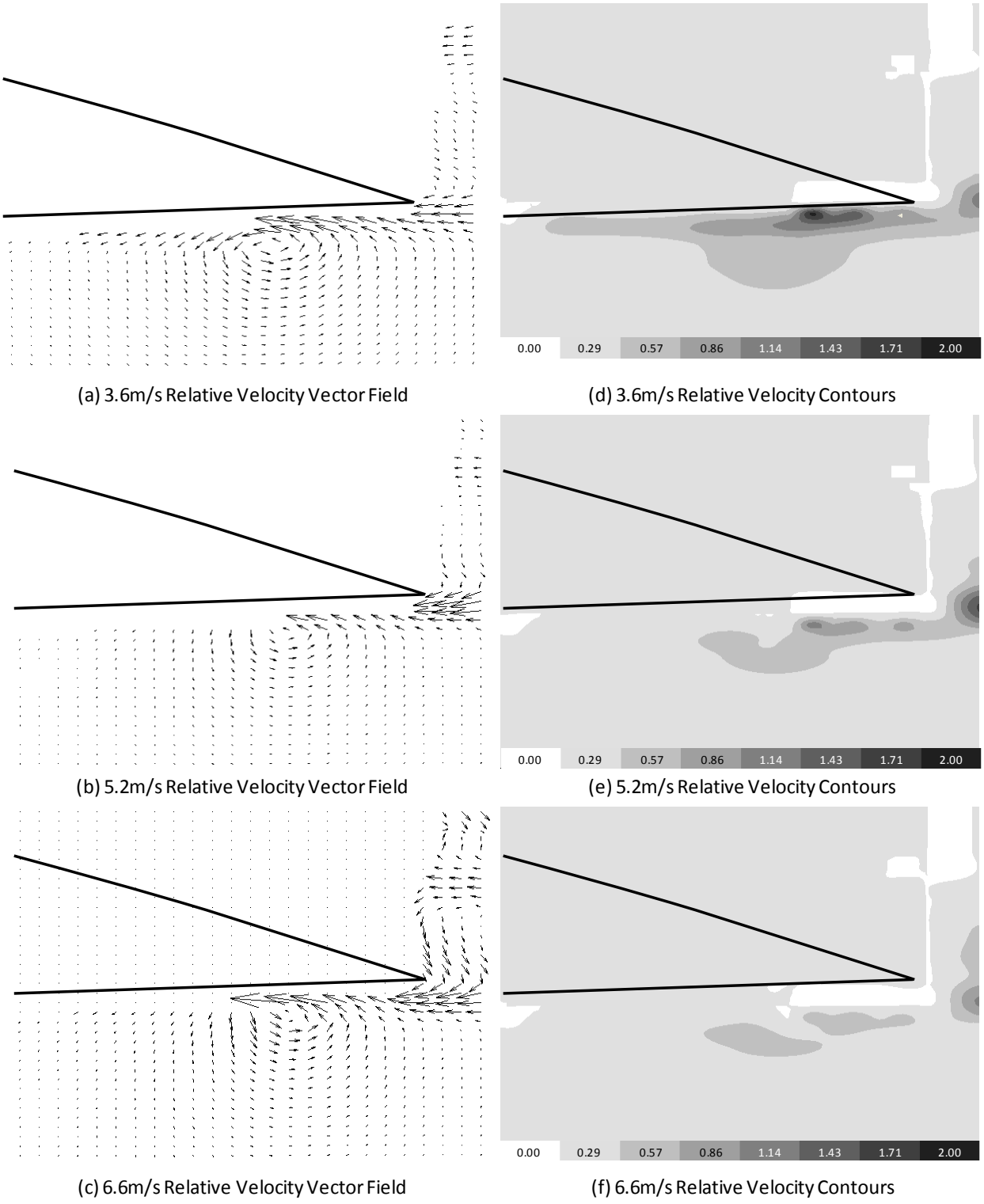

(a) 3.6m/s Relative Velocity Vector Field

(d) 3.6m/s Relative Velocity Contours

(b) 5.2m/s Relative Velocity Vector Field

(e) 5.2m/s Relative Velocity Contours

(c) 6.6m/s Relative Velocity Vector Field

(f) 6.6m/s Relative Velocity Contours

Figure III.3 Detailed Flow Study at AoA=-4: Relative Velocity Vector Fields (a)-(c) and Relative Velocity Contours (d)-(f)

APPENDIX IV

1% and 2% Gurney Flap on NACA 4424 Wing (26cm Chord)

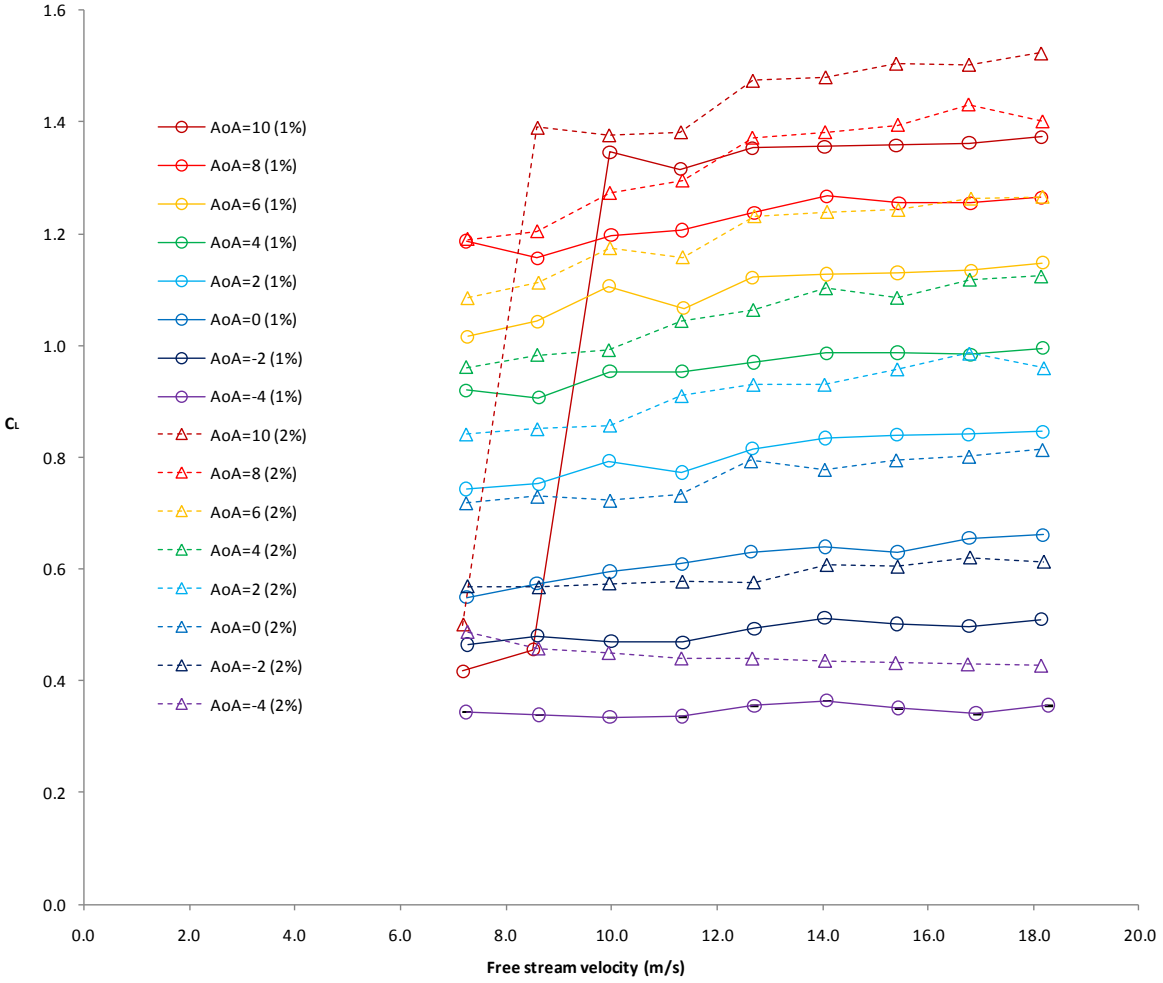

Figure IV.1 Experimental Results of 1% and 2% Gurney Flap on a NACA 4424 Wing (26cm Chord)

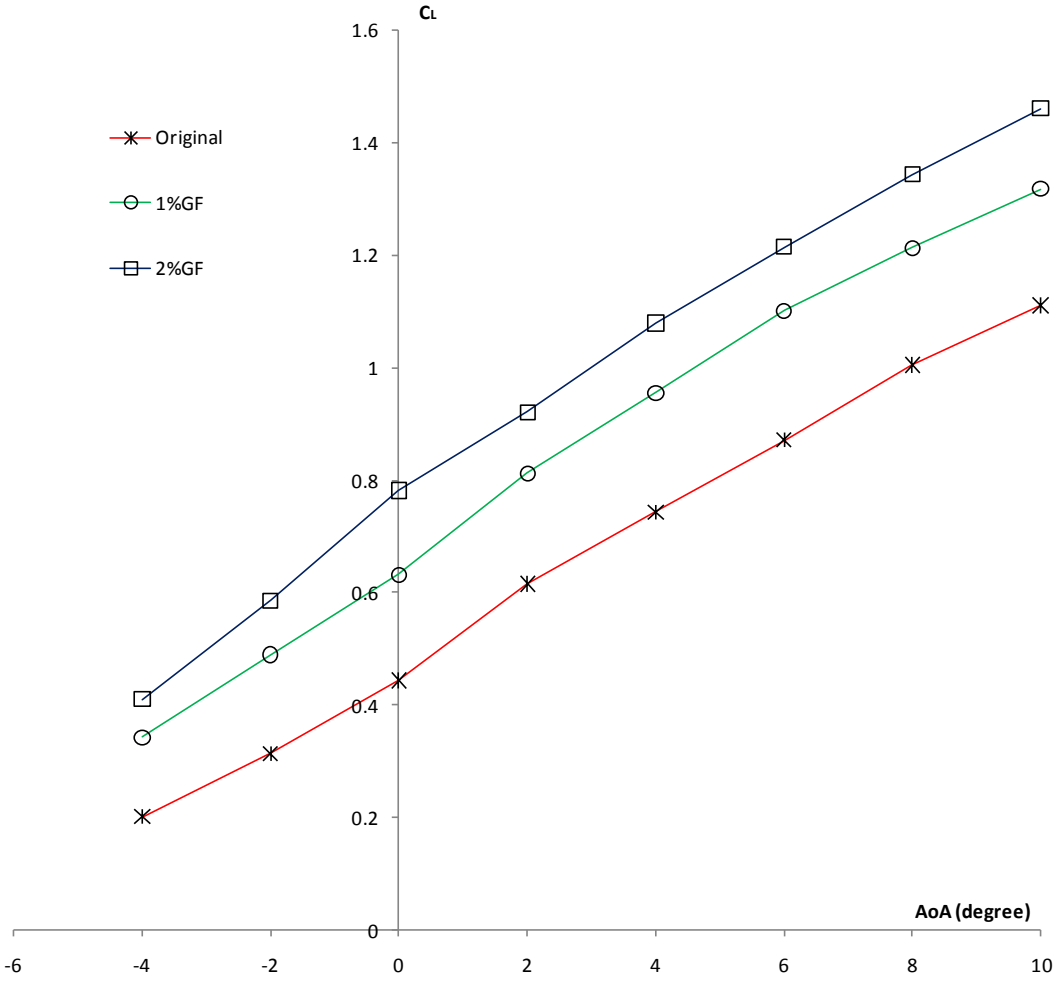

Figure IV.2 Lift Curves of 1% and 2% Gurney Flap on a NACA 4424 Wing (26cm Chord)